

UNCLASSIFIED

AD 4 6 4 7 2 2

DEFENSE DOCUMENTATION CENTER

FOR

SCIENTIFIC AND TECHNICAL INFORMATION

CAMERON STATION ALEXANDRIA, VIRGINIA



UNCLASSIFIED

NOTICE: When government or other drawings, specifications or other data are used for any purpose other than in connection with a definitely related government procurement operation, the U. S. Government thereby incurs no responsibility, nor any obligation whatsoever; and the fact that the Government may have formulated, furnished, or in any way supplied the said drawings, specifications, or other data is not to be regarded by implication or otherwise as in any manner licensing the holder or any other person or corporation, or conveying any rights or permission to manufacture, use or sell any patented invention that may in any way be related thereto.

CATALOGED BY: **DDC**  
AS AD NO. **464722**

**464722**

# LARGE MOTOR CASE TECHNOLOGY EVALUATION

First Year Summary Progress Report

June - 1965

VOLUME I

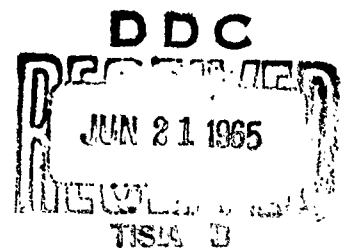
Contract AF 33(615) - 1623

Prepared for

Air Force Materials Laboratory

Wright-Patterson Air Force Base - Ohio

THE BOEING COMPANY  
Aero-Space Division  
Seattle, Washington



LARGE MOTOR CASE TECHNOLOGY EVALUATION

First Year Summary Progress Report

June - 1965

VOLUME I

Contract AF 33(615) - 1623

Prepared for

Air Force Materials Laboratory

Wright-Patterson Air Force Base - Ohio

THE BOEING COMPANY

Aero-Space Division

Seattle, Washington

## FOREWORD

This document is Volume I of a report presenting work accomplished by The Boeing Company during the first twelve month period from June 11, 1964 through June 11, 1965 in "Large Motor Case Technology Evaluation", Air Force Contract AF 33(615)-1623. Because of its length, this publication is presented in two volumes. The work was administered by the AF Materials Engineering Branch, Materials Application Division, Wright-Patterson Air Force Base, Ohio. The project engineer is Lt. Robert M. Dunco, MAAE.

The performance of this contract is under the direction of the Structural Development Unit, Structures and Materials Department, Aero-Space Division, The Boeing Company, with C. F. Tiffany as Project Supervisor, J. N. Masters, as Project Leader, and Howard A. Johnson as Non-destructive Test Program Leader.

## NOTICE

This document may not be reproduced or published in any form, in whole or in part, without prior approval of the Government. Because this is a Progress Report, information herein is tentative and subject to changes, corrections, and modifications.

## TABLE OF CONTENTS

### VOLUME I

LIST OF ILLUSTRATIONS	iv
LIST OF TABLES	v
I ABSTRACT	1
II INTRODUCTION	2
III BACKGROUND	3
IV WORK ACCOMPLISHED	11
A. 623A Materials	11
B. Alternate Materials	21
V CONCLUSIONS	32
REFERENCES	33
APPENDIX A	

## ILLUSTRATIONS

<u>FIGURE NUMBER</u>	<u>TITLE</u>	<u>PAGE</u>
1	Program Summary Chart	34
2	Parent Metal Fracture Toughness Data	35
3	GTA Weld Toughness Data	36
4	Significance of Proof Testing in Estimation of Minimum Tank Life	37
5	Failure Mode Prediction 260" Diameter Case	38
6	Failure Mode Prediction 156" Diameter Case	39
7	Sustained Load Tests 18 N1 (200) GTA	40
8	Sustained Load Tests 18 N1 (250) Submerged Arc	41
9	Sustained Load Tests 18 N1 (250) GTA	42
10	Residual Stresses	43
11	Subcritical Flaw Growth	44
12	Heat Treat Response for Two Quench and Temper Steels	45
13	900°F Aging Response for HY 180/210 (12 N1-5Cr-3Mo)	46
14	Effect of Post Weld Heat Treatment on Hardness of 9Ni-4Co-25C Weldments	47
15	Weld Edge Configuration	48
16	Composite Porosity Scatter Data	49
17	Lack of Fusion Scatter Data	50
18	Weld Cracking Scatter Data	51
19	Weld Toughness Scatter Data	52
20	Weld Quality Comparison by Alloy and Process (Porosity and Lack of Fusion)	53
21	Weld Quality Comparison by Alloy and Process (cracking)	54
22	Weld Toughness Comparison by Alloy and Process	55

TABLES

<u>TABLE NUMBER</u>	<u>TITLE</u>	<u>PAGE</u>
I	Materials Investigated	56
II	.60" Thick 18 Ni (200) GTA	57
III	.40" Thick 18 Ni (200) GTA	58
IV	.75" Thick 18 Ni (250) Sub-Arc	59
V	.48" Thick 18 Ni (250) Sub-Arc	60
VI	.39" Thick 18 Ni (250) GTA (Shells)	61
VII	.39" Thick 18 Ni (250) GTA (Heads)	62
VIII	Allowable Flaw Size Comparison	63
IX	Allowable Flaw Size 260" Case, 18 Ni (200) GTA	64
X	Allowable Flaw Size 260" Case, 18 Ni (250) Sub-Arc	65
XI	Allowable Flaw Size 156" Case, 18 Ni (250) GTA	66
XII	Screening Test Data - HY-150	67
XIII	Screening Test Data - 9 Ni - 4 Co - .20C	68
XIV	Screening Test Data - 12 Ni 5 Cr - 3 Mo (180)	69
XV	List of Process Variables Controlled in Multiple Balance Experiment	70
XVI	Composition of Alternate Materials (Base Metal & Filler Wire)	71
XVII	Alternate Material Processing History	72
XVIII	Work Sheet for Multiple Balance Design Experiment (GTA) Weld Process	73
XIX	Effects of Process, Gas, Alloy and Filler on Weld Toughness	74
XX	Typical Welding Rates	75
XXI	Summary of Multiple Balance Experiment	76
XXII	Material Comparisons	77



## I. ABSTRACT

In this volume, the results of base metal and weldment tests, and analyses of design deviations on materials and configurations of large solid motor cases of the 623A class are presented. A resultant end product of the above is the development of tables and curves depicting allowable initial flaw sizes in weldments of three large motor case designs. Such data considers the combined effect of material toughness, anticipated subcritical flaw growth, and total applied stresses which includes the effects of designed and manufactured discontinuities.

A second phase of this program summarized in this volume is the data generated during a statistically designed experiment devoted to the development of welding processes on three promising new materials. The effects of welding process variables on weld quality and toughness (KIC) are shown.

Volume II describes the work performed to date in the area of nondestructive inspection and includes specifications for fabrication of an automated ultrasonic inspection system suitable for use on large diameter motor case weldments.

## II. INTRODUCTION

The objective of this program is to assess material and process requirements for large solid propellant motor cases fabricated with roll-and-weld technology. Emphasis is placed on definition of material requirements for reliable performance, development and evaluation of advanced welding and inspection methods, and improvement in the engineering standards used to produce reliable motor cases.

The short-range goal includes the definition of the effects of defects, design deviations, and material quality on the performance of the two alloys presently being used in the 623A programs, and a review of the capability of present nondestructive testing techniques. The long-range goal is the establishment of large-motor-case material selection criteria and the development of sufficient detailed material, process, inspection, and subscale case performance data on motor-case materials to ensure a rational material selection prior to the initiation of potential future motor-case designs.

Initially, efforts included the evaluation of 260 inch case material-process combinations, and welding development on three alternate alloys. This was to be followed by detailed specimen and subscale case testing of the two most promising alternate alloys, and of the two 260 inch case materials. Since release of the September Progress Report, however, the program has been re-directed to include an evaluation of the 156 inch case material-process combination. This has required the elimination, subsequent to the multiple balance experiment, of two alternate alloys instead of one.

A summary chart of the program plan showing the major areas of investigation is shown in Figure 1.

### III. BACKGROUND

Before discussing detailed data being developed on this program, it appears appropriate to briefly describe the role fracture toughness testing and fracture mechanics analysis play in material selection efforts. Further, it is felt necessary to define the more important relations of these items with design, stress analysis, fabrication, and non-destructive inspection procedures in obtaining reliable and economical motor cases.

From examination of many past motor case and pressure vessel failures it becomes apparent that the primary causes for failure are pre-existing flaws. Also these past investigations have indicated that failure occurs when the flaw tip stress intensity attains a critical value which is commonly called the plane strain fracture toughness,  $K_{IC}$ . In a simplified form, the stress intensity,  $K$ , at the leading border of a surface or internal flaw can be described by the following:

$$K = 1.1\sqrt{\pi} \sigma (a/Q)^{\frac{1}{2}} M_K \quad (1)$$

where

$a$  = semi-minor axis of an elliptical flaw

$\sigma$  = applied gross stress

$Q$  = Flaw shape parameter

$M_K$  = magnification factor to account for deep flaws,  
multiple flaw interactions, etc.

1.1 applies for surface flaws, and drops to unity for internal flaws.

At onset of rapid propagation and fracture;

$$K_{IC} = 1.1\sqrt{\pi} \sigma (a/Q)_{cr}^{\frac{1}{2}} M_K \quad (2)$$

By describing the critical flaw size,  $(a/Q)_{cr}$ , as the allowable initial size,  $(a/Q)_1$ , plus anticipated subcritical flaw growth, Equation (2) can be rewritten as:

$$\text{Allowable } (a/Q)_1 + \text{Subcritical growth} = \frac{1}{1.21\pi} \left( \frac{K_{IC}}{M_K \sigma_T} \right)^2 \quad (3)$$

where:

$\sigma_T$  = total applied stress

Analysis of each element of Equation (3) is required and will be discussed in this report.

In considering large diameter motor cases, one must consider the following questions:

- 1) What  $K_{IC}$  values are of primary interest?
- 2) What determines the total applied stress level,  $\sigma_T$ ?
- 3) What type of subcritical flaw growth might one expect?

In answer to the first question, it is apparent that weldments and heat affected zones (HAZ) are of primary importance for  $K_{IC}$  determination for two reasons. First, weldment and HAZ toughness values are generally lower than parent metal values, and secondly, the probability of flaw occurrence is highest in these areas.

Accordingly, primary emphasis in the alternate materials portion of this program is placed on the determination of weldment and HAZ  $K_{IC}$  values and in determining the influence of process variable on these values. Additional emphasis will be placed on thick section properties.

In answer to the second question, the applied primary stresses in a motor case are dependent upon the design factors of safety and the selected heat treat strength level. But as important, the determination of critical flaw sizes or allowable initial flaw sizes must include consideration of:

- 1) Secondary or discontinuity stresses inherent in the design (e.g., head to shell joints).
- 2) Secondary stresses resulting from design deviations (e.g., linear and angular mismatch).
- 3) Possible residual stresses

Later paragraphs will discuss procedures used to determine these secondary stresses and show the probable influence of these stresses on critical flaw sizes. Also, included are the results of residual stress measurements made on the Aerojet and Thiokol 260 inch diameter motor cases.

With regard to subcritical flaw growth, probably the most important consideration is the possibility of environmentally induced sustained stress growth during proof testing or during actual motor firing. Also, if there are high residual tensile stresses, there is the possibility of flaw growth under zero pressure.

While one might expect that the pressurization times are not sufficiently long to worry about sustained stress flaw growth, this cannot be assumed. For instance extremely large amounts of flaw growth have been observed in the 4340 type steels operating in a damp environment. For this reason each of the 623A materials and the alternate alloys were tested (both base metal and weldments) to define flaw growth characteristics.

Our inhouse research on motor case materials which is being extended on this program included the investigation of some 14 alloys. These efforts were based on the investigation of parent metal and weldment fracture toughness, subcritical flaw growth, and fabrication characteristics. Yield strength levels ranged from about 140 KSI to 280 KSI. These materials are summarized in Table I. The typical base metal plane strain fracture toughness values are shown in Figure 2, and typical weld metal fracture toughness data is shown in Figure 3. In both Figures 2 and 3, arrows depict those data points where specimens failed after net section yielding, and thus  $K_{IC}$  values are known to be greater than indicated. From these illustrations, it is apparent that toughness reductions would be expected with increasing strength levels. In considering these trends, two fundamental questions are raised:

- 1) What material strength level is required for large diameter solid motor cases?
- 2) How high a toughness value is needed to guarantee a reliable motor case?

In an attempt to obtain an answer to the first question, in 1963, a systems study was initiated on two large launch vehicles utilizing 260" first stage motors and liquid upper stages. One vehicle was designed to place 500,000# of payload in a 300 mile earth orbit, the other to place 1,000,000# in orbit. These studies have been reported elsewhere (Reference 1), and can briefly be summarized as follows. First, by holding all propellant weights constant, it was seen that a decrease of first stage case tensile strength from 250 down to 150 KSI results in a payload reduction of only three to four percent. Secondly, three cases were designed utilizing 150, 200, and 250 KSI strength materials (HPL50, Ladish D6 at 200 KSI, and 18 Ni 250). Cost estimates were

developed by Boeing and by three companies experienced in constructing large structures. The results of these estimates were then used in constructing a curve of case strength versus relative cost per pound of payload in orbit. The overall result was that total vehicle economics was completely insensitive to first stage case strength level. Recognizing that any contingencies such as an expected higher proof test failure rate in the higher strength materials, it became apparent that actual vehicle cost savings might accrue from use of the lower strength materials.

Based upon this study, no apparent advantage could be seen in using the very high strength materials in 260-inch diameter cases. With regard to the 156-inch diameter cases, the question as to required strength is still unanswered. Intuitively, it is felt that vehicle performance may be slightly more sensitive to case strength level, but to our knowledge there is no such data available.

The answer to the second question (i.e., what  $K_{IC}$  values are required to ensure reliability?) is not a simple one, however, the following illustrates what is felt to be a practical approach.

It is clear that from an economics standpoint we cannot afford many proof test failures, and from the standpoint of both economics and personnel safety, the prevention of service failures is mandatory. Obviously, if an accurate job of defining allowable flaw sizes is done, materials and fabrication processes are selected which result in a low probability of flaw occurrence, and if non-destructive inspection procedures are developed which guarantees detection of all flaws larger than allowable, neither proof

test nor service failures should be encountered. Unfortunately, this goal has not yet been attained, and other tools must be investigated to help guard against failure.

The potential value of the proof test in assuring subsequent service life was discussed in the 5th report of the ASTM Committee on Fracture Testing (reference 2). This is illustrated in Figure 4. As seen in this figure, maximum initial to critical flaw size ratio,  $(a/Q)_1 / (a/Q)_{cr}$  is equal to  $1/a^2$ , where  $a$  is the proof test factor. Similarly, the maximum initial-to-critical stress intensity ratio,  $K_{I1} / K_{Ic}$ , is equal to  $1/a$ . Both are independent of the actual proof stresses, and the actual material toughness values. This is significant since the actual proof stresses may be different because of design or manufactured discontinuities, and because the toughness values will likely vary between base metal, weldments, and forgings.

Also, as noted in the Figure, the minimum flaw growth potential in the tank  $(a_{cr}/Q_{cr} - a_1/Q_1)$  is equal to  $(1 - 1/a^2)$ . The task then lies in evaluating the flaw growth characteristics of the case materials, to ensure that flaw growth during service is indeed less than the growth potential noted above. As will be seen in the body of the report this does not appear to be a critical problem for the materials under study, and for the expected service requirements of large cases.

The final question remains, then, of how to prevent proof test failures. An obvious approach would be to utilize a material with sufficient toughness such that any subcritical flaw would have to grow through the thickness



prior to reaching critical size. Such a case would then leak rather than fail catastrophically and it could be subsequently repaired.

Such a criterion could be met in a case if the critical flaw size at proof pressure for the worst shape flaw (i.e., a long elliptical surface flaw) is greater than the case thickness. Such a criterion could obviously not be met if under the same pressure the most favorably shaped flaw (i.e., an internal penny shaped crack) attained critical size prior to exceeding a diameter greater than the case thickness. Using this approach, Figures 5 and 6 have been constructed. In Figure 5, a hypothetical 260-inch case is illustrated, with design pressures and factors as noted. The relation of weld toughness versus yield strength shown earlier in Figure 3 is repeated. Superimposed on this band, are two cut-off lines depicting the two extremes just mentioned. It is seen that through the use of materials with yield strengths greater than about 200 KSI failure prior to leakage is a certainty for even the most favorable flaw shape. Through the use of materials with yield strengths of about 150 KSI and under, critical long surface flaws are greater than thickness, and a leak before failure condition prevails. Between these two extremes, failure mode is dependent upon actual flaw shapes and locations. Figure 6 illustrates the same approach for a 156-inch case with the same design factors. Here it is seen that because of thinner cylindrical shell requirements, higher allowable design strengths are acceptable.

This background discussion has attempted to convey the following major points.

- 1) Pre-existing flaws are the primary cause of unreliable motor case behavior.
- 2) Allowable flaw size determination requires an accurate knowledge of  $K_{IC}$  values, subcritical flaw growth, and total motor case stresses.
- 3) From the primary standpoint of reliability (although vehicle economics are not ignored) it is desirable to have weldment  $K_{IC}$  values in excess of about 160 or 170 KSI  $\sqrt{IN}$  for 156-inch motor cases, and in excess of about 200 KSI  $\sqrt{IN}$  for the 260-inch cases.

The program described in the following paragraphs has been planned around these three major points.

#### IV. DISCUSSION

The following sections describe the work accomplished to date in the three major areas of investigation (i.e., 623A Class materials, alternate materials, and non-destructive testing). Early program results are summarized where necessary for understanding of the detailed presentation of the results of the last quarter.

##### A. 623A Class Materials

The specific goal of this portion of the program is the establishment of flaw acceptance criteria and allowable weldment design deviations (i.e., mismatch and sink-in) for the large diameter maraging steel motor cases of the 623A type. This necessarily requires an evaluation and understanding of static fracture and subcritical flaw growth characteristics of the appropriate material - process combinations and analyses of total stresses in typical weldments in the three 623A cases.

##### 1. Testing Approach

In order to establish realistic baseline toughness values and flaw growth characteristics of existing large case materials, all weldment tests are being performed on panels fabricated by the three 623A motor-case contractors. In each case, material thicknesses were selected to duplicate full scale head and shell requirements. Limited tests were performed on base metal, with primary emphasis on weldments (centerline and heat affected zones, HAZ). Base metal was purchased specifically for use on this program, weld wire (and flux where applicable) was supplied by the case contractor. Weldment-grain direction orientations were selected to represent what was felt to be the most critical combination. That is, welds in gages representing cylindrical shells were placed perpendicular to the primary plate rolling

direction, thus duplicating the longitudinal shell weld. For the thinner gages representing head thickness, weldments were placed parallel to the primary plate rolling direction. All specimens were pulled transverse to the weld. Fatigue cracked surface flaw specimens were used for toughness and flaw growth studies for most weldments. One exception was the use of cracked round notch bars on .75 inch thick 18 Ni (250) weld panels.

Static specimens were tested in air at room temperature by loading at a rate required to produce a complete failure within one to three minutes. Sustained load tests were performed by loading to approximately 85% of the critical stress intensity ( $K_{IC}$ , as determined from the prior static tests) and holding at this level until failure or for 24 hours. If failure did not occur at this time, the stress intensity level was increased five percent. With no failure for an additional 24 hours, the load was increased directly to failure. As described later, these tests were performed in either air, or under a 3-1/2% salt solution spray environment.

Flaws in the HAZ specimens were placed so as to intersect the coarse grained zone immediately adjacent to the fusion line. Flaw shape on these specimens was semi-circular where possible, so that stress intensity around the crack periphery was essentially constant. Such flaw placement was suggested from a series of smooth tensile specimen fatigue tests. Here, specimens were cycled at a maximum tensile stress of 80% of yield until failure or until a crack was observed. Three out of four 18 Ni (250) specimens (GTA and submerged arc weldments) developed cracks in the noted coarse grained location, and one in the weld centerline. Both 18 Ni (200) specimens failed in base metal, distant from any weld affected structure.

## 2. 18 Ni (200) Test Results

Compositions of base metal and filler wires used in this series of tests are as shown below:

FORM	HEAT	C	M <sub>m</sub>	P	S	Si	Ni	Cr	Mo	Al	Ti	Co
Base Repub	3951104	.014	.05	.004	.007	.02	18.20	.10	4.32	.11	.25	7.75
Wire Spcl Mtls	6-3343	.010	.01	.005	.004	.004	18.02	-	3.62	.079	.27	7.74

Base metal tests as reported in earlier reports indicated longitudinal and transverse  $K_{IC}$  values from surface flaw specimens (with flaw normal to plate surface) of approximately 156 and 138 KSI  $\sqrt{IN}$  respectively at a yield strength averaging 230 KSI. Single edge notch specimens (with crack moving parallel to plate surface) gave average  $K_{IC}$  values of 115 and 103 KSI  $\sqrt{IN}$  for longitudinal and transverse directions respectively.\* Both sets of specimens had been aged at 900°F for 4 hours.

Toughness values from panels welded (and aged 900°F 8 hours) by Sun Shipbuilding and Drydock Company shown in earlier reports are reproduced in Table II and III. Briefly, these data show HAZ and .62 thick weld centerline toughness values from five to ten percent lower than base metal. An additional small reduction in manual repair weld toughness is suggested, and a more significant reduction is seen in the .40 weld centerline values of 113 and 119 KSI  $\sqrt{IN}$ .

Sustained load surface flaw tests were then run, utilizing the data generated in the static tests. The data developed during this series of

\*Distinct discontinuity in load deflection curves were not usually observed in this series of tests.

tests are shown in Figure 7 . It is noted that in eleven out of twelve test runs in ambient air (50% average humidity) failure did not occur during the 24 hour hold, even with initial applied  $K_I$  levels from 90 to 95 percent of critical. This behavior is as good as that seen on most base metal alloys tested in air. The only exception was a .40 inch thick HAZ specimen (note, transverse grain) which failed within the band of data from specimens tested in salt spray. Such band suggests a sustained load stress intensity threshold level of approximately 75 percent of critical. The significance of the above noted data will be discussed in later paragraphs.

### 3. 18 Ni (250) Test Results (Submerged arc welds)

Compositions of base metal and filler wires used in this series of tests is as shown below.

FORM	MFG	HEAT	C	M <sub>m</sub>	P	S	Si	Ni	Co	Mo	Al	Ti
Base	Repub.	3321290	.017	.10	.005	.005	.07	17.93	7.80	4.98	.10	.46
Wire*	ARMETCO	09391	.02	.08	.002	.007	.02	17.95	7.88	4.82	.08	.65
Wire**	ARMETCO	09395	.01	.08	.002	.005	.02	18.28	7.88	4.59	.08	.49

Base metal, (.48 and .75 inch plate) fracture tests as reported in earlier reports indicated a longitudinal  $K_{IC}$  of 116 KSI  $\sqrt{IN}$  and long transverse of 86 KSI  $\sqrt{IN}$  from surface flaw specimens (with flaw normal to plate surface) and values in the 80's and 90's in both principal directions from single edge notch and round notch specimens. This material has been aged at 835°F for four hours and exhibited yield strengths of 260 KSI transverse

\* Sub-arc Welds

\*\*Manual GTA Repairs

(.48 inch plate) and 250 KSI longitudinal (.75 inch plate).

Panel welds from Newport News Shipbuilding and Drydock Company displayed yield strengths of 198 and 184 KSI for the .48 and .75 inch panels respectively. Though some fracture specimens were tested at this strength level, most were aged two-and-one-half hours (in addition to the Newport four-hour age) at 835°F to increase the strengths to what was felt to be more representative of the full scale structure. Though the resulting strengths (225 and 213 KSI respectively) and microstructure more closely represent the case, such history must raise the question of applicability of the generated specimen data. Valid static toughness values that were obtained on the panel welds after re-aging were in the order of 55 to 58 KSI  $\sqrt{IN}$  in the .48 inch plate. The .75 inch panel was first tested using round notch bars, which resulted in calculated values of around 40 KSI  $\sqrt{IN}$ . In attempting to determine if variations in toughness existed between the first and second sub-arc pass, two specimens were prepared from a .75 inch panel. One with a surface flaw extending into the first pass side, and one in the opposite side. The resultant values\* were 79.3 and 81.8 KSI  $\sqrt{IN}$ . This compares favorably with values of 89.0 and 77.5 KSI  $\sqrt{IN}$  taken earlier in .48 inch "second pass" surface flaw tests in as received material. Weld test data is summarized in Table IV and V.

Because of the above noted findings, sustained load tests were performed only on the .48 inch panels from which surface flaw specimens had already been machined. The results of these tests are shown in Figure 8. For comparative purposes, the data is superimposed on the 18 Ni (200) weld

\*These specimens were "as received" (i.e., not re-aged)

data presented in Figure 7. Little difference is seen in the two sets of specimens. That is, the flaws appear to be extremely stable in ambient air environment and stress intensity threshold level for initiation of subcritical growth is about 75 percent of critical in a salt spray environment.

#### 4. 18 Ni (250) Test Results (GTA Welds)

Composition of base metal and filler wire used in this series of tests are as shown below:

FORM MFG	HEAT	C	M <sub>m</sub>	P	S	Si	Ni	Co	Mo	Al	Ti
Base USS	X53690	.02	.06	.004	.011	.02	18.06	8.10	4.82	.13	.38
Wire ARMETCO	08850	.01	.03	.002	.005	.03	18.10	8.00	4.52	.10	.46

Tensile and fracture data of base metal (.39 plate) aged 900° for three hours is shown below:

	F <sub>tu</sub> KSI	F <sub>ty</sub> KSI	K <sub>IC</sub> Surface Flaw	KSI $\sqrt{IN}$ Single Edge Notch
Longitudinal	-	-	88.8	84.5
Transverse	246	237	82.9	75.9

Toughness values from panels welded (and aged 900°F 3 hours) by Excelco Developments are shown in Table VI and VII. As with the 18 Ni (250) submerged arc weld tests, weld centerline K<sub>IC</sub> values appear to be significantly lower than that of base metal. Likewise HAZ test results, again from surface flaw specimens, show calculated values consistently higher than that of base metal. Such values are obviously affected by layered structure and should be treated with caution. As shown in Table VII, a significant difference in weld centerline K<sub>IC</sub> values were observed between groups of specimens taken from two panels which were supposedly processed in a



similar manner. Significant differences in ductility were also observed (4% RA versus 38% RA), while tensile strengths compared favorably.

Sustained load data developed from the Excelco weld panels are illustrated in Figure 9. As before, the data is superimposed on the 18 Ni (200) scatter-band. From this figure it can be seen that in ambient air environment the flaws are extremely stable, but significant growth is experienced in salt spray. Growth rates are slightly higher than in the lower strength materials discussed earlier; however, a threshold level of 75 percent of  $K_{IC}$  appears to be a safe estimate. The significance of this data is discussed in Paragraph IV.A.6.

#### 5. Design Deviation Analyses

The planned design deviation analyses has now been completed and is included as Appendix A. These analyses deal primarily with longitudinal and girth weld mismatch and sink-in. The ultimate objective of these studies, when coupled with previously noted test phases, is to define allowable weldment flaw sizes in vessels containing what is considered to be typical deviations from ideal contour.

As might be expected, it has been observed that the most important deviation (in terms of expected dimensional control problems, as well as in terms of the impact of the given deviation) are probably associated with head to-y-ring girth welds\*. The primary reason for this is that applied moments caused by a given deviation tend to be linearly proportional to the dimensional value of the deviation (e.g., the sink-in in inches), and the resultant stress is inversely proportional to the square of the thickness.

\*Nozzle-ring to head junctures are not included in this study.

A brief discussion of the effects of what are considered to be typical deviations on critical flaw sizes of existing cases is included in Paragraph IV.A.7.

#### 6. Residual Stress Measurements

Residual surface stresses were measured utilizing X-ray diffraction techniques (Reference 3) at several areas of each of the two 260 inch diameter cases. The measurements were made after the aging cycle on I.D. and O.D. surfaces, on the weld centerline, in the heat affected zone, and in virgin base metal. The surfaces were sufficiently smooth so that additional surface preparation was unnecessary.

Detailed results were included in earlier reports and are summarized in Figure 10. The numbers shown in tabular form are the averages (in thousands of pounds per square inch) of several readings taken at the locations shown. Each data point is believed to be accurate within plus or minus ten KSI.

Data from flat panels welded and aged by Sun Ship and Newport News are also shown in Figure 10. Diffraction measurements were made on as-received surfaces, and on successively deeper surfaces exposed by electropolishing, in three mil increments. Longitudinal and transverse values, in weld centerline and heat affected zones from both panels are included in the same illustration. It is seen that readings taken on the original surface are generally comparable to those measured on the actual cases, and though tension stresses are occasionally observed, the trend approaches zero stress at approximately 15 to 25 mils from the surface.

On the basis of these measurements, it has been chosen to ignore the effects of residual stresses in the computation of allowable flow sizes in the large maraged cases.

#### 7. Allowable Flaw Size

The allowable flaw size in a motor case is defined as the critical flaw size minus the subcritical flaw growth anticipated during service life of the case. Use of the sustained load flaw growth data reported earlier can be illustrated as in Figure 11 (a), (b), and (c). Figure 11 (b) relates critical flaw size versus total applied stress for material of any toughness. If critical flaw size at an operating stress of unity is designated 100 percent, it can be seen that critical size at a proof stress of 1.1 times operating, is  $(1/1.1)^2 \times 100$ , or 83 percent of critical at operating. That is, any case which successfully passes a 1.1 proof pressure could not have contained a crack-like flaw any larger than 83 percent of critical at operating pressure, or else the case would have failed before reaching the proof pressure. By cross plotting the lower bound of the sustained load tests shown earlier\*, it is seen that it would take an approximately 60 minute operational load cycle before a flaw 83 percent of critical would be expected to grow sufficiently to cause failure at the firing pressure. Flaw growth during one firing cycle, therefore, is not felt to be significant.

Recognizing that hydrostatic test pressurization rates in the large cases might be relatively slow and that the case might actually be held at pressure several times for instrumentation read-out, the possibility of

\*Note that the ordinate of Figure 7 thru 9 is squared to construct the Figure 11 (c) curve.

growth during the proof test cycle should probably be considered. This is illustrated in Figure 11 (a). By assuming that a flaw exists before testing which is just barely under critical size at proof pressure, measurable growth might be expected at pressures above 70 percent of proof (since the lower-bound  $K_{I1}/K_{IC}$  threshold lies at about 70 percent.) Therefore, a conservative estimate of allowable flaw size would be a size equal to 90 percent of the critical size at proof stress.

With this approach, allowable flaw sizes for three 623A cases are shown in Table VIII. These represent the effects of membrane stresses only (i.e., they do not account for designed or manufactured discontinuities), and are based on weld centerline  $K_{IC}$  values shown earlier. Stress levels indicated are based on proof pressures and minimum design thicknesses as indicated.

Though detailed discussion of the effects of weld contour deviations is included in Appendix A, examples of typical deviation effects are illustrated for the three cases in Tables IX, X, and XI. Membrane stress allowable flaw sizes are included for comparative purposes. Rather rapid decreases in allowable flaw sizes with only moderate deviations are apparent. For instance, where bulkhead allowable flaw size due to membrane stress in the 18 Ni (200) large case is approximately .14 inches, this is reduced by about 50 percent in a Y-ring weldment containing a five percent ( $\delta = .05 \times .34 = .017$  inch) mismatch. The probability of having deviations of this magnitude is extremely high.

## B. Alternate Materials

As illustrated earlier in Figure 1, the overall plan of the alternate materials phase of this program included the screening of several candidate materials, weld evaluation of three of the most promising alloys, and detailed testing (specimens and vessels) of a single alloy. From results of the screening tests performed early in the program two quench and temper steels (5Ni and 9Ni) and one maraged steel (12Ni) were selected. The screening test data for these three alloys is shown in Tables XII, XIII, and XIV. Note that in many instances  $K_{IC}$  values are conservative and are so indicated. During the last quarter the first part of the weld development program was completed (i.e., the multiple balance experiment) and the 9Ni alloy was selected for continued study. Final weld optimization, detailed tests of the selected weld process, repair weld evaluation, thick section property tests, and the subscale case fabrication are now in work. The following paragraphs discuss the approach and results of the weld development program.

### 1. Multiple Balance Experiment

At the outset of this program, it was decided that the program objectives would most assuredly be reached if a statistically designed experiment were to be employed. The experimental procedure selected was the Multiple Balance Design. This test plan permits evaluation of an unlimited number of test variables without undue complexity or cost. Table XV lists the variables evaluated.

Base Alloy: Three steels (two quench and temper and one maraging steel) were selected based upon early screening tests as being most promising as alternate materials. Tables XVI and XVII.

Filler Alloy: Three filler alloys were selected for each base alloy, one being the composition shown best by preliminary studies and two

modifications to improve toughness, strength or weldability.

Compositions C, D and H in Table XVI are similar to compositions shown good by previous studies. Compositions B and I approach base metal composition of the 5Ni and 12Ni steels. Alloy A is a low strength modification of C. Alloy E is a modification of D with increased Mn and Si to improve GMA weldability. Alloy F is a high Co Modification of the base metal to promote self tempering by raising the Ms temperature. Alloy G offers a strength level intermediate between H and I and increased Mo and decreased Cr should provide better toughness.

Filler alloy size: Two wire sizes .045 and .062 inch diameter were employed primarily to affect current densities in GMA process.

Pre-Weld Heat Treatment: The 12Ni maraging steel was welded only in the solution annealed condition; the two quench and temper steels were tempered at one of three levels between 850 and 1075°F. Figures 12 and 13 show the heat treat response of the three steels.

Post-Weld Heat Treatment: The 12Ni steel was given one of three post weld age treatments, 4, 8, or 12 hours at 900°F. The 5Ni and 9Ni steels were given one of four post weld treatments: none, temper weld pass, 2-hour temper at 600°F, or a re-temper in accord with the pre-weld heat treatment. Figure 14 shows a hardness traverse across a 9Ni-4Co weldment after each heat treatment.

Pre Heat and Interpass Temperature: Two temperatures 150 and 300°F were employed.

Post Heat Hold: The interpass temperature was held for 0 or 30 min. after completion of the final pass and then the part allowed to

naturally air cool.

Welder: Two welders were used one for each shift.

Engineer: Two engineers directed the operation one for each shift.

Shift: The welding was done in two shifts approximately 2/3 on the day shift and 1/3 on the night shift.

Priority Number: The order in which the panels were to be welded was determined by a random draw.

Weld Process: The bulk of the effort was placed on one of three processes, GTA, GMA and GMA (HD) with a lesser effort on GMA (short arc) and Submerged arc.

Weld Joint: Two joint configurations were used for each process, one wide and one narrow. Figure 15 illustrates the joint details.

Weld Energy: Four energy levels were used, 10, 20, 30, and 40 kilojoules/inch/pass.

Weld Speed: Two relative speeds were used for each heat setting, a relatively fast and a slow.

Shielding gas: Five gases were employed: Argon, Helium, Helium + Argon + CO<sub>2</sub>, Helium + Argon + Oxygen and Argon + CO<sub>2</sub>.

Gas Flow Rates: Two flow rates were used, 40 and 80 cfh.

Cup to Work Distance: Two separation distances between the torch cup and the work were used in the GMA processes .7 and 1.0 inch.

Tip to Work Distance: Two electrode extensions were used in the GMA processes .5 and .7 inch.

Filler Wire Feed: Two feed rates for the auxiliary wire were used, fast and slow.

Cleanliness: Two cleanliness ratings were given, clean and not clean.

Trailer Shield: A trailer shield with Argon gas was or was not used.

Three independent multiple balance plans were constructed, one for each of the three weld processes under consideration. This breakdown was selected to reduce the complexity of each plan and because each process had slight variations which could not be matched.

A typical plan layout is illustrated in Table XVIII. It is subdivided into four subgroups; each subgroup contains no more combinations than tests to be performed. The first has 24 combinations, the second 16, etc. Sample numbers were selected at random and assigned to a cell of subgroup 1 until all were filled. The same sample numbers were then redrawn using a table of random numbers and assigned to cells in subgroup 11 until these were all filled. The extra numbers were then assigned in such a manner as to maintain balance. This process of drawing numbers continued until all four subgroups of each multiple balance plan were filled and all sample numbers had been assigned.

The welding proceeded according to the plan. Test panels were assigned a priority number and pulled from the stack according to lowest priority. Base metal and filler wire delivery delays forced extensive changes in the originally planned schedule but the random selection philosophy was maintained.

An example of how the multiple balance plan worked with pre-determined settings follows: Sample #71 was welded using 10 kilojoules, wide joint, fast speed, fast feed rate, 40 cfh of A, no trailing shield, well cleaned parts, 9N1-4Co-.25C, .045" dia. "d" filler, 975°F temper, 150°F preheat and interpass



temperature with no hold time after completion of the weld. The variables of operator and observer were not preplanned; the parts were welded as they came and whichever operator was on duty at the time welded it. The post-weld heat treatment was selected at random and for #71 was 1 (as-welded).

Prior to welding each test part, a "bead on plate" weld was made to establish the specific voltage, current and travel speed to establish a stable weld and yet have the predicted heat input. A plus or minus 10% variation was allowed in the heat input to permit improved weld stability but in spite of this, many of the welds were far from ideal. Very little could be gained from earlier welds because of the hundreds of combinations available. In general, welding voltages were established within a 2-volt range by the shielding gas, the amperage by the travel speed range and electrode diameter and the welding speed was the final adjustment to attain the desired heat input. Minor variations of each were then made to achieve stability. Once a setting was established, it was used in the test panel. Further minor variations were made in the settings if determined necessary. If gross surface porosity were encountered, this was ground out and rewelded. Manual repairs were employed as necessary to complete the weldment. No repair was used on crack-like defects.

Upon completion of the welding, each panel was radiographed. The films were then inspected for three distinct defect types, porosity, cracks and lack of fusion. Porosity was rated 1-5 with 1 and 2 being good, 3 fair and 4 and 5 poor. Cracks and lack of fusion were both measured by the cumulative total length of weld containing the defect. This was reported as ranging from 0 to 9 inches. Visual observations were made and recorded on the log sheets as the welds were made but the lengths of cracks noted were not recorded. Additional crack-like defects have been noted on the fracture surfaces but these have not been correlated.

Following radiographic inspection those samples considered to be of testable quality were given the post weld heat treatment and then machined and tested.

Each of the four evaluation criteria, fracture toughness, cracking, lack of fusion and porosity, were subjected to analysis by use of scatter plots.

Scatter plots have been made for each process-criterion combination for a total of 12. These have been condensed into 4 composite plots in Figures 16 through 19, which show the scatter as affected by the major variables.

### Porosity

Figure 16 shows the scatter plots based upon porosity; from this diagram it can be seen that the entire sample had a 39, 22, 16, 13, 15 distribution. How each of 20 factors affected this distribution is shown. The mean is indicative of relative effects. This chart shows that the most important factors affecting porosity are the base alloy and welding process. Other factors having significant influence are welding speed, heat input, filler size and the shielding gas. In the GMA process the higher heat welds had more porosity whereas in the GTA process the higher heat welds had less porosity. The 9 Ni- 4Co consistently had the highest porosity and the 5 Ni consistently had the least porosity. The porosity level of the GTA welds was considerably below that of the GMA welds. The 062" dia. electrode produced less porosity than the 045" dia. by the GMA process but the wire size had little or no effect on the porosity of the GTA and GMA (HD) processes. Slow welding speed reduced the porosity level. The effect of the gas composition appears somewhat erratic and has not been clearly evaluated. All other factors appear to have a very minor effect on the porosity level of the weldments.

### Lack of Fusion

Figure 17 is a scatter plot based upon lack of fusion instead of porosity but only process and alloy are defined. The most important factor is base alloy with the 12 Ni being the least prone to lack of fusion and the 5 Ni being most prone to lack of fusion. Other factors affecting fusion include wire size, speed and joint. The larger diameter wire, slower speed and wider joint favored the lesser degree of lack of fusion.

Replicate samples did not show a close duplication with respect to lack of fusion as they did with respect to toughness, porosity and cracking. Because of the poor duplication, less certainty can be placed on conclusions regarding lack of fusion than on any of the other factors.

### Cracking

Figure 18 is a scatter plot for weld cracking. The most important factors are alloy and process. The 5 Ni exhibits a much shorter average crack length than the 9 Ni and 12 Ni. The 9 Ni exhibits a slightly shorter average crack length than the 12 Ni. Other factors affecting the cracking are: heat, joint and speed. The higher heat, wider joint and slower speeds promote less cracking. The GTA process appears to exhibit the best quality.

### Toughness

Figure 19 is an abbreviated scatter plot for weld toughness showing only the more important variables. Differences which appear apparent between processes are a result of confounding between the processes and gases. Detailed examination revealed the shielding gases to be the primary factors and in particular the O<sub>2</sub> and CO<sub>2</sub> are the ingredients reducing the toughness.

A detailed description as to how the multiple balance data can be analyzed is contained in Reference 4. A brief description follows:

Once the scatter plot is drawn, a visual check shows which factor or factors are most important. The means of each column of the most important factor are determined and the differences subtracted out, e.g., the mean toughness of 5 Ni is 168+, for 9 Ni 125 and for 12 Ni 120. Consequently, every sample of 5 Ni is adjusted by adding -43 and every sample of 12 Ni is adjusted by adding +5. After the adjustment is made, the data is again plotted and again checked for main effects. Gas and filler wire are then found to be important. After these three factors are corrected, the original scatter of 130 KSI is reduced to 65, allowing analysis of the other variables.

The analysis of the multiple balance plans was carried only so far as to insure proper selection of an alloy to be carried into the factorial optimization plan wherein only one alloy will receive process optimization. This alloy selection has been made although the two alloys 9Ni and 12 Ni are nearly equal in all respects. A detailed comparison between alloys is contained in Figures 20 through 22. These bar charts serve to show the similarities and differences of the three alloys investigated to the exclusion of the other factors and summarize the data previously presented by the scatter plots.

Figure 20 compares the alloy and welding process in terms of porosity and lack of fusion. The superiority of the 12 Ni is the result of its increased fluidity with respect to the other two alloys. The 5 Ni has the least porosity because it is the only one of the three alloys with sufficient scavengers Mn and Si to be effective in GMA welding.

The GTA process offers a much greater latitude of useful welding conditions; consequently better overall weld quality was attained. The extra instability added to the GMA process by the cold wire addition caused the GMA (HD) process

to have the highest porosity level of the three processes. The reason is partly due to operation in non-ideal ranges.

Figure 21 compares the average crack length for each alloy and process by X-ray inspection. The obvious superiority of 5 Ni is apparent. The low average crack length in the GTA process is partly attributable to the low metal build-up per pass. All GTA panels of 9 Ni and 12 Ni had cracks in the root passes but subsequent passes were able to either melt them out or close the cracks so tightly as to be undetectable by X-ray. The degree of excess penetration was less in the GMA processes so fewer cracks were healed. The addition of a second filler supply to the weld puddle in the GMA (HD) process supplies a sufficient amount of strength to the hot weld to cause a substantial reduction in cracking.

The cracking frequency as determined by unaided visual inspection shows the relative crack susceptibility of the three alloys under normal welding conditions rather than by an artificial "bead-on-plate" test. The 5 Ni is far less susceptible to cracking, the 12 Ni is most susceptible to cracking and the 9 Ni has an intermediate susceptibility.

Figure 22 compares the alloys and processes in terms of weld toughness. Very little difference is noted between the 9 Ni and 12 Ni but the 5 Ni is significantly toughest. The low toughness of the 12 Ni in the GMA (HD) process is due to a confounding of process and shielding gas. No significant difference in toughness was noted between the GMA and GMA (HD) processes. The GTA process did produce tougher welds by a small margin but most of the apparent differences are due to the effect of the shielding gases. Oxygen and CO<sub>2</sub> are detrimental to the weld toughness.

Table XIX illustrates the weld toughness in a matrix of the more important variables. Replicate results are indicated by toughness numbers connected with a hyphen. The excellent reproducibility is indicative that all significant variables have been considered. The specimen size was too small for the 5 Ni to ensure elastic fracture; therefore, all the numbers followed by a + are conservative. One sample was a single edge notch configuration which is capable of measuring higher toughnesses for a given specimen cross-section than the surface notch configuration. This specimen recorded a  $K_{IC}$  of 203 KSI  $\sqrt{IN}$  with general yielding so the value is conservative.

The one 12 Ni  $K_{IC}$  value of 101 KSI  $\sqrt{IN}$  is felt to be unconservative because of a weld defect located laterally from the fatigue crack.

Table XX lists typical welding rates employed in the Multiple Balance Study. The conditions selected for listing in this table were selected at random; no particular pattern was followed.

Table XXI lists the factors which were found to be important and the direction in which they affected the four criteria: porosity, lack of fusion, crack susceptibility and fracture toughness.

## 2. Material Selection

The weld data generated from the 623A materials tests and the alternate material tests have been compiled in Table XXII in a manner which reflects the philosophies expressed earlier in the background discussion and, by using consistent design factors, in a manner allowing direct comparisons.

For yield strengths noted shell gages are shown for 260 and 156 inch cases operating at fixed design factors. Critical flaw sizes at proof for each of the cases are also calculated using the same design factors. By comparing

the critical flaw size\* with the design thicknesses, an estimate of failure mode can be made. It is seen that only the 5 Ni alloy approaches a "leak-before-failure" mode in the 260 inch case. Also, the 5 Ni, 9 Ni, and 12 Ni alloys approach this condition in the 156 inch case.

It was noted earlier that insufficient systems data is available to suggest the use of 5 Ni in the smaller cases. Since present Air Force interest lies primarily in the smaller boosters 5 Ni has been dropped from further study in this program.

Though from a case performance standpoint (i.e., strength and toughness) both the 9 Ni and 12 Ni alloys appear worthy of additional investigation program funds require elimination of one of them. The overall difference in behavioral characteristics that were observed in this program were minor. At this time it is not possible to make an irrevocable choice. Final choice of the 9 Ni alloy was based on the observation that the alloy was slightly less susceptible to weld cracking.

\* Note that flaw sizes are noted in terms of  $(a/Q)$ , and by assuming unfavorable flaw shape ( $Q = 1$ ), surface flaw depth in inches is equal to  $(a/Q)$ .

## V. CONCLUSIONS

1. From the test results of panels produced by 623A contractors, minimum  $K_{IC}$  values for 18 Ni (200) GTA, 18 Ni (250) - Submerged Arc, and 18 Ni (250) GTA weldments are believed to be 110, 55, and 60 KSI  $\sqrt{\text{in}}$ , respectively. When considering primary design stresses only, these values yield allowable flaw sizes,  $(a/Q)_I$ , in the order of .14, .02, and .05 respectively.
2. Analyses of the effects of weldment mismatch in bulkheads indicate that allowable flaw sizes can be reduced by as much as fifty percent as a result of drawing tolerance deviations.
3. Residual stresses and subcritical flaw growth do not appear to be significant problems for the expected service requirements of the existing 623A case materials and processes.
4. The 5 Ni quench and temper steel shows extremely attractive properties and processing characteristics for 260 inch case application. Its usefulness on smaller first stage cases has not been assessed from a vehicle economics standpoint.
5. Both the 9 Ni and 12 Ni alloys show promise for use on the 156-inch cases.



## REFERENCES

1. Masters, J. N., "Booster Case Materials Evaluation," Fourth Maraging Steel Project Review, ML-TDR-64-225, Vol. 1, July 1964, p. 226.
2. ASTM Committee on FTESMM, "Progress in the Measurement of Fracture Toughness and Using Fracture Mechanics," Materials Research and Standards, Vol. 4, No. 3, March 1964
3. Bolstad, D. A., Davis, R. A., Quist, W. E., and Roberts, E. C., "Measuring Stress in Steel Parts by X-ray Diffraction," Metal Progress, 88, July, 1963.
4. "Reliability: Management, Methods, and Mathematics", Book, p. 389, D. K. Lloyd and M. Lipow, Prentiss-Hall, 1964

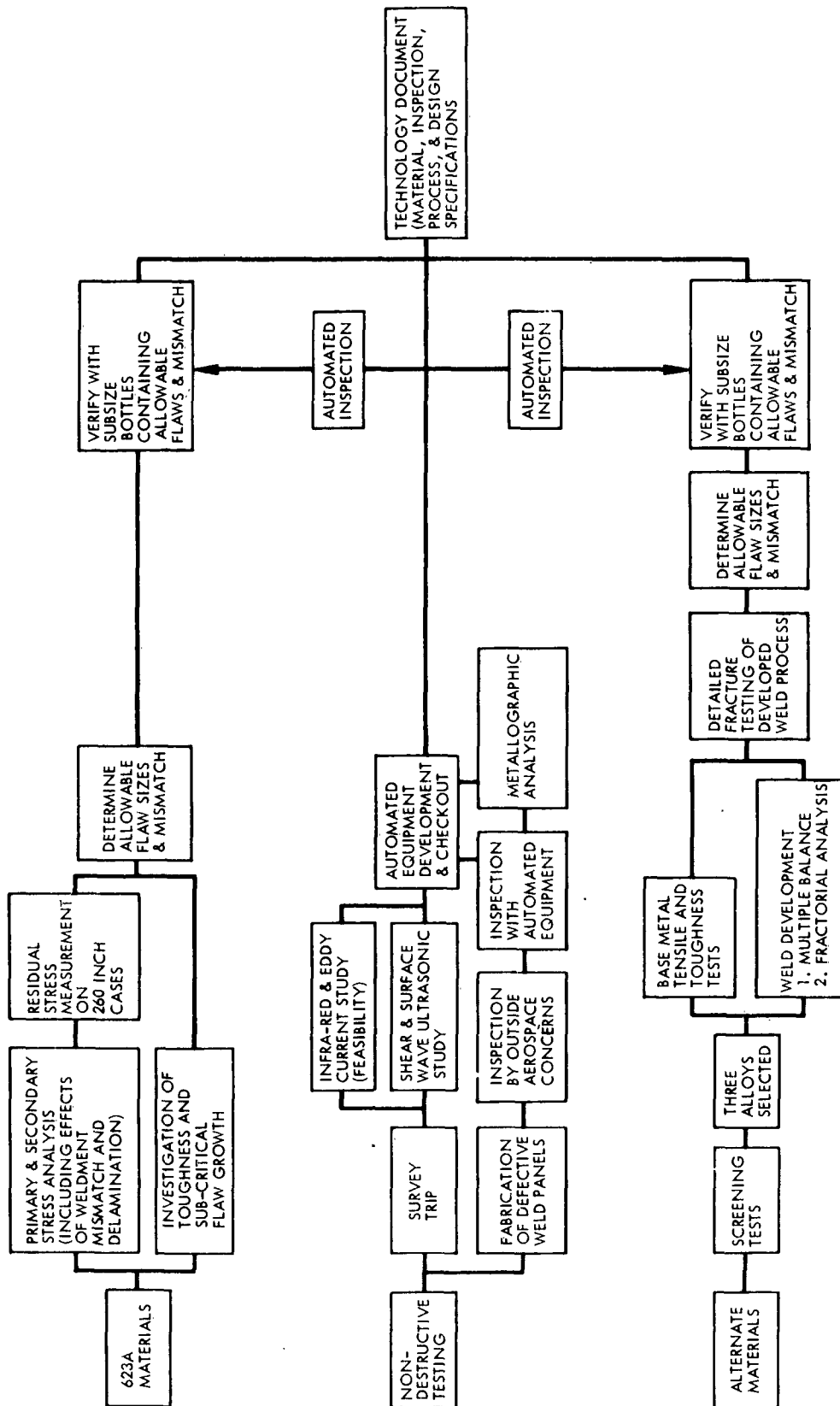


Figure 1: Program Summary Chart

FIGURE 2:  
PARENT METAL  
FRACTURE TOUGHNESS DATA

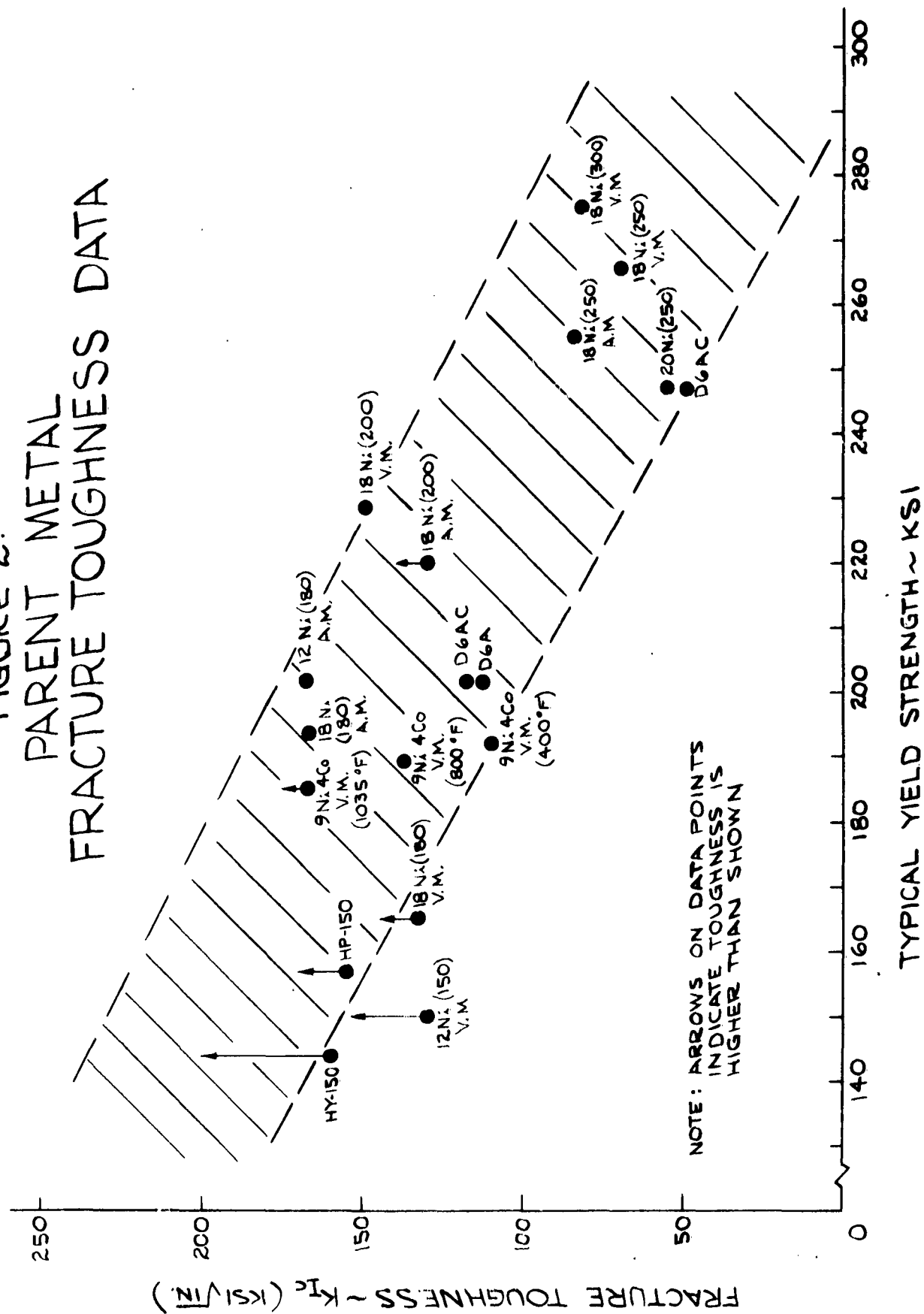
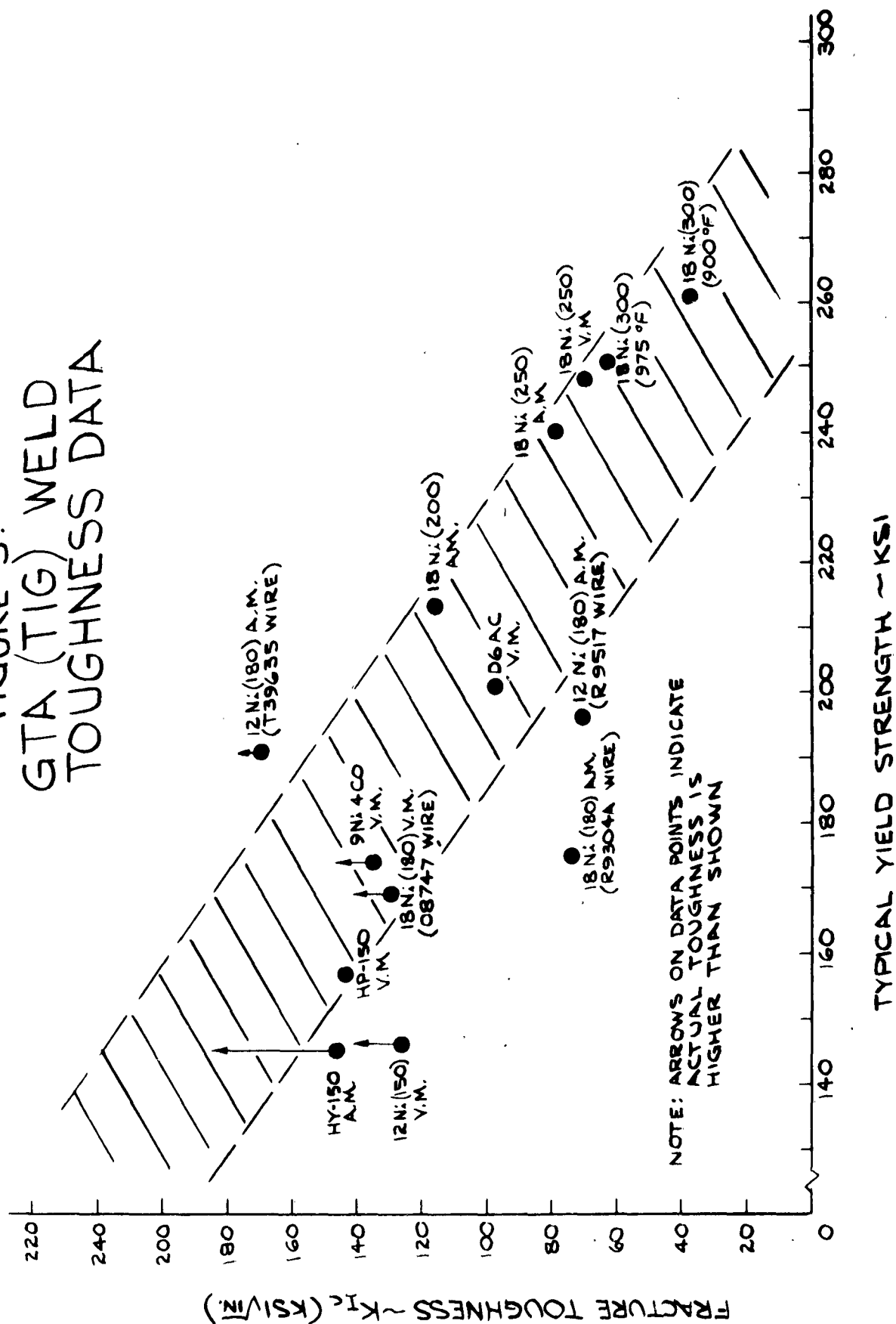


FIGURE 3:  
GTA (TIG) WELD  
TOUGHNESS DATA



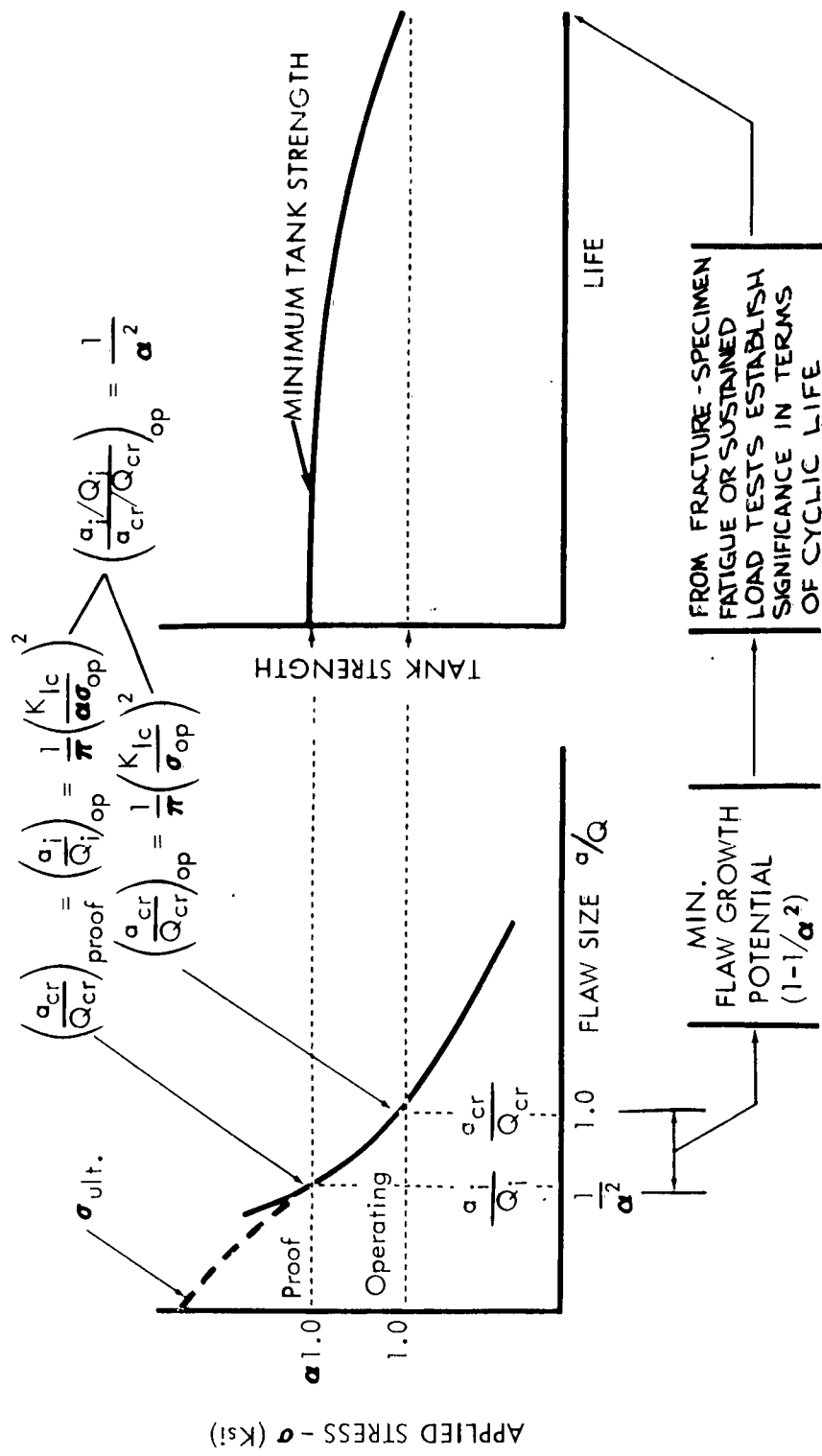


Figure 4: SIGNIFICANCE OF PROOF TESTING IN ESTIMATION OF MINIMUM TANK LIFE

FIGURE 5:  
FAILURE MODE PREDICTION  
260" DIA CASE

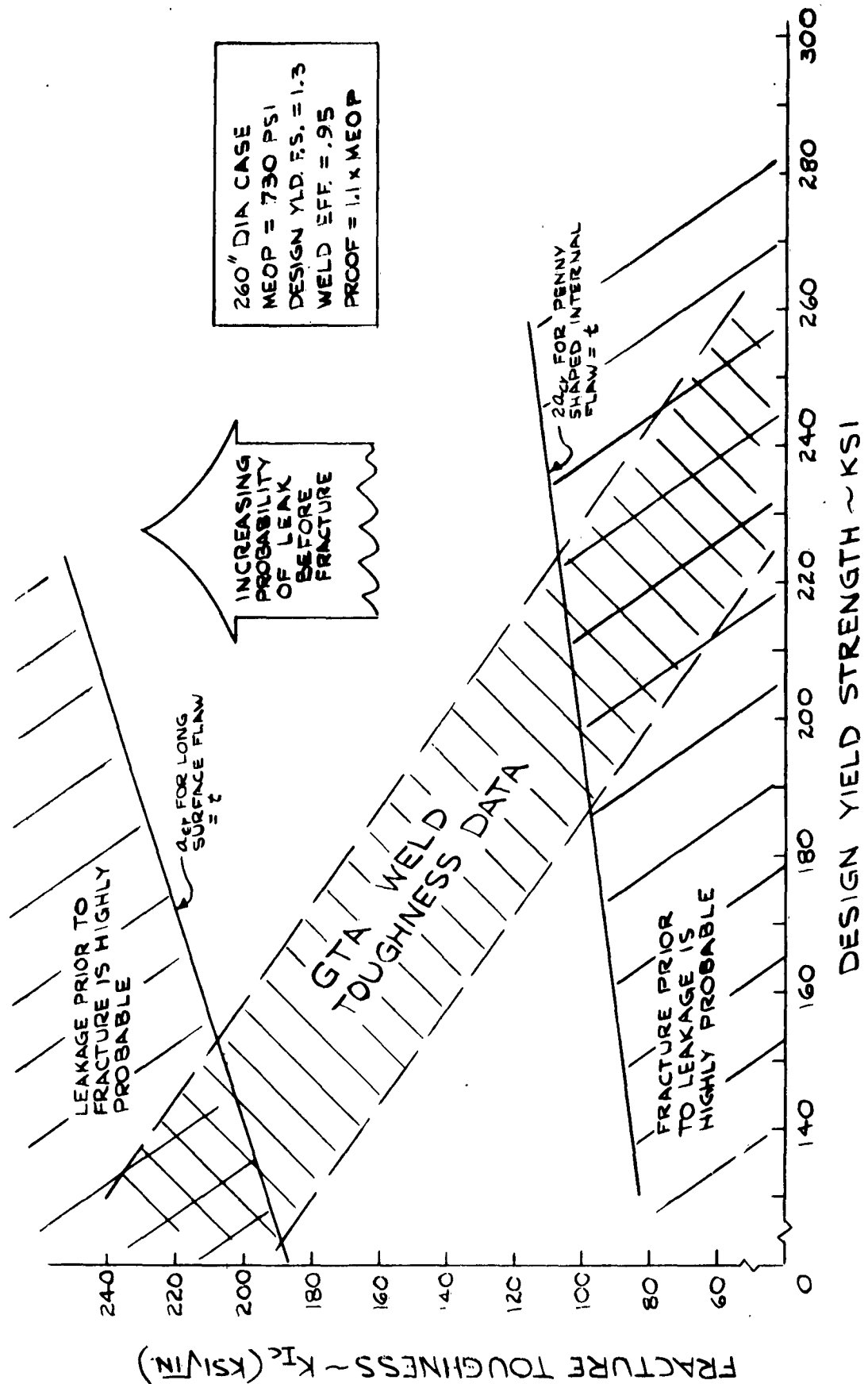


FIGURE 6:  
FAILURE MODE PREDICTION  
156" DIA CASE

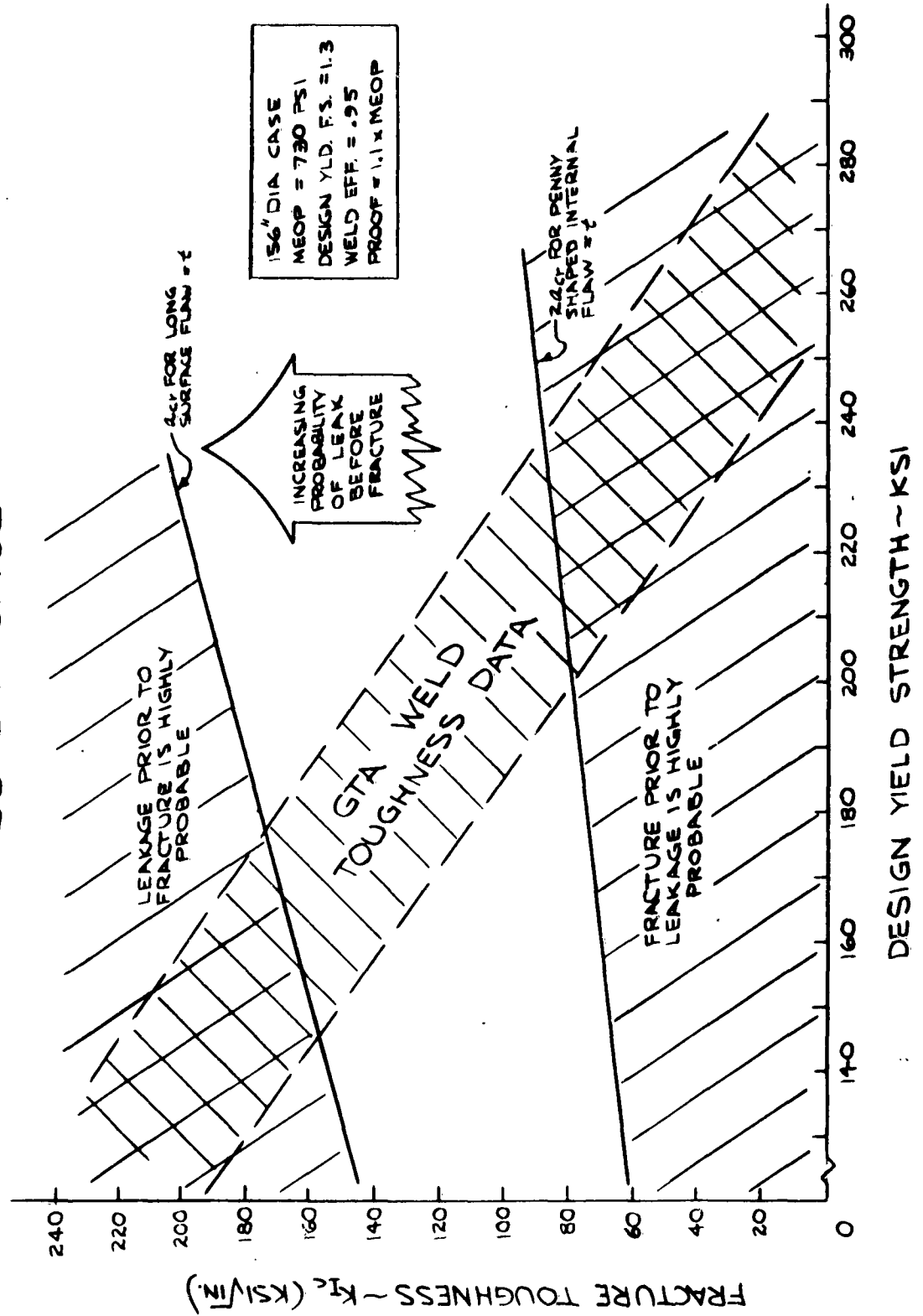


FIGURE 7:  
SUSTAINED LOAD TESTS  
18 Ni (200) GTA

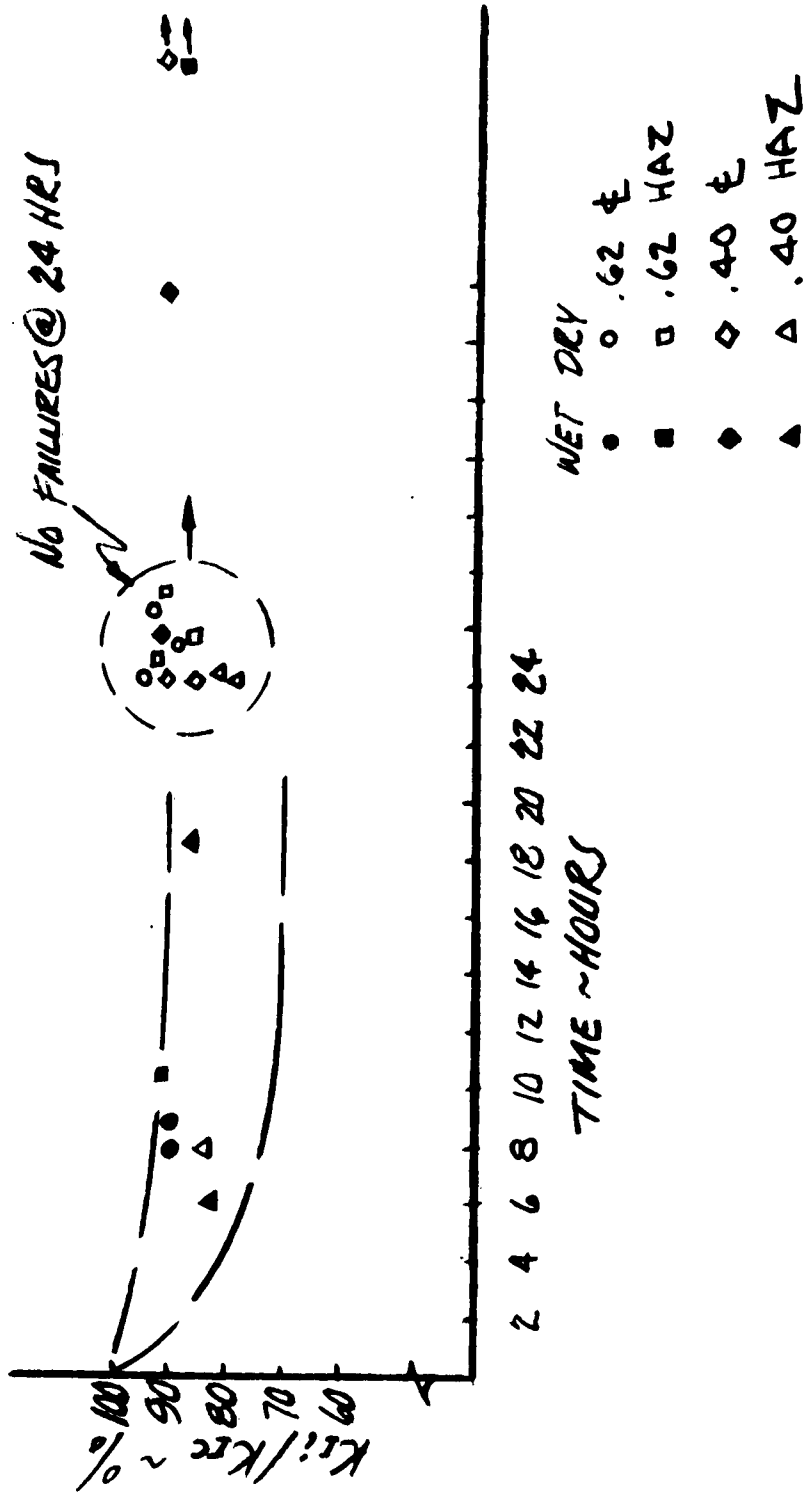
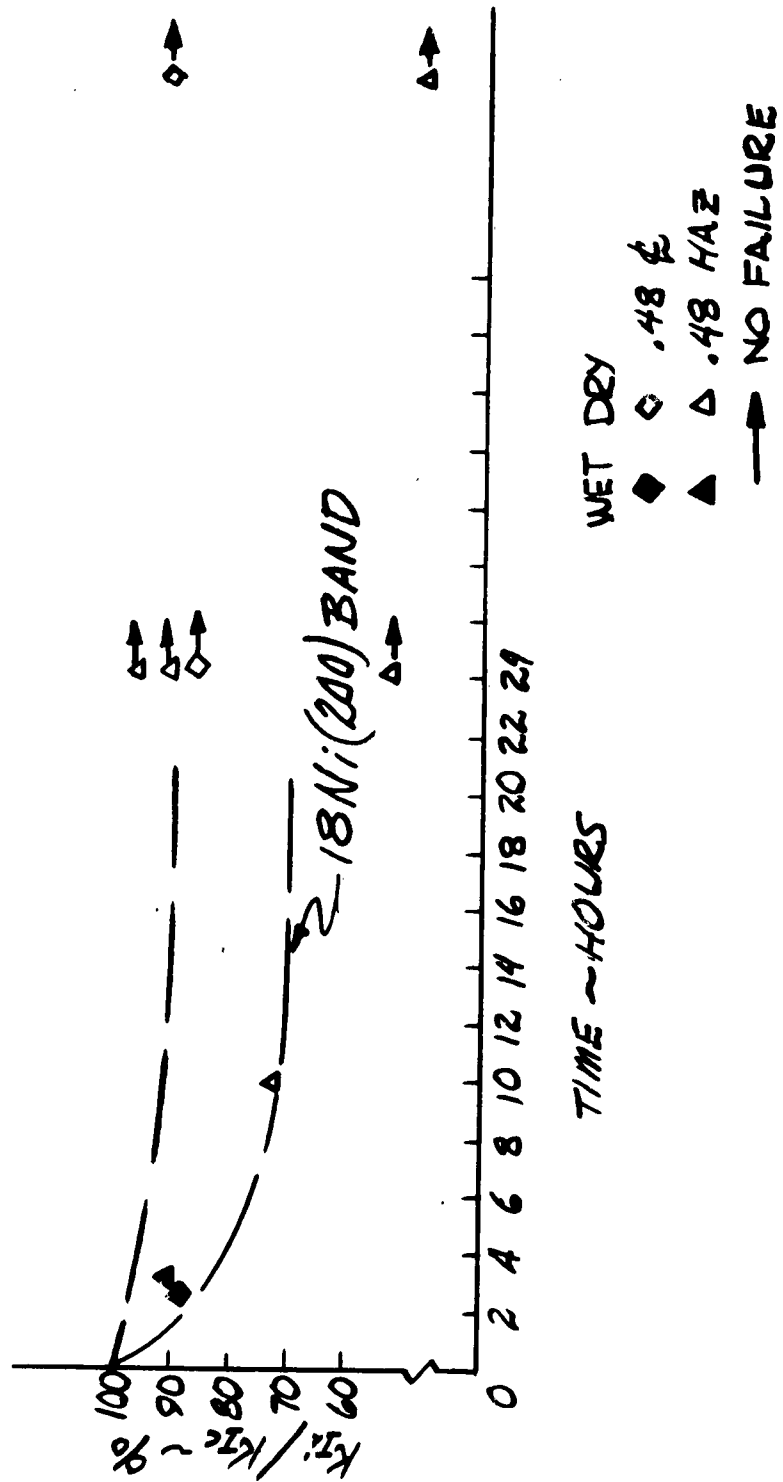




FIGURE 8:  
SUSTAINED LOAD TESTS  
18Ni(250) SUB-ARC



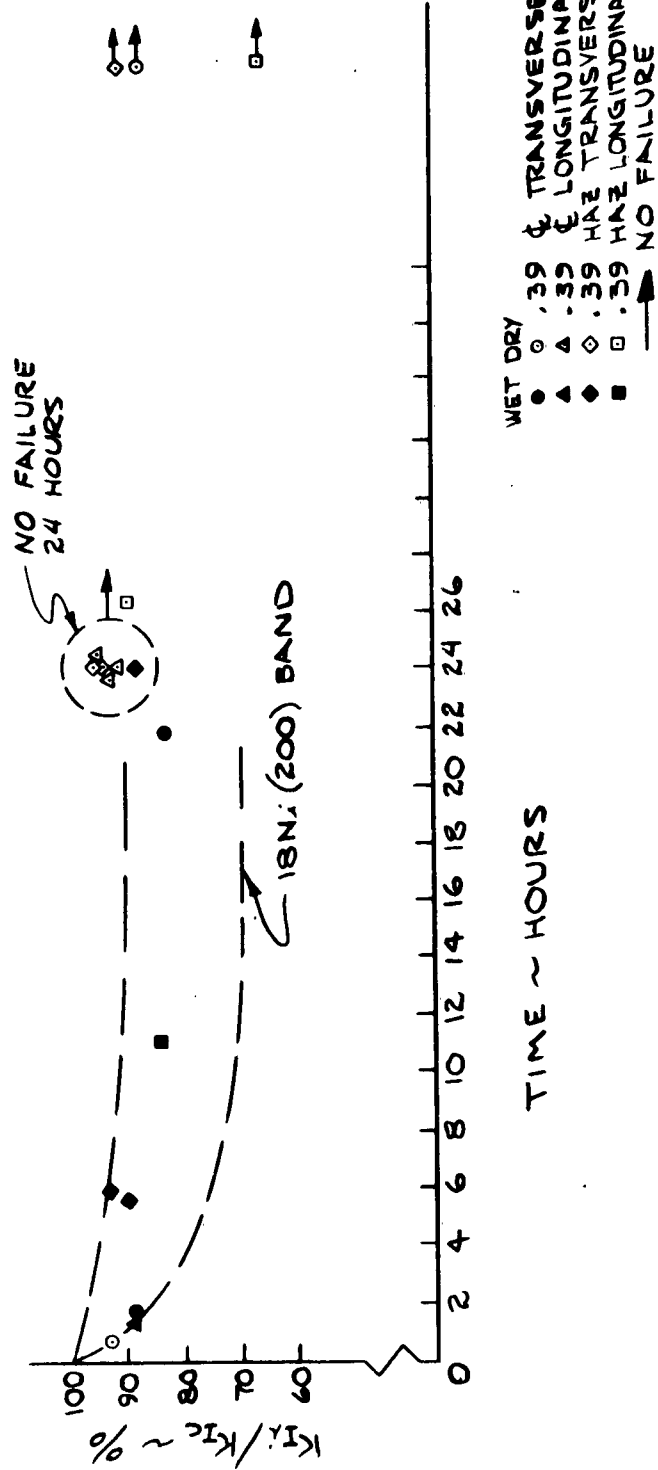


FIGURE 9:  
SUSTAINED LOAD TESTS  
18Ni(250) GTA WELDS

# FIGURE 10 RESIDUAL STRESSES

260" SUN CASE

STRESS ~ KSI	
OUT	IN
Φ	-30 -50
HAZ	-10 -40
B.M.	-10 -40

260" NEWPORT CASE

STRESS ~ KSI	
OUT	IN
Φ	-30 -40
HAZ	-50 -60
B.M.	-60 -30

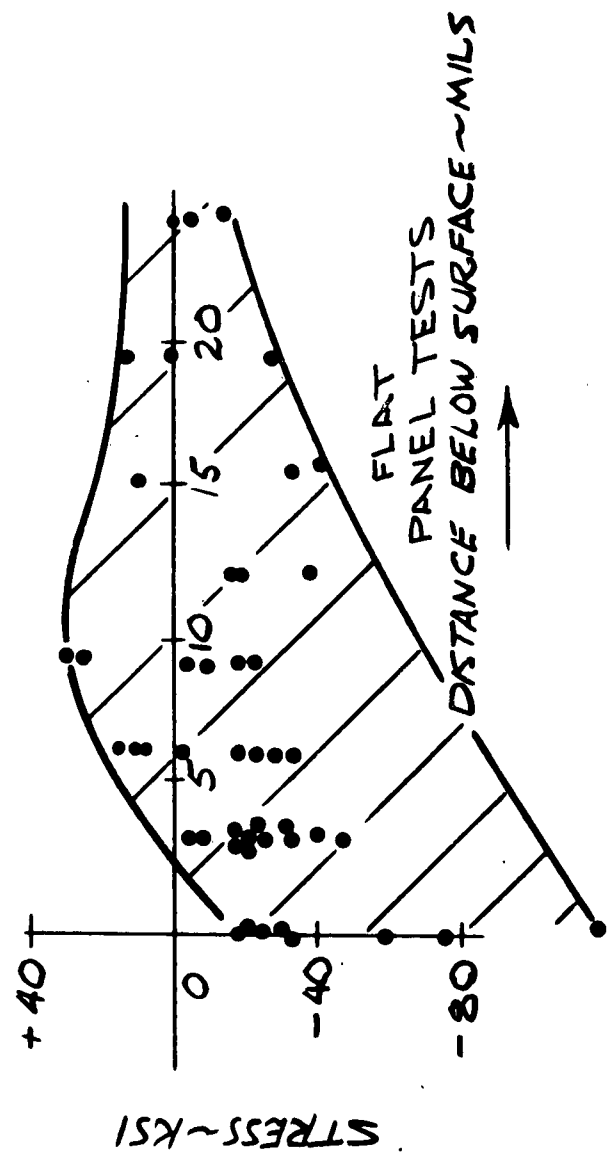
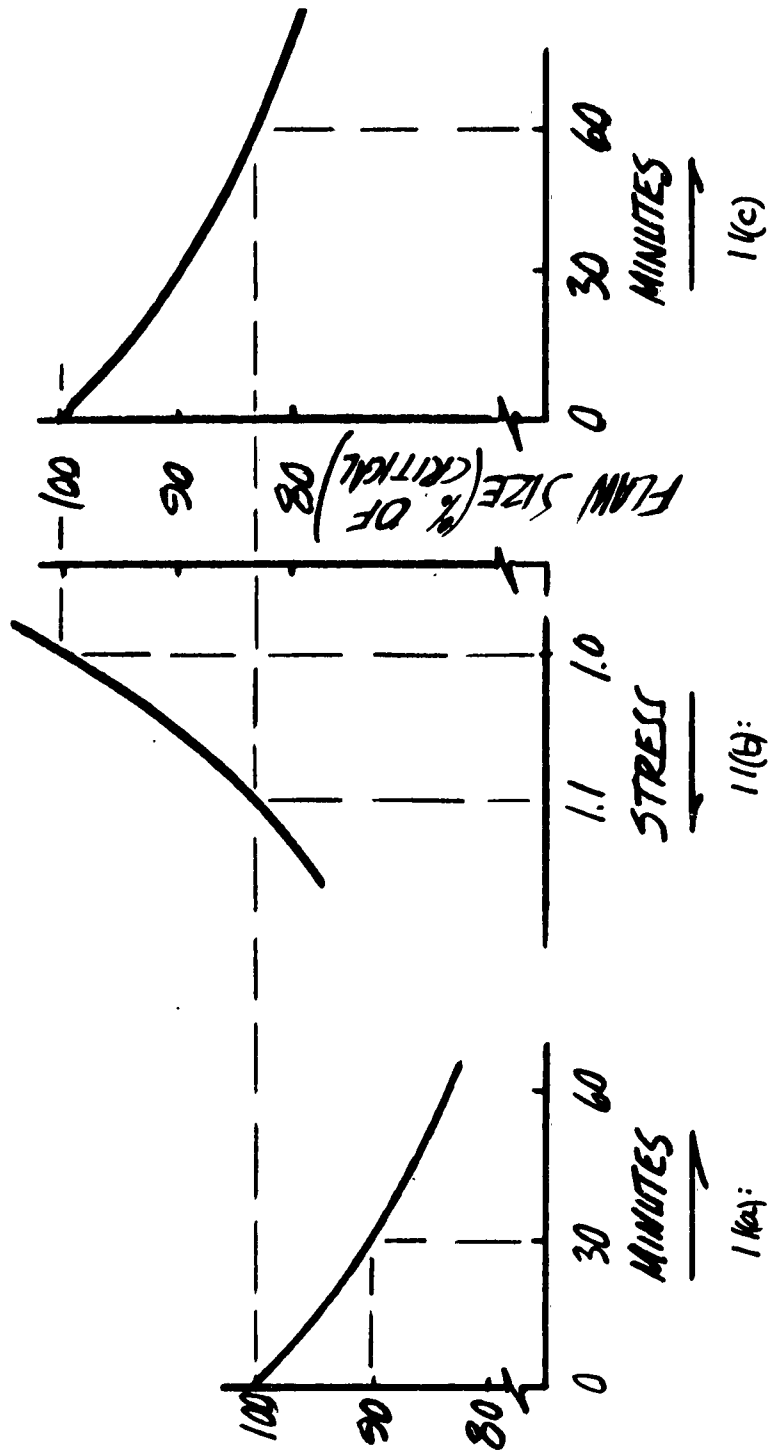
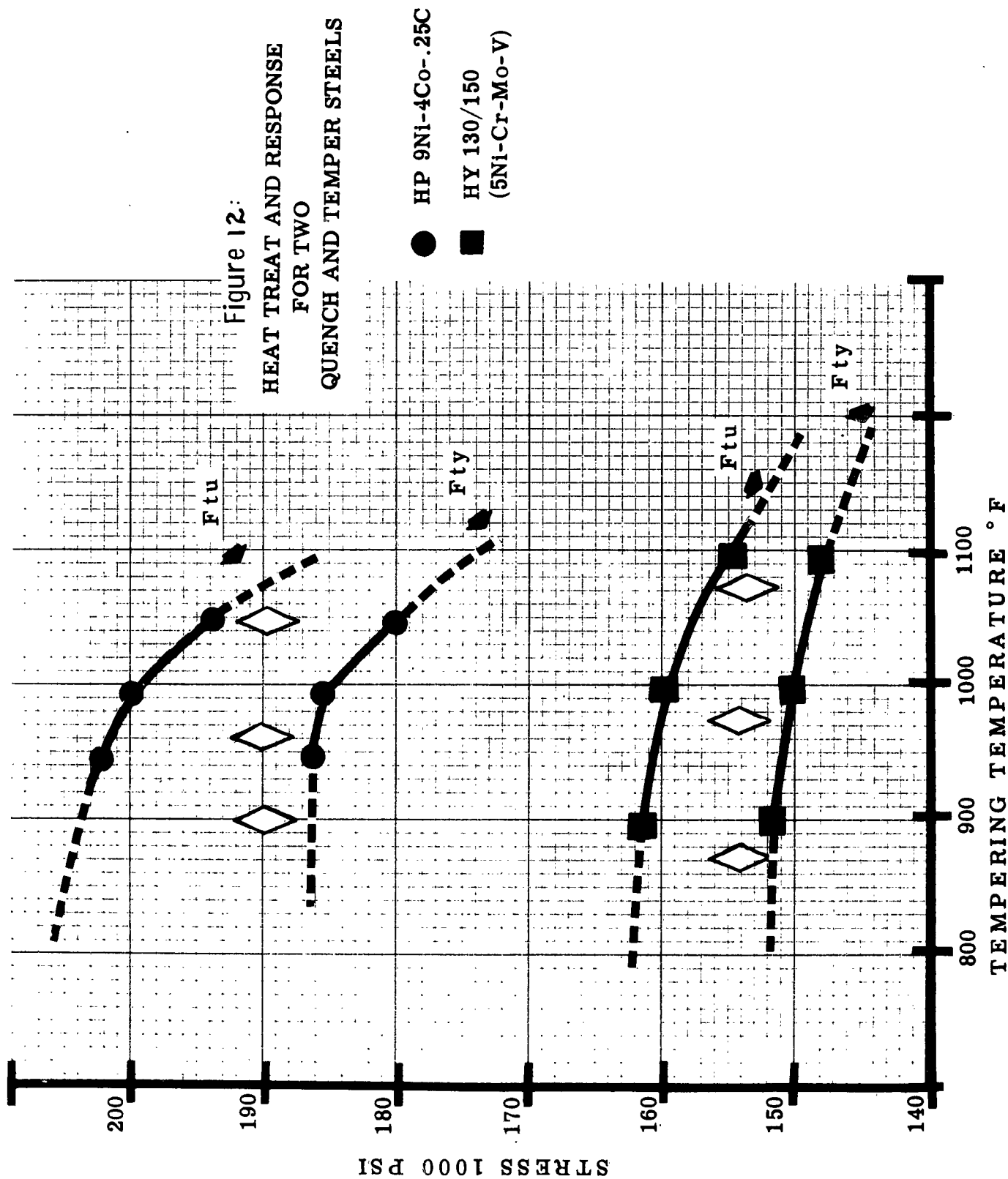


FIGURE 11:  
SUBCRITICAL FLAW GROWTH



$$\therefore \left( \frac{\sigma}{\sigma_c} \right)_{\text{allowable}} = 90 \times 10^{-6} = \text{load } @ \left( \frac{\sigma}{\sigma_c} \right)_{\text{at proof}}$$



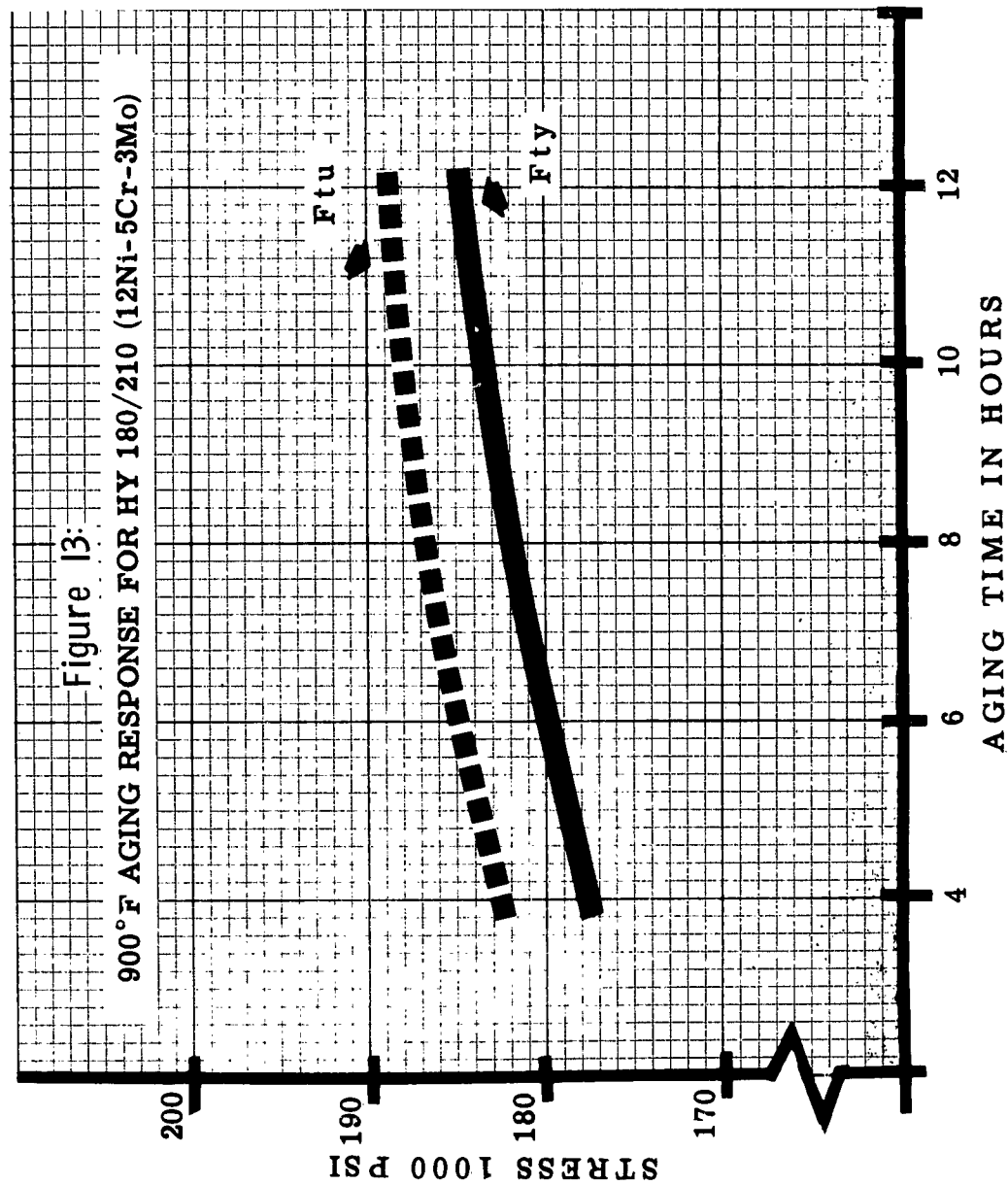


Figure 14: EFFECT OF POST WELD HEAT TREATMENTS ON  
HARDNESS OF 9Ni - 4Co - .25C WELDMENTS

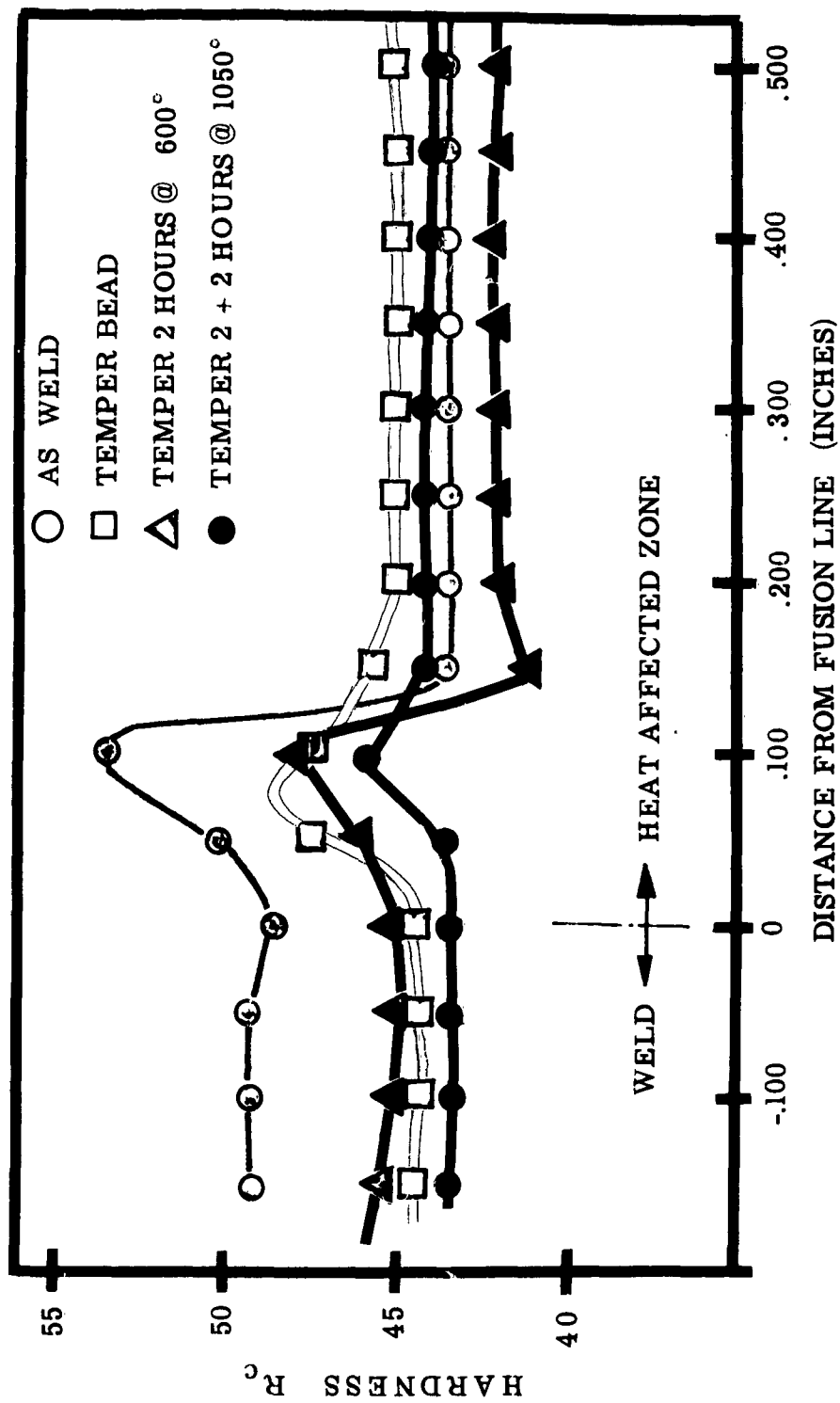
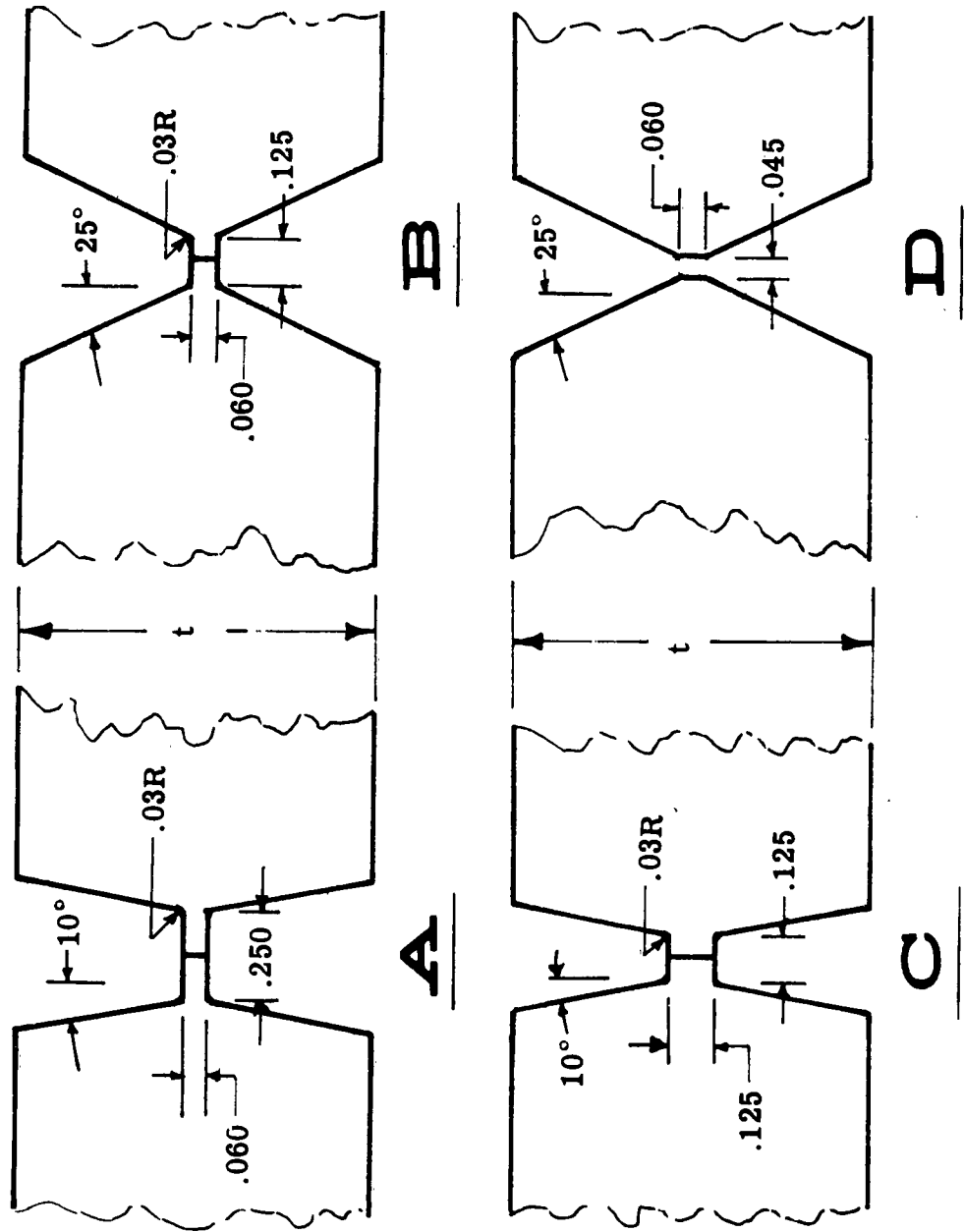
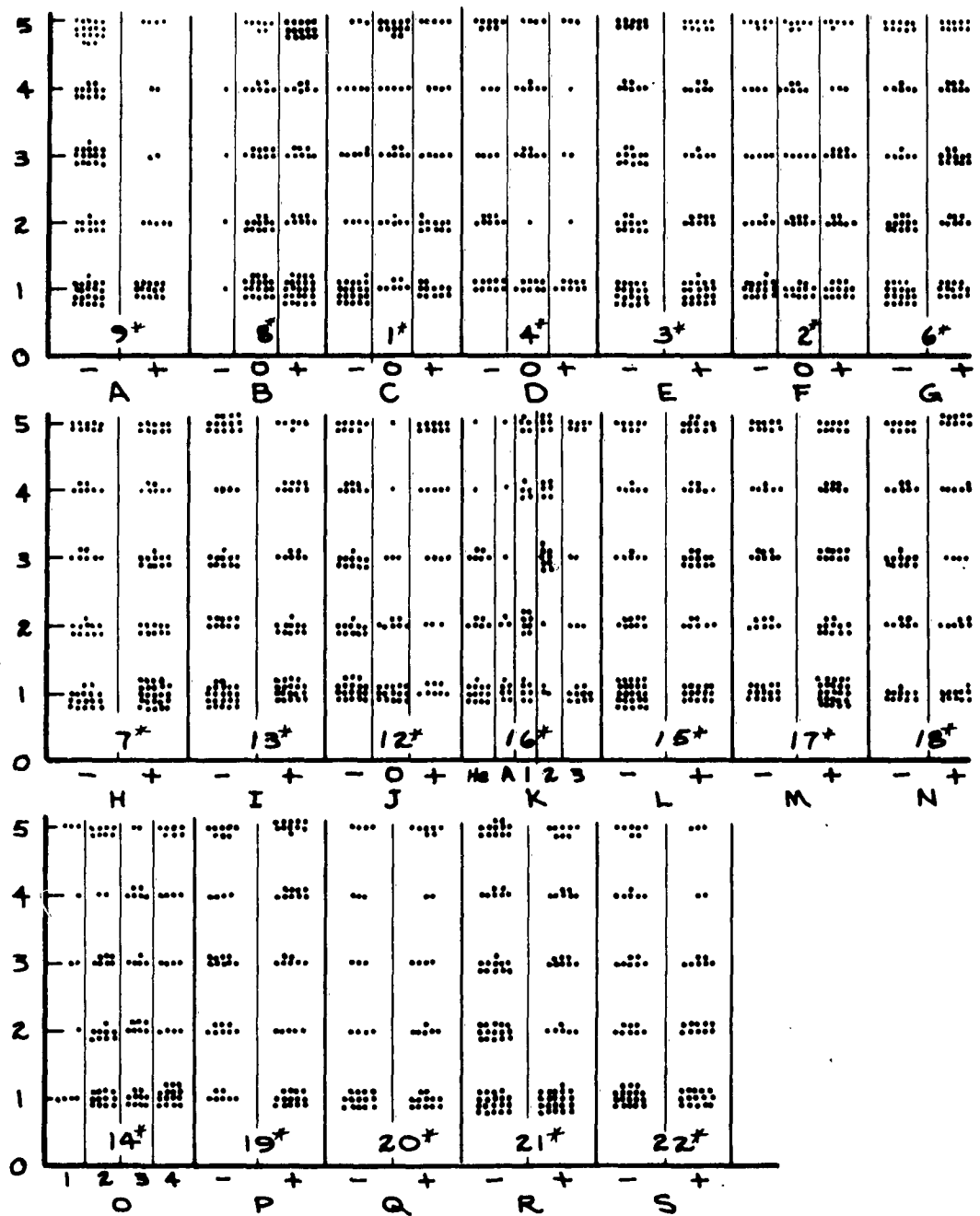


Figure 15:  
WELD EDGE CONFIGURATIONS







\* NUMBER CORRESPONDS TO PARTICULAR VARIABLE SHOWN  
IN TABLE XV

FIGURE 16: COMPOSITE POROSITY SCATTER  
DATA

Figure 17:  
LACK OF FUSION SCATTER DATA

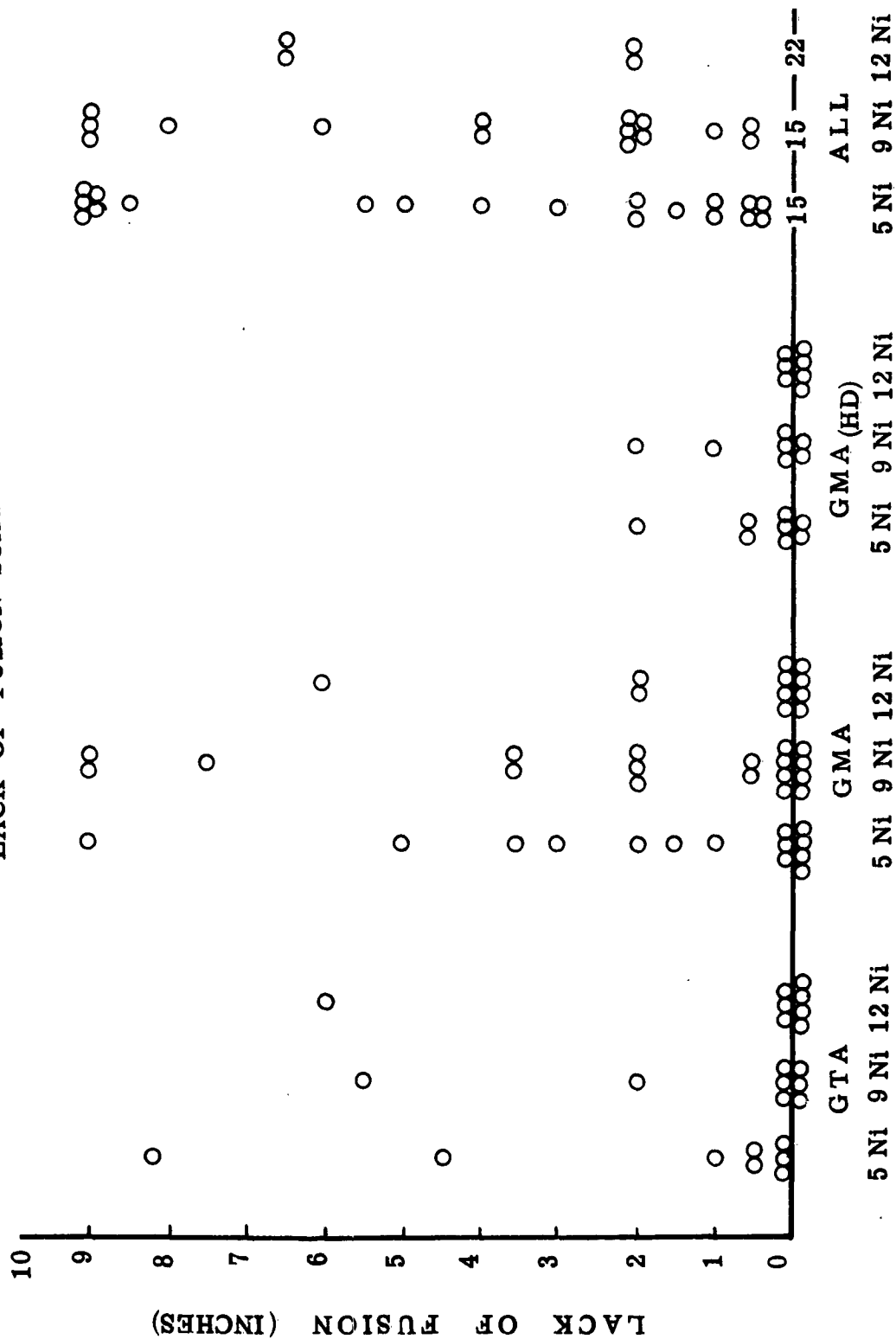


Figure 18:  
WELD CRACKING SCATTER DATA

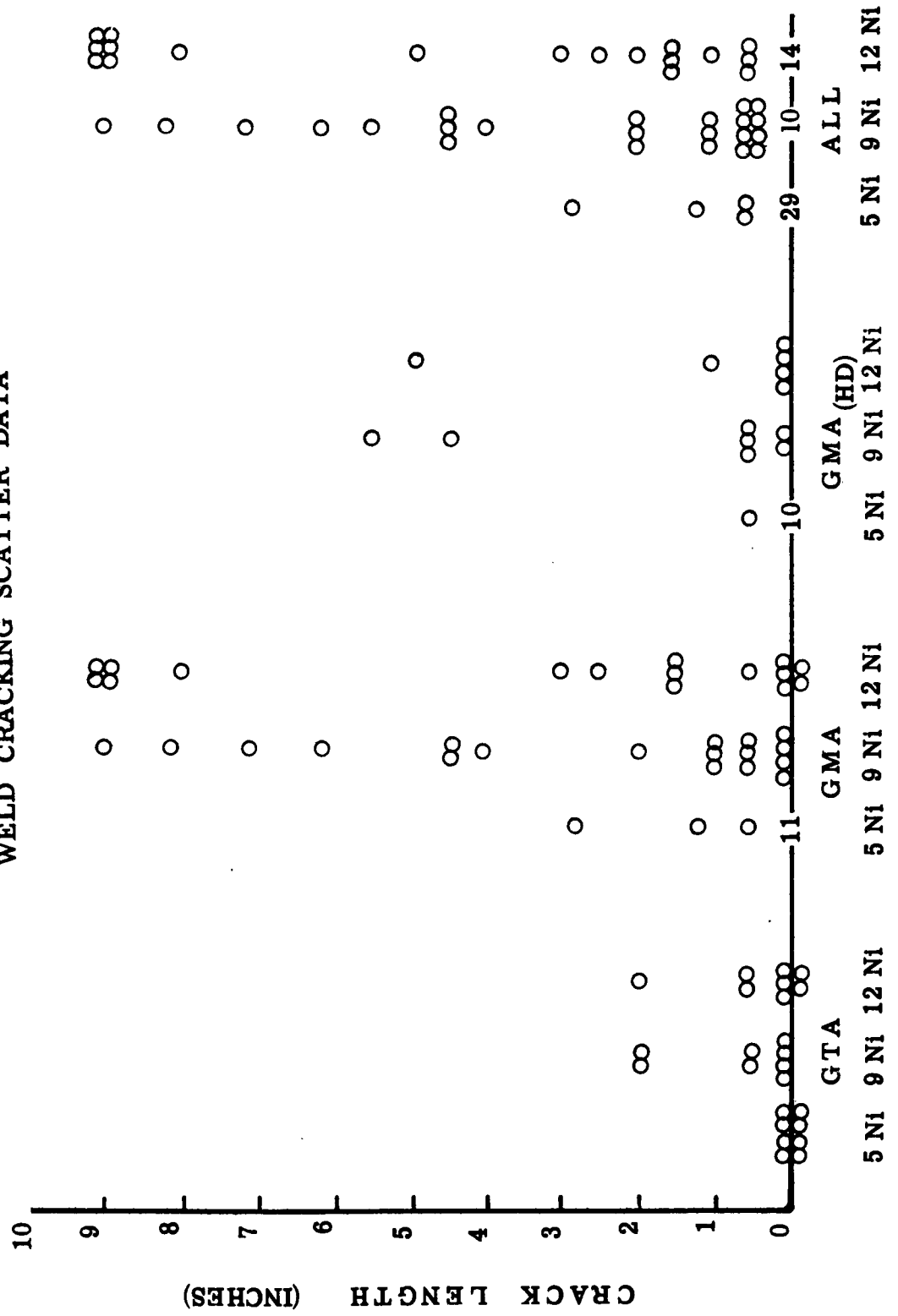


Figure 19:  
WELD TOUGHNESS SCATTER DATA

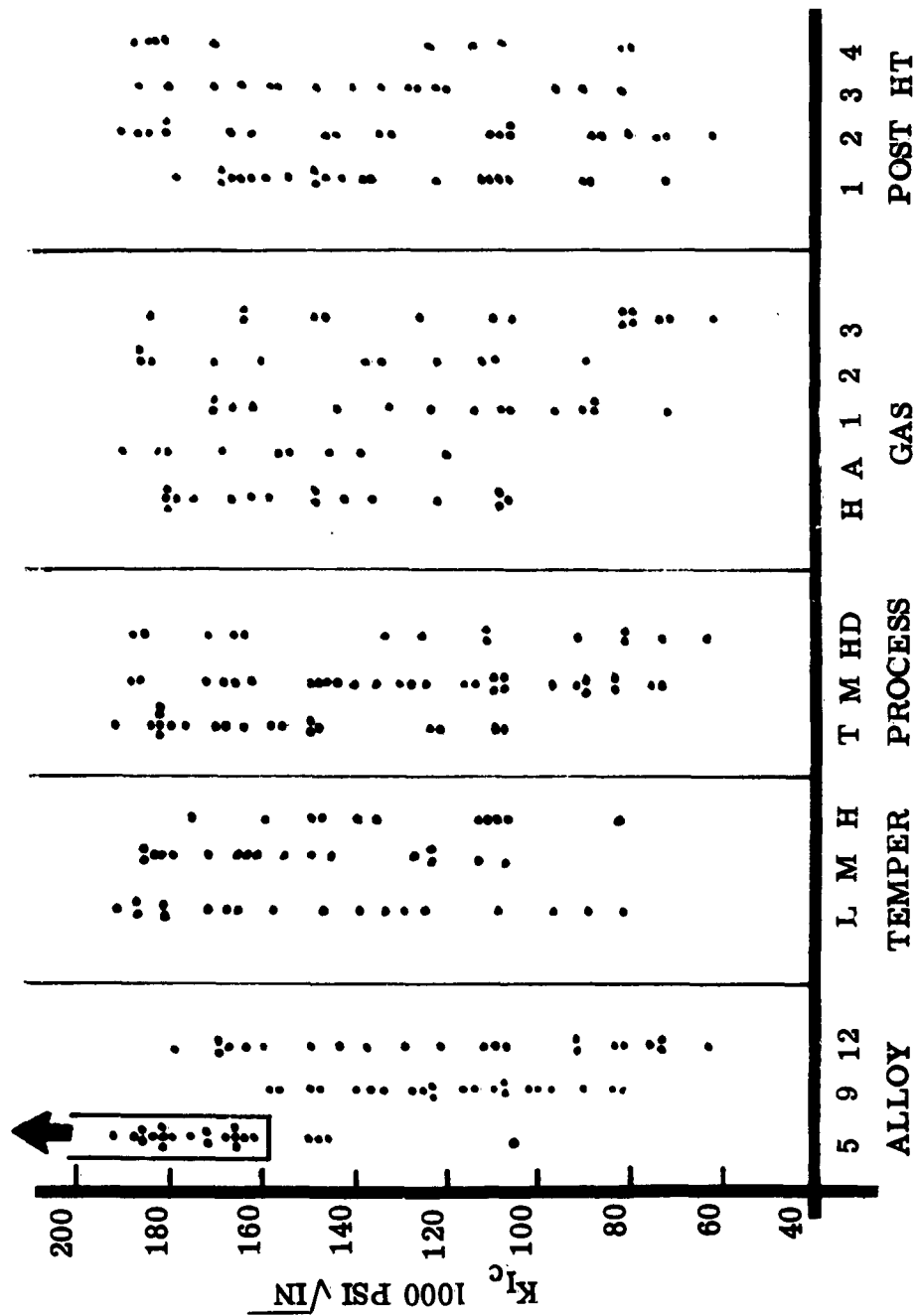


FIGURE 20

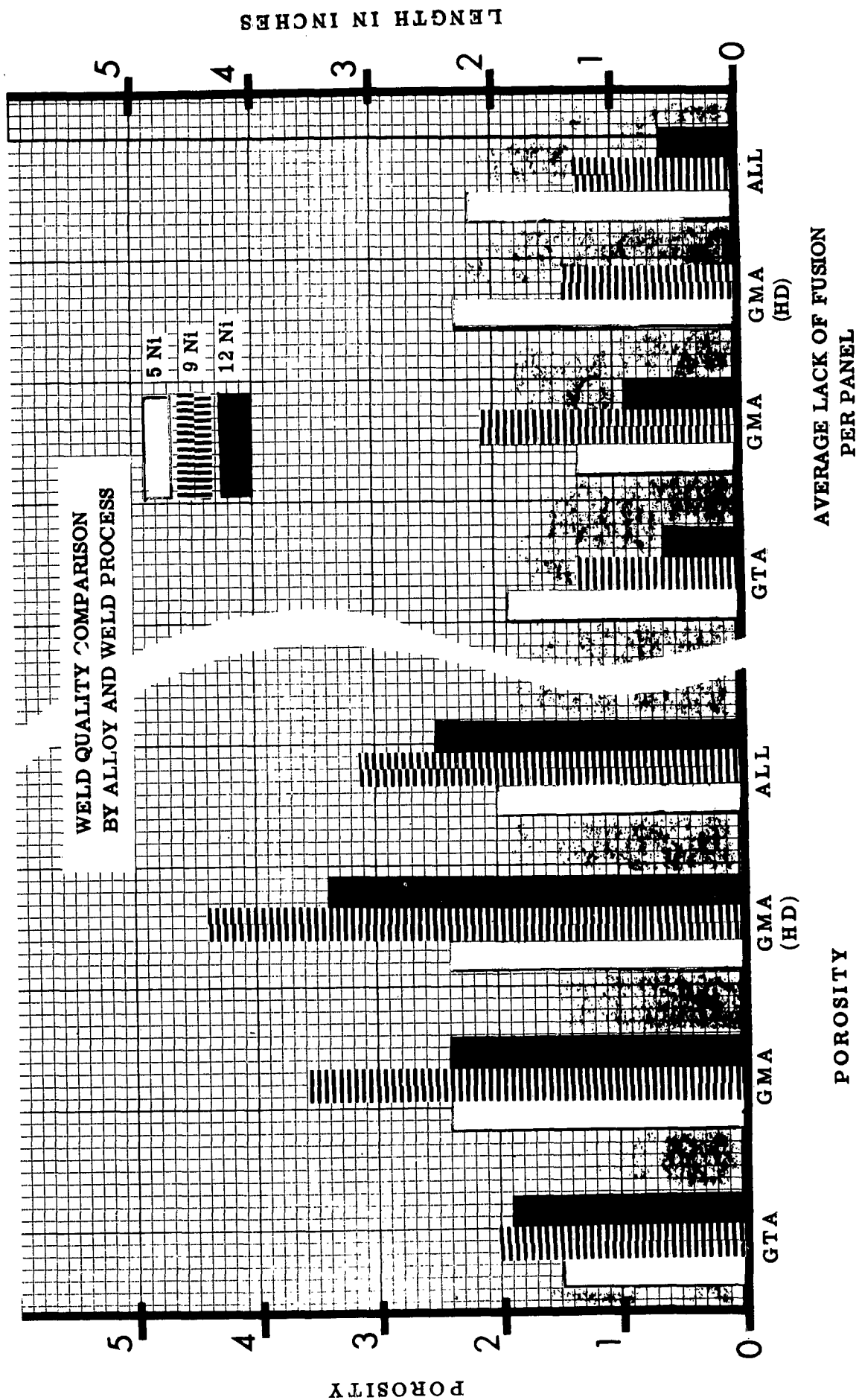
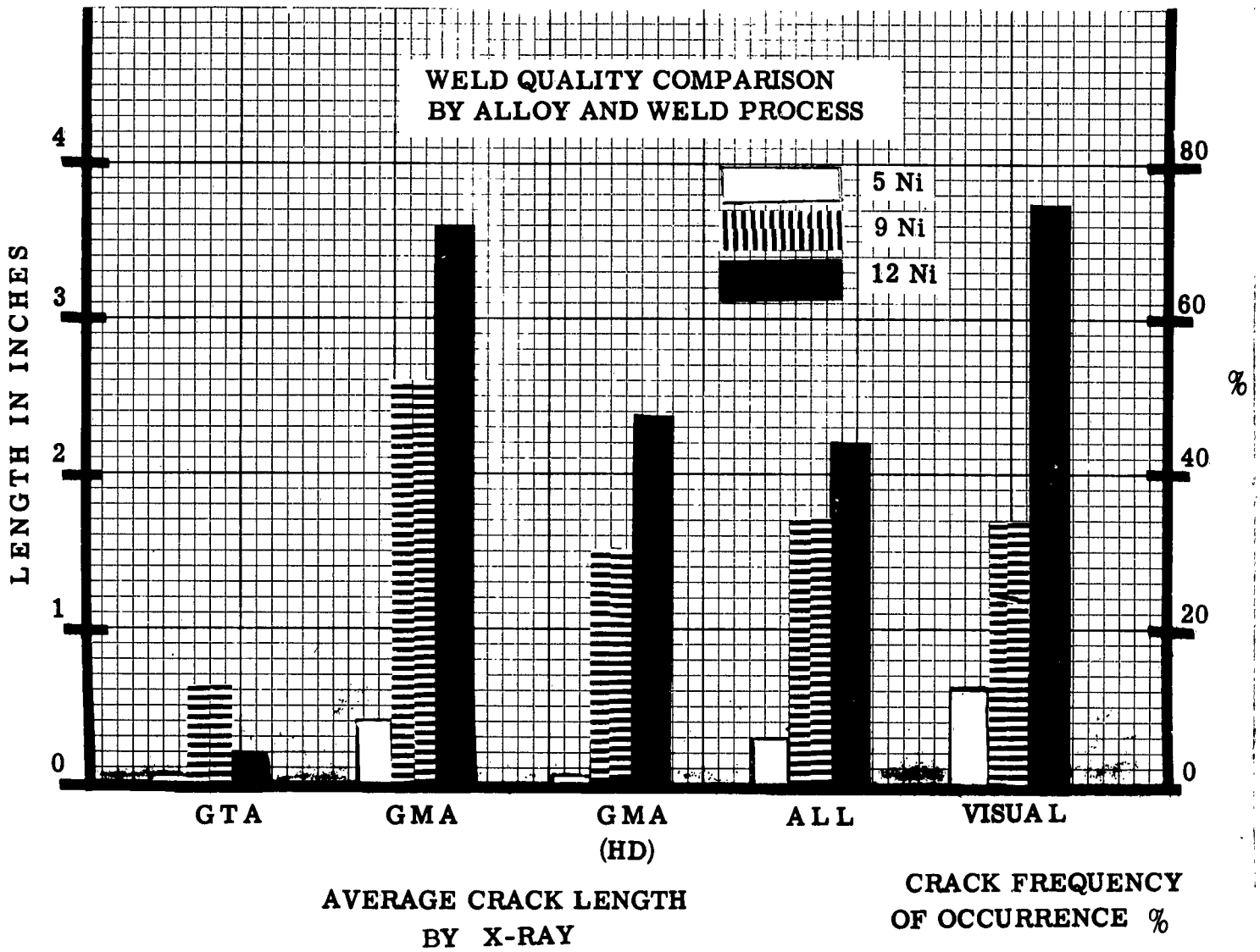
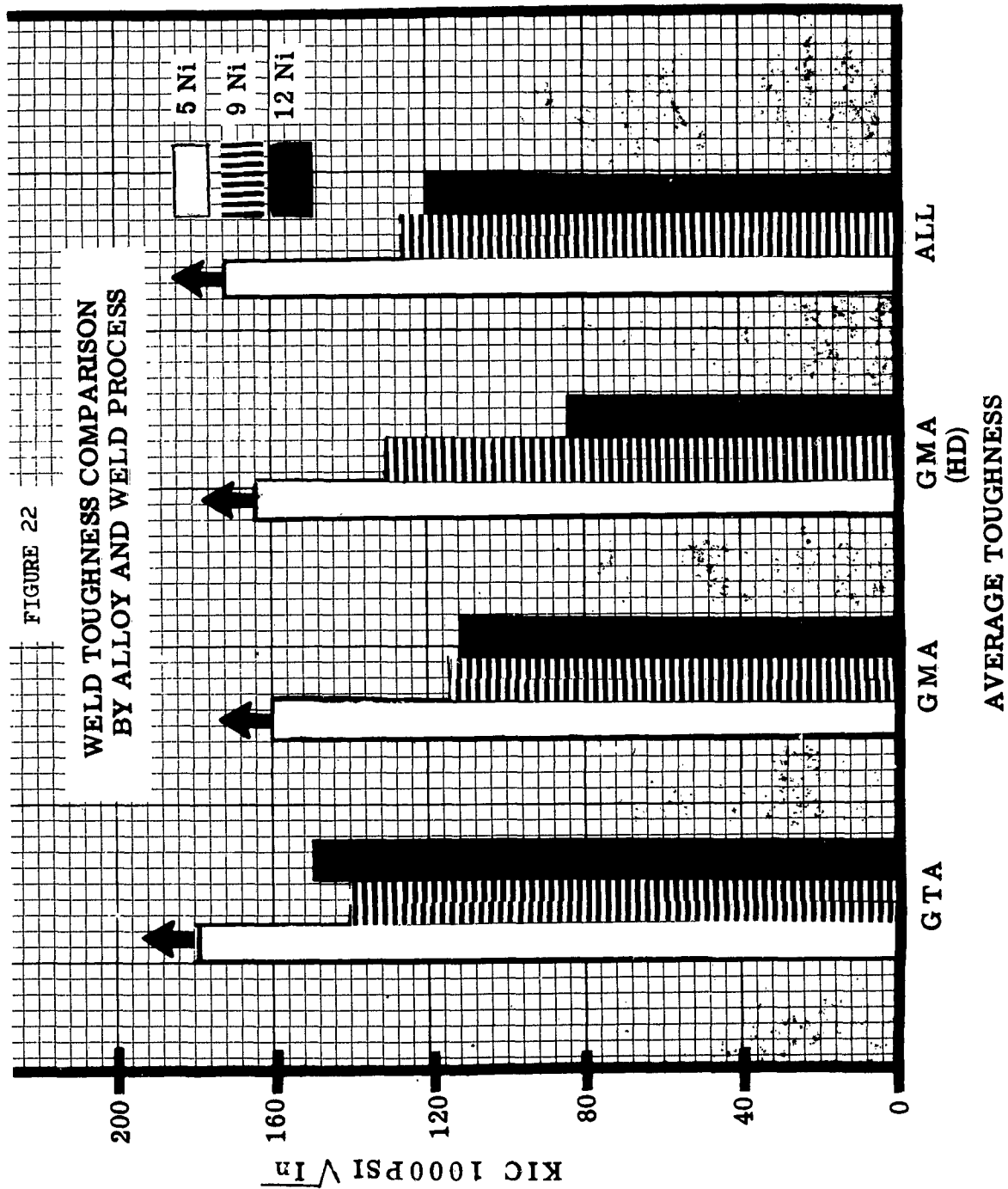


FIGURE 21





**TABLE I**  
**MATERIALS INVESTIGATED**  
**(Boeing Independent Research and**  
**Screening Tests on AF33(615)-1623)**

	<u>Tempered or Aged Condition</u>	<u>Typical Yield Strength KSI</u>
I	<b>QUENCH &amp; TEMPERED STEELS</b>	
	Republic HP-150 (Vac Melt) [3Ni - 1.4 Cr - .9 Mo - .11 Mn - .26 C]	1015 <sup>0</sup> F 157
	USS HY-150 (Air Melt) [5 Ni - .4 Cr - .4 Mo - .25 Mn - .13C]	1125 <sup>0</sup> F 144
	Republic 9 Ni - 4 Co - .20C (Vac Melt) [8.5 Ni - 4 Co - .45 Cr - .4 Mo - .25 Mn - .26C]	400 <sup>0</sup> F 193 800 <sup>0</sup> F 189 1035 <sup>0</sup> F 185
	Ladish D6A (Air Melt)	1015 <sup>0</sup> F 203 1050 <sup>0</sup> F 198 1085 <sup>0</sup> F 196
	Ladish D6AC (Vac. Melt)	1015 <sup>0</sup> F 205 1050 <sup>0</sup> F 203 1085 <sup>0</sup> F 199
II	<b>MARAGING STEELS</b>	
	12 Ni - 5 Cr - 3 Mo (150) (Air Melt)	900 <sup>0</sup> F, 3 Hrs 150
	12 Ni - 5 Cr - 3 Mo (180) (Vac Melt)	900 <sup>0</sup> F, 3 Hrs 202
	18 Ni (180) (Air Melt)	900 <sup>0</sup> F, 3 Hrs 193
	18 Ni (180) (Vac Melt)	900 <sup>0</sup> F, 3 Hrs 162 900 <sup>0</sup> F, 6 Hrs 169
	18 Ni (200) (Air Melt)	900 <sup>0</sup> F, 3 Hrs 220
	18 Ni (200) (Vac Melt)	900 <sup>0</sup> F, 3 Hrs 211
	18 Ni (250) (Air Melt)	900 <sup>0</sup> F, 3 Hrs 248
	18 Ni (250) (Vac Melt)	900 <sup>0</sup> F, 3 Hrs 268
	18 Ni (300) (Vac Melt)	825 <sup>0</sup> F, 3 Hrs 236 900 <sup>0</sup> F, 3 Hrs 261 975 <sup>0</sup> F, 3 Hrs 251



TABLE II  
 .60" THICK  
 18Ni(200) GTA

		$f_{ty} \sim \text{KSI}$	$K_{Ic} \sim \text{KSI}\sqrt{\text{IN.}}$
WELD (1)	W	224	137+
	HAZ	—	141+
	REPAIR	—	129
B.M. (2)		227	158

(1) AGED @ 900°F, 8 HOURS  
 (2) AGED @ 900°F, 4 HOURS

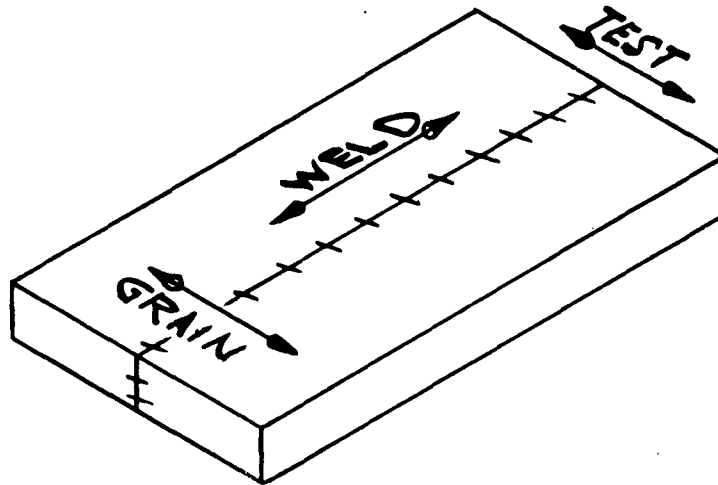


TABLE III  
 .40" THICK  
 18Ni(200)GTA

		$f_{LY} \sim KSI$	$K_{IC} \sim KSI\sqrt{IN.}$
WELD	¢	225 <sup>(1)</sup>	116
	HAZ		133
B. M.		232 <sup>(2)</sup>	142

- (1) AGED @ 900°F, 8 HOURS  
 (2) AGED @ 900°F, 4 HOURS

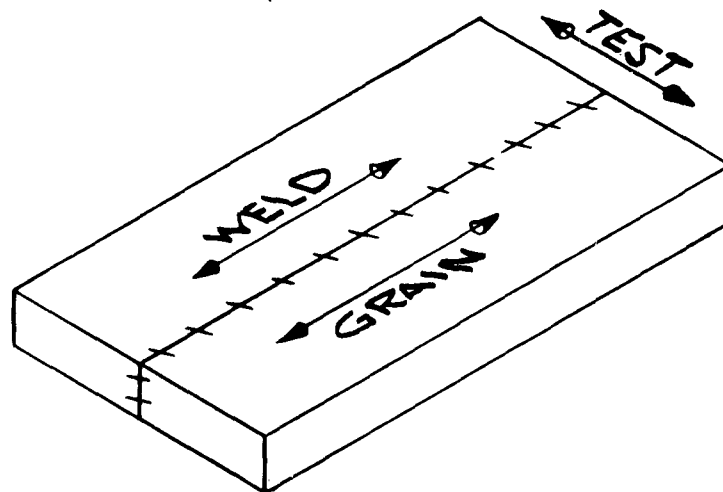


TABLE IV  
 .75" THICK  
 18 Ni (250) SUB-ARC

		$f_{ty} \sim \text{KSI}$		$K_{Ic} \sim \text{KSI}\sqrt{\text{IN.}}$	
		4 HRS	6 1/2 HRS	4 HRS	6 1/2 HRS
WELD	£	184	213	79(1) 82(2) (-)(3)	(-)(3)
	REPAIR	—	—	(-)(3)	—
B. M.		250	—	96.5	—

- (1) 1<sup>ST</sup> PASS SIDE } SURFACE FLAWED  
 (2) 2<sup>ND</sup> PASS SIDE }  
 (3) ROUND NOTCHED BAR — ECCENTRIC

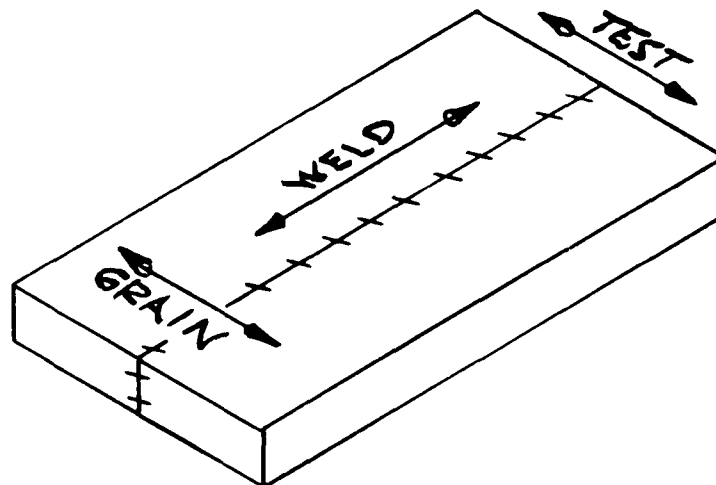


TABLE V  
 .48" THICK  
 18 Ni (250) SUB-ARC (1)

		$f_{ty} \sim KSI$		$K_{Ic} \sim KSI\sqrt{IN.}$	
		4 HRS	6 1/2 HRS	4 HRS	6 1/2 HRS
WELD (2)	¢	198	225	83	57
	HAZ	—	—	—	93
B.M.		260	—	86	—

- (1) AGED @ 835 °F, TIMES NOTED  
 (2) SURFACE FLAWS, 2<sup>ND</sup> PASS SIDE

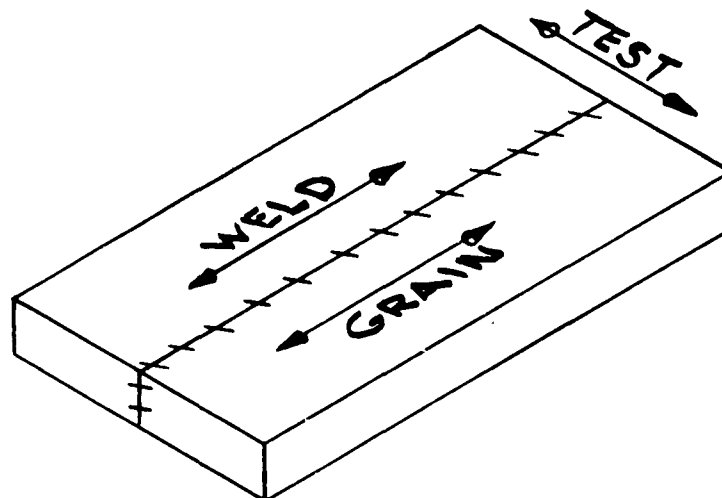


TABLE VI  
 .39" THICK  
 18Ni(250)GTA<sup>(1)</sup>  
 (SHELLS)

		$f_{ty} \sim \text{KSI}$	$K_{IC} \sim \text{KSI}\sqrt{\text{IN.}}$
WELD	Ø	231	78.5
	HAZ	—	126 ?
	REPAIR	—	65.8 - 84.3
B. M.		—	89

(1) AGED @ 900°F, 3 HOURS

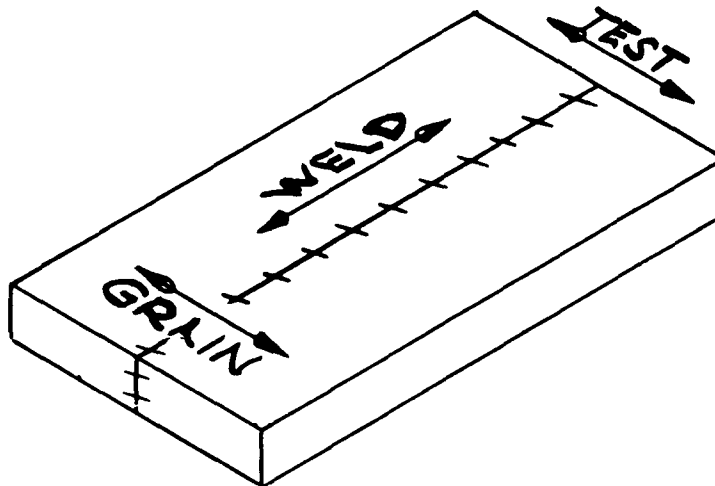
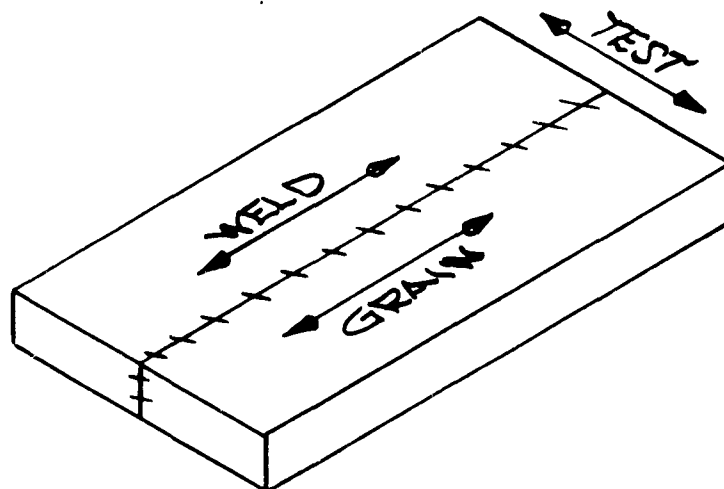


TABLE VII  
 .39" THICK  
 18Ni(250) GTA<sup>(1)</sup>  
 (HEADS)

		$f_{ty} \sim \text{KSI}$		$K_{IC} \sim \text{KSI}\sqrt{\text{IN.}}$	
		# 1	# 2	# 1	# 2
WELD	E	238	239	83 76	63 66
	HAZ			105?	96?
B. M.		237		83	

(1) AGED @ 900° F, 3 HOURS



**TABLE VIII**  
**ALLOWABLE FLAW SIZE**  
**COMPARISON**

	$(a/q)_i$ * SURFACE FLAW							
	SHELL				HEAD			
	THICKNESS (IN.)	$\frac{PR}{t}$ (KSI)	$K_{Ic}$ (MIN) KSI $\sqrt{IN}$	$(a/q)_i$ (IN.)	THICKNESS (IN.)	$\frac{PR}{2t}$ (KSI)	$K_{Ic}$ (MIN) KSI $\sqrt{IN}$	$(a/q)_i$ (IN.)
260" CASE 18Ni (200) GTA	.60	165	130	.147	.34	145	110	.136
260" CASE 18Ni (250) SUB-ARC	.72	173	55	.024	.47	133	55	.040
156" CASE 18Ni (250) GTA (THIOKOL)	.47	162	75	.051	.30	127	75 60	.083 .053

$$* (a/q)_i = (a/q)_{Cr} @ \text{PROOF} \times .90 = \frac{1}{1.21 \pi} \left( \frac{K_{Ic}}{\sigma_{\text{PROOF}}} \right)^2 \times .90$$

**TABLE IX**  
**ALLOWABLE FLAW SIZE**  
**260" CASE, 18 Ni(200) GTA**

	$(a/Q)_i$ = ALLOWABLE INITIAL SIZE <sup>(1)</sup> (INCHES)	
	SHELL <sup>(3)</sup> $K_{Tc}=130 \quad \sigma_m=164.7$	HEAD <sup>(3)</sup> $K_{Tc}=110 \quad \sigma_m=145.3$
MEMBRANE	0.147	0.136
Y-RING TO HEAD	—	0.116 <sup>(2)</sup>
5% ANGULAR MISMATCH	0.115	0.105 <sup>(2)</sup>
5% ANGULAR MISMATCH AT Y-RING	—	0.071 <sup>(2)</sup>

(1) FLAWS NORMAL TO HOOP STRESS  
EXCEPT AS NOTED

(2) FLAWS NORMAL TO LONGITUDINAL STRESS

(3) @ 760 psig PROOF



**TABLE X**  
**ALLOWABLE FLAW SIZE**  
**260" CASE, 18 Ni(250) SUB-ARC**

	$(a/q)_i$ = ALLOWABLE INITIAL SIZE <sup>(1)</sup> (INCHES)	
	SHELL <sup>(3)</sup> $K_{Ic} = 55 \quad \sigma_m = 172.9$	HEAD <sup>(3)</sup> $K_{Ic} = 55 \quad \sigma_m = 133.1$
MEMBRANE	0.024	0.040
Y-RING TO HEAD	—	0.027 <sup>(2)</sup>
5% ANGULAR MISMATCH	0.018	0.032 <sup>(2)</sup>

(1) FLAWS NORMAL TO HOOP STRESS  
EXCEPT AS NOTED

(2) FLAWS NORMAL TO LONGITUDINAL STRESS

(3) @ 960 psig PROOF

**TABLE XI**  
**ALLOWABLE FLAW SIZE**  
**156' CASE, 18Ni(250) GTA**

	$(a/Q)_i$ = ALLOWABLE INITIAL SIZE <sup>(1)</sup> (INCHES)	
	SHELL <sup>(3)</sup> $K_{Ic} = 75 \quad \sigma_m = 162.3$	HEAD <sup>(3)</sup> $K_{Ic} = \frac{60}{75} \quad \sigma_m = 127.0$
MEMBRANE	0.051	0.053 0.083
Y-RING TO HEAD	—	0.035 <sup>(2)</sup> 0.055 <sup>(2)</sup>
5% ANGULAR MISMATCH	0.041	0.046 <sup>(2)</sup>

(1) FLAWS NORMAL TO HOOP STRESS  
EXCEPT AS NOTED

(2) FLAWS NORMAL TO LONGITUDINAL STRESS

(3) @ 985 psig PROOF

# SURFACE FLAW SPECIMENS

SPECIMEN NUMBER	B= BASE METAL W= WELD WIRE	HEAT NUMBER		SPECIMEN			FATIGUE CRACK EXTENSION				CRACK	
		PLATE	WELD WIRE	THICKNESS ~IN.	WIDTH ~IN.	GROSS AREA ~IN <sup>2</sup>	TEST TEMP. OF	MAXIMUM TENSION FA- TIGUE STRESS ~KSI	STRESS RATIO MIN/MAX	TOTAL NUMBER OF CYCLES	LENGTH ~IN.	DEPTH ~IN.
SFL-1	B	X14332	-	1.02	3.005	3.065	RT	28	.06	15,000	1.04	.40
SFL-3	B	"	-	1.021	5.005	5.110	"	27	.06	18,000	2.13	.49
SFL-4	B	"	-	1.019	5.005	5.100	"	27	.06	16,000	2.11	.50
SFW-4	W	X14332	R9376	.907	4.000	3.628	RT	27	.06	6,000	2.14	.39
SFW-2	W	"	"	.702	3.007	2.110	"	30	.07	6,000	1.07	.32
SFW-1	W	"	"	.704	3.004	2.115	"	30	.07	5,000	1.04	.29

# TENSILE SPECIMENS

SPECIMEN NUMBER	B= BASE METAL W= WELD WIRE	HEAT NUMBER		GAGE ~IN.	AREA ~IN. <sup>2</sup>	TEST ATMOSPHERE	GRAIN DIRECTION L= LONGITUDINAL T= TRANSVERSE	TEST TEMP. OF	ULTIMATE STRENGTH ~ KSI	YIELD STRENGTH ~ KSI	% ELONG O.F.
		PLATE	WELD WIRE								
TFL-1	B	X14332	-	1.0198	.5102	AIR	L	RT	147.3	143.0	-
TFL-2	B	"	-	1.0186	.5084	"	L	"	147.1	143.1	-
TFL-3	B	"	-	1.0110	.5038	"	L	"	148.0	144.5	58
TFW-3	W	X14332	R9376	.9975	.4994	AIR	-	RT	149.7	138.7	62
TFW-2	W	"	"	1.0068	.5051	"	-	"	148.0	139.3	62
TFW-1	W	"	"	1.0062	.5044	"	-	"	148.2	140.3	62

# SURFACE FLAW SPECIMENS

SPECIMEN			FATIGUE CRACK EXTENSION				CRACK GEOMETRY					SUSTAINED LOADING			FRACTURE
THICKNESS ~ IN.	WIDTH ~ IN.	GROSS AREA ~ IN <sup>2</sup>	TEST TEMP. OF	MAXIMUM TENSION FATIGUE STRESS ~ KSI	STRESS RATIO MIN/MAX	TOTAL NUMBER OF CYCLES	LENGTH ~ IN.	DEPTH ~ IN.	LENGTH (AFTER SUSTAINED LOADING)	DEPTH (AFTER SUSTAINED LOADING)	FLAW LOCATION	TEST ATMOSPHERE	GROSS AREA SUSTAINED STRESS ~ KSI	TIME OF SUSTAINED STRESS ~ HRS	TEST ATMOSPHERE
02	3.005	3.065	RT	28	.06	15,000	1.04	.401	—	—	—	—	—	—	AIR
21	5.005	5.110	"	27	.06	18,000	2.13	.495	—	—	—	—	—	—	"
19	5.005	5.100	"	27	.06	16,000	2.11	.500	2.11	.500	—	NaCl	110.2	1.0	"
07	4.000	3.628	RT	27	.06	6,000	2.14	.397	—	—	¢	—	—	—	AIR
02	3.007	2.110	"	30	.07	6,000	1.07	.325	1.07	.325	¢	NaCl	117.7	2.0	"
04	3.004	2.115	"	30	.07	5,000	1.04	.296	—	—	¢	—	—	—	"

# TENSILE SPECIMENS

GAGE IN.	AREA ~ IN <sup>2</sup>	TEST ATMOSPHERE	GRAIN DIRECTION L=LONGITUDINAL T=TRANSVERSE	TEST TEMP. OF	ULTIMATE STRENGTH ~ KSI	YIELD STRENGTH ~ KSI	ELONGATION % PER INDICATED L			REDUCTION IN AREA %	
							0.50	1.00	2.00		
198	.5102	AIR	L	RT	147.3	143.0	—	44	26	65	
186	.5084	"	L	"	147.1	143.1	—	44	27	64	
110	.5038	"	L	"	148.0	144.5	58	45	25	59	
075	.4994	AIR	—	RT	149.7	138.7	62	42	24	61	
068	.5051	"	—	"	148.0	139.3	62	42	25	63	
062	.5044	"	—	"	148.2	140.3	68	42	25	62	

NS

CRACK GEOMETRY					SUSTAINED LOADING			FRACTURE TEST TO FAILURE IN STATIC TENSION							
NGTH IN.	DEPTH ~ IN.	LENGTH (AFTER SUSTAINED LOADING)	DEPTH (AFTER SUSTAINED LOADING)	FLAW LOCATION	TEST ATMOSPHERE	GROSS AREA SUSTAINED STRESS ~ KSI	TIME OF SUSTAINED STRESS ~ HRS	TEST ATMOSPHERE	GROSS AREA STRESS ~ KSI G	NET AREA STRESS ~ KSI G	YIELD STRENGTH (BASED ON TENSILE DATA) G	$\sigma_N/\sigma_Y$	a/g	K <sub>IC</sub> ~ KSI√IN	INDICATED K <sub>IC</sub> ~ KSI√IN
04	.401	—	—	—	—	—	—	AIR	134.3	150.5	143.0	1.05	.226	—	124.2
13	.495	—	—	—	—	—	—	"	130.3	155.6	143.0	1.09	.399	—	159.8
11	.500	2.11	.500	—	NaCl	110.2	1.0	"	129.0	154.0	143.0	1.08	.398	—	158.0
14	.397	—	—	£	—	—	—	AIR	126.0	154.3	139.8	1.10	.356	—	146.0
07	.325	1.07	.325	£	NaCl	117.7	2.0	"	132.7	152.4	139.8	1.08	.224	—	121.9
14	.296	—	—	£	—	—	—	"	135.6	153.1	139.8	1.10	.215	—	121.8

DEPTH IN.	ELONGATION % PER INDICATED L			REDUCTION IN AREA %
	0.50	1.00	2.00	
0	—	44	26	65
1	—	44	27	64
5	58	45	25	59
7	62	42	29	61
5	62	42	25	63
5	68	42	25	62

TABLE XII  
SCREENING TEST DATA

ALLOY: HY-150

MELT PRACTICE: AIR MELT

# SURFACE FLAW SPECIMENS

SPECIMEN NUMBER	B=BASE METAL W=WELD WIRE	HEAT NUMBER		SPECIMEN			FATIGUE CRACK EXTENSION				CRACK	
		PLATE	WELD WIRE	THICKNESS ~ IN.	WIDTH ~ IN.	GROSS AREA ~ IN <sup>2</sup>	TEST TEMP. OF	MAXIMUM TENSION FA- TIGUE STRESS ~ KSI	STRESS RATIO MIN/MAX	TOTAL NUMBER OF CYCLES	LENGTH ~ IN.	DEPTH ~ IN.
* H-400	B	3950924	—	.754	3.00	2.262	RT	60.0	.06	3,600	.8755	.2701
* H-800	B	"	—	.760	3.00	2.280	"	50.0	.06	6,200	.895	.301
* H-1035	B	"	—	1.038	3.02	3.132	"	45.0	.06	5,000	1.095	.335
* SCW-3	W	3930786 3888650		.706	2.515	1.776	RT	27.0	.09	18,000	.790	.208
* SCW-2	W	"	"	.711	2.999	2.132	"	27.0	.08	17,000	.820	.220
SCW-1	W	"	"	.711	3.001	2.134	"	27.0	.08	13,000	.785	.200

\* SPECIMENS NOTED MEET REF (1) TENTATIVE REQUIREMENTS

- 1 ▷ THICKNESS OF RECTANGULAR SPECIMEN
- 2 ▷ ALL WELDMENTS LEFT "AS DEPOSITED" ON PLATE  
ORIGINALLY TEMPERED AT 1035°F

# TENSILE SPECIMENS

SPECIMEN NUMBER	B=BASE METAL W=WELD WIRE	HEAT NUMBER		DIA ~ IN.	AREA ~ IN <sup>2</sup>	TEST ATMOSPHERE	GRAIN DIRECTION L=LONGITUDINAL T=TRANSVERSE	TEST TEMP. OF	ULTIMATE STRENGTH ~ KSI	YIELD STRENGTH ~ KSI	EL % RET 0.5C
		PLATE	WELD WIRE								
TCL-1	B	3330786	—	.2486	.0485	AIR	L	RT	196.7	187.4	—
TCL-2	B	"	—	.2489	.0487	"	L	"	193.7	185.3	—
TCL-3	B	"	—	.2494	.0489	"	L	"	195.5	184.6	26
H-9	B	"	—	.6151	.3076	"	L	"	194.4	186.9	56
H-10	B	"	—	.6149	.3111	"	L	"	192.9	185.8	60
TCW-3	W	3930786 3888650		.2502	.0492	AIR	—	RT	191.0	168.4	6
TCW-2	W	"	"	.2498	.0490	"	—	"	194.2	173.4	—
TCW-1	W	"	"	.2496	.0489	"	—	"	194.3	174.1	—

1

# SURFACE FLAW SPECIMENS

SPECIMEN			FATIGUE CRACK EXTENSION				CRACK GEOMETRY					SUSTAINED LOADING			FRAC
KNES N.	WIDTH ~ IN.	GROSS AREA ~ IN <sup>2</sup>	TEST TEMP. OF	MAXIMUM TENSION FATIGUE STRESS ~ KSI	STRESS RATIO MIN/MAX	TOTAL NUMBER OF CYCLES	LENGTH ~ IN.	DEPTH ~ IN.	LENGTH (AFTER SUSTAINED LOADING)	DEPTH (AFTER SUSTAINED LOADING)	FLAW LOCATION	TEST ATMOSPHERE	GROSS AREA SUSTAINED STRESS ~ KSI	TIME OF SUSTAINED STRESS ~ HRS	TEST ATMOSPHERE
54	3.00	2.262	RT	60.0	.06	3,600	.8755	.2701	—	—	—	—	—	—	AIR
60	3.00	2.280	"	50.0	.06	6,200	.895	.301	—	—	—	—	—	—	"
38	3.02	3.132	"	45.0	.06	5,000	1.095	.335	—	—	—	—	—	—	"
56	2.515	1.776	RT	27.0	.09	18,000	.790	.208	—	—	£	—	—	—	AIR
1	2.999	2.132	"	27.0	.08	17,000	.820	.220	.830	.254	£	NaCl	160.3	1.0	"
1	3.001	2.134	"	27.0	.08	13,000	.785	.200	—	—	£	—	—	—	"

UTATIVE REQUIREMENTS  
ECIMEN


POSITED" ON PLATE  
5°F

# TENSILE SPECIMENS

N.	AREA ~ IN. <sup>2</sup>	TEST ATMOSPHERE	GRAIN DIRECTION L=LONGITUDINAL T=TRANSVERSE	TEST TEMP. OF	ULTIMATE STRENGTH ~ KSI	YIELD STRENGTH ~ KSI	ELONGATION % PER INDICATED L			REDUCTION IN AREA %	TEMPERING TEMPERATURE °F
							0.50	1.00	2.00		
86	.0485	AIR	L	RT	196.7	187.4	—	18	—	62	1035
89	.0487	"	L	"	193.7	185.3	—	18	—	63	1035
94	.0489	"	L	"	195.5	184.6	26	15	—	64	1035
1	.3076	"	L	"	194.4	186.9	56	37	21	62	1035
1	.3111	"	L	"	192.9	185.8	60	37	22	63.9	1035
02	.0492	AIR	—	RT	191.0	168.4	6	4	—	4	(POROSITY OBSERVED ON FRAC
98	.0490	"	—	"	194.2	173.4	—	16	—	62	
96	.0489	"	—	"	194.3	174.1	—	16	—	61	

2

MEL

CRACK GEOMETRY					SUSTAINED LOADING			FRACTURE TEST TO FAILURE IN STATIC TENSION								TEMPER. TEMPERATURE °F 
GTN N.	DEPTH ~ IN.	LENGTH (AFTER SUSTAINED LOADING)	DEPTH (AFTER SUSTAINED LOADING)	FLAW LOCATION	TEST ATMOSPHERE	GROSS AREA SUSTAINED STRESS ~ KSI	TIME OF SUSTAINED STRESS ~ HRS	TEST ATMOSPHERE	GROSS AREA STRESS ~ KSI ON	NET AREA STRESS ~ KSI ON	YIELD STRENGTH (BASED ON TENSILE DATA) ON	$\sigma_N/\sigma_Y$	$a/a_0$	$K_{Ic} \sim$ KSI/IN	INDICATED $K_{Ic} \sim$ KSI/IN	
55	.2701	—	—	—	—	—	—	AIR	130.5	142.3	192.7	.739	.1723	110.8	—	400
5	.301	—	—	—	—	—	—	"	164.2	182.3	189.1	.964	.1885	138.3	—	800
95	.335	—	—	—	—	—	—	"	179.3	197.5	185.1	1.067	.2310	—	167.2	1035
0	.208	—	—	£	—	—	—	AIR	168.8	182.0	173.7	1.05	.159	—	130.2	
20	.220	.830	.254	£	NaCl	160.3	1.0	"	167.4	181.2	173.7	1.04	.174	—	135.3	
5	.200	—	—	£	—	—	—	"	176.8	187.5	173.7	1.08	.157	—	136.2	


ELONGATION % PER INDICATED L				REDUCTION IN AREA %	TEMPERING TEMPERATURE °F 
	0.50	1.00	2.00		
—	18	—	—	62	1035
—	18	—	—	63	1035
26	15	—	—	64	1035
56	37	21	—	62	1035
60	37	22	—	63.9	1035
6	4	—	—	4	(POROSITY OBSERVED ON FRACTURE SURFACE)
—	16	—	—	62	
—	16	—	—	61	

TABLE XIII  
SCREENING TEST DATA

ALLOY: 9Ni-4Co-.20C  
MELT PRACTICE: VACUUM MELT



# SURFACE FLAW SPECIMENS

SPECIMEN NUMBER	B=BASE METAL W=WELD WIRE	HEAT NUMBER		SPECIMEN			FATIGUE CRACK EXTENSION				CRACK	
		PLATE	WELD WIRE	THICKNESS IN.	WIDTH IN.	GROSS AREA IN <sup>2</sup>	TEST TEMP. °F	MAXIMUM TENSION FA- TIGUE STRESS ~ KSI	STRESS RATIO MIN/MAX	TOTAL NUMBER OF CYCLES	LENGTH IN.	DEPTH IN.
*SEL-1	B	X15339	—	1.054	3.001	3.163	RT	27.0	.06	9,000	1.07	.36
*SEL-2	B	"	—	1.054	3.008	3.170	"	27.0	.06	10,000	1.05	.38
*SEL-15	B	X15216	—	1.460	3.990	5.830	"	28.0	.06	11,000	1.51	.52
*SEWI-6	W	X15339	T39635	.961	3.012	2.895	RT	29.4	.06	6,000	1.05	.31
*SEWI-5	W	"	"	.984	3.011	2.963	"	29.4	.06	5,000	1.04	.32
*SEWI-4	W	"	"	.969	3.004	2.911	"	29.4	.06	5,000	1.04	.31
SEW-3	W	"	R9517	.713	3.011	2.147	"	27.0	.08	6,000	1.07	.33
SEW-2	W	"	"	.704	3.002	2.113	"	27.0	.08	6,000	1.07	.3
SEW-1	W	"	"	.708	2.993	2.119	"	27.0	.08	6,000	1.08	.31

\* SPECIMENS NOTED MEET REF(1) TENTATIVE REQUIREMENTS

# TENSILE SPECIMENS

SPECIMEN NUMBER	B=BASE METAL W=WELD WIRE	HEAT NUMBER		DIA ~ IN.	AREA ~ IN <sup>2</sup>	TEST ATMOSPHERE	GRAIN DIRECTION L=LONGITUDINAL T=TRANSVERSE	TEST TEMP. °F	ULTIMATE STRENGTH ~ KSI	YIELD STRENGTH ~ KSI	% O.
		PLATE	WELD WIRE								
TEL-1	B	X15339	—	.2494	.0488	AIR	L	RT	207.2	202.4	
TEL-2	B	"	—	.2493	.0488	"	L	"	207.7	202.8	
TEL-3	B	"	—	.2490	.0487	"	L	"	208.2	203.0	1
TEWI-5	W	X15339	T39635	.2482	.0484	AIR	—	RT	194.2	191.4	
TEWI-4	W	"	"	.2493	.0488	"	—	"	194.2	189.9	
TEW-2	W	"	R9517	.2495	.0489	"	—	"	199.6	195.1	
TEW-1	W	"	"	.2495	.0489	"	—	"	201.4	196.9	

# SURFACE FLAW SPECIMENS

SPECIMEN			FATIGUE CRACK EXTENSION				CRACK GEOMETRY					SUSTAINED LOADING			FRAC
THICKNESS IN.	WIDTH IN.	GROSS AREA IN <sup>2</sup>	TEST TEMP. OF	MAXIMUM TENSION FA- TIGUE STRESS ~ KSI	STRESS RATIO MIN/MAX	TOTAL NUMBER OF CYCLES	LENGTH IN.	DEPTH IN.	LENGTH (AFTER SUSTAINED LOADING)	DEPTH (AFTER SUSTAINED LOADING)	FLAW LOCATION	TEST ATMOSPHERE	GROSS AREA SUSTAINED STRESS ~ KSI	TIME OF SUSTAINED STRESS ~ HRS	TEST ATMOSPHERE
1.054	3.001	3.163	RT	27.0	.06	9,000	1.07	.365	—	—	—	NaCl	152.2	1.0	AIR
1.054	3.008	3.170	"	27.0	.06	10,000	1.05	.385	—	—	—	—	—	—	"
1.460	3.990	5.830	"	28.0	.06	11,000	1.51	.525	—	—	—	—	—	—	"
961	3.012	2.895	RT	29.4	.06	6,000	1.05	.350	—	—	HAZ	—	—	—	AIR
984	3.011	2.963	"	29.4	.06	5,000	1.04	.325	1.04	.355	¢	NaCl	143.7	.5	"
969	3.004	2.911	"	29.4	.06	5,000	1.04	.333	—	—	¢	—	—	—	"
713	3.011	2.147	"	27.0	.08	6,000	1.07	.330	—	—	¢	—	—	—	"
704	3.002	2.113	"	27.0	.08	6,000	1.07	.340	1.08	.364	¢	NaCl	57.8	1.0	"
708	2.993	2.119	"	27.0	.08	6,000	1.08	.330	—	—	¢	—	—	—	"

## ITATIVE REQUIREMENTS

# TENSILE SPECIMENS

DIA IN.	AREA ~ IN. <sup>2</sup>	TEST ATMOSPHERE	GRAIN DIRECTION L=LONGITUDINAL T=TRANSVERSE	TEST TEMP. °F	ULTIMATE STRENGTH ~ KSI	YIELD STRENGTH ~ KSI	ELONGATION % PER INDICATED L			REDUCTION IN AREA %	
							0.50	1.00	2.00		
494	.0488	AIR	L	RT	207.2	202.4	—	13	—	49	
493	.0488	"	L	"	207.7	202.8	—	13	—	48	
490	.0487	"	L	"	208.2	203.0	18	10	—	51	
482	.0484	AIR	—	RT	194.2	191.4	—	9	—	42	
493	.0488	"	—	"	194.2	189.9	—	8	—	44	
495	.0489	"	—	"	199.6	195.1	—	9	—	26	
495	.0489	"	—	"	201.4	196.9	—	6	—	18	

2

NS

CRACK GEOMETRY					SUSTAINED LOADING			FRACTURE TEST TO FAILURE IN STATIC TENSION							
LENGTH IN.	DEPTH IN.	LENGTH (AFTER SUSTAINED LOADING)	DEPTH (AFTER SUSTAINED LOADING)	FLAW LOCATION	TEST ATMOSPHERE	GROSS AREA SUSTAINED STRESS ~ KSI	TIME OF SUSTAINED STRESS ~ HRS	TEST ATMOSPHERE	GROSS AREA STRESS ~ KSI ON	NET AREA STRESS ~ KSI ON	YIELD STRENGTH (BASED ON TENSILE DATA) KSI ON	$\sigma_N/\sigma_Y$	$a/q$	$K_{Ic} \sim$ KSI $\sqrt{IN}$	INDICATED $K_{Ic} \sim$ KSI $\sqrt{IN}$
.07	.365	—	—	—	NaCl	152.2	1.0	AIR	180.6	200.0	202.6	.99	.227	167.0	—
.05	.385	—	—	—	—	—	—	"	179.0	199.0	202.6	.98	.224	164.2	—
.51	.525	—	—	—	—	—	—	"	166.5	186.0	192.7	.96	.318	182.4	—
.05	.350	—	—	HAZ	—	—	—	AIR	179.5	199.5	190.6	1.05	.224	—	165.2
.04	.325	1.04	.355	¢	NaCl	143.7	.5	"	187.0	207.3	190.6	1.09	.225	—	172.0
.04	.333	—	—	¢	—	—	—	"	188.1	207.5	190.6	1.09	.223	—	172.7
.07	.330	—	—	¢	—	—	—	"	71.0	81.5	196.0	.42	.203	62.1	—
.07	.340	1.08	.364	¢	NaCl	57.8	1.0	"	82.2	97.0	196.0	.49	.212	73.5	—
.08	.330	—	—	¢	—	—	—	"	86.4	99.6	196.0	.51	.209	76.7	—

D PTH IN.	ELONGATION % PER INDICATED L			REDUCTION IN AREA %
	0.50	1.00	2.00	
4	—	13	—	49
8	—	13	—	48
0	18	10	—	51
—	—	—	—	—
—	—	—	—	—
—	—	—	—	—
—	—	—	—	—
—	9	—	—	42
—	8	—	—	44
—	9	—	—	26
—	6	—	—	18

TABLE XIV  
SCREENING TEST DATA

ALLOY: 12Ni-5Cr-3Mo (180)

MELT PRACTICE: AIR MELT

3

TABLE XV

## LIST OF PROCESS VARIABLES CONTROLLED IN MULTIPLE BALANCE EXPERIMENT

1. Base Alloy	12. Weld Process
2. Filler Alloy	13. Joint Configuration
3. Filler Alloy Size	14. Energy
4. Pre-Weld Heat Treatment	15. Speed
5. Post-Weld Heat Treatment	16. Shielding Gas
6. Pre-Heat and Interpass Temperature	17. Gas Flow Rate
7. Post Heat Hold	18. Cap-Work Distance
8. Welder	19. Tip-Work Distance
9. Engineer	20. Filler Feed Rate
10. Shift	21. Cleanliness
11. Priority	22. Trailer Shield

**TABLE XVI**  
**COMPOSITIONS OF ALTERNATE MATERIALS**  
**(BASE METAL & FILLER WIRE)**

		Heat No.	C	Mn	P	S	Si	Ni	Cr	Mo	Al	Ti	Co	V
5N1	Base Metal	X53957	.11	.72	.006	.006	.26	4.98	.52	.54	.023			.07
	Wire A	T5596B	.045	2.23	.008	.008	.38	2.02	.79	.55	-	.015	-	-
	Wire B	T5788C	.085	.72	.003	.005	.33	5.31	.70	.55	.007	.020	-	.07
	Wire C	T5256A	.071	1.98	.001	.005	.34	1.86	.86	.55	-	.016	-	-
9N1	Base Metal	3930960	.26	.33	.006	.010	.01	8.38	.39	.49	-	-	3.90	.08
	Wire D	3888727	.22	.30	.006	.006	.26	7.50	.99	1.02	-	-	3.65	.07
	Wire E	3888722	.25	.80	.003	.005	.40	7.20	.87	1.03	-	-	3.60	.10
	Wire F	3888726	.25	.48	.008	.006	.25	7.20	.45	.42	-	-	5.20	.07
12N1	Base Metal	X10058	.02	.06	.006	.010	.07	12.02	5.10	3.00	.24	.32	-	-
	Wire G	T5755BT	.006	.028	.001	.007	.018	11.9	5.03	2.00	.015	.44	-	-
	Wire H	T5759AT	.009	.016	.002	.006	.019	11.8	3.60	2.76	.002	.45	-	-
	Wire I	T5264C	.006	.010	.001	.005	.026	11.9	5.05	3.04	.18	.65	-	-

TABLE XVII

PROCESSING HISTORY OF ALTERNATE MATERIALS

5Ni-Cr-Mo-V

Supplier: United States Steel Corporation  
 Melting Practice: Air Melt - Electric furnace - Lime Alumina Slag  
 Heat No.: X-53957 Size: 80 ton  
 Ingot Size: 32" x 60" Hot Rolled 2000° finish at 1900°F  
 Rolling Ratio 1.8/1.0 (L.T.)  
 Austenitized 1500° 1½ hrs. Water Quenched  
 Tempered 1½ hrs. at 875-1075° Air Cooled

9Ni-4Co-.25C

Supplier: Republic Steel Corporation  
 Melting Practice: Vacuum Arc Remelt-Carbon De-Ox.  
 Air Melt Heat No.: 3311846 Size: 90 ton  
 VAR. Heat No.: 3930960 Size: 5 ton  
 Ingot Size: 24" Dia. Press Forged from 24" RD to 18" x 4"  
 Hot Rolled 1750° finish at 1500°F  
 Annealed 1125° 3 hrs. Air Cooled  
 Austenitized 1550° 1 hr. Oil Quenched  
 Tempered 2 hrs. + 2 hrs. at 900-1050° Air Cooled

12Ni-5Cr-3Mo

Supplier: United States Steel Corporation  
 Melting Practice: Air Melt Electric Furnace - Lime Alumina Slag  
 Heat No.: X-10058 Size: 20 ton  
 Ingot size 29" x 54" Hot Rolled 2000° finish 1800°F  
 Rolling Ratio 2.4/1.0 (L.T.)  
 Annealed 1500° 1 hr. Water Quenched  
 Aged 4-12 hrs. at 900°

Filler Speed	Weld Speed	10		20		30		Weld Heat Weld Joint
		N	W	N	W	N	W	
S	S	93	77	74	84*	89	81	
	F	73	76	72	85	79	75	
F	S	91	87	83	92	80	90	
	F	78*	71	94*	86	82	88	

Trail Shield	Cleanliness	A		He		Gas Gas Flow
		40	80	40	80	
No	A	71-94*	84*	79-92	72	
	B	87	75-93	83	81-90	
Yes	A	80	85-91	77	73-86	
	B	88-89	74	78-82*	76	

Filler Alloy	Wire Size	HY 150		HP 9-4		12Ni(180)		Base Metal
(a)(d) (g)	0	90-94*		71		86		
	+	77		82		79-89		
(b)(h) M	0	80-93		72		81		
	+	76		73		75-78		
(c)(f) (i) H	0	87		84-88*		85		
	+	91		74-83		92		

Pre/Post Heat	Post Heat Hold Time	L		M		H		Prior H.T. Cond.
150	0	80-90		71-94*		78-83*		
	30	85-91		73-82		81-92		
300	0	84-93*		72-77		74-75		
	30	79-89		86-87		76-88		

TABLE XVIII Work Sheet for Multiple Balance Design Experiment  
Gas-Tungsten-Arc (GTA) Weld Process

\*Denotes Location of Replicate Samples

**TABLE XIX**  
**EFFECTS OF PROCESS, GAS, ALLOY AND FILLER ON WELD TOUGHNESS**

	GTA		GMA			
	A	He	He	70% He 24 A 6 CO <sub>2</sub>	70% He 29.5 A .502	75% A 25% CO <sub>2</sub>
A	182-183+	178+ 189+	-	146	-	149 166 166
B	191+	178+ 182+	-	172+ 172+	-	112 146 147
C	184+	-	-	167 164	186-190+ 185+ 187+ 203**	185+
D	156	150	-	109	136	88 82
E	-	108 124	-	115 98 134	124	84
F	148 141 153-162	-	-	125-127	113 140	107 127
G	169	159 181	138	107 90 91	111 91	84
H	-	110 149 164	143-143	-	129 136	74 82
I	121	168	-	73	-	74-76 64



**TABLE XX**  
**TYPICAL WELDING RATES**

Weld Process	1.5 Inch 5 Ni-Cr-Mo-V		1.0 Inch 12Ni-5Cr-3Mo		0.8 Inch 9Ni-4Co-.25C	
	<u>No. Passes</u>	<u>Arc Time per Inch</u>	<u>No. Passes</u>	<u>Arc Time</u>	<u>No. Passes</u>	<u>Arc Time</u>
GTA	27	5.8	18	3.0	15	2.2
GMA	46	1.3	10	1.0	9	.9
GMA (HD)	17	0.8	8	.5	6	.3
GMA (SA)	12	1.5	6	1.0	6	.8
Sub Arc	8	.7	6	.5	6	.5

TABLE XXI  
SUMMARY OF MULTIPLE BALANCE EXPERIMENT  
EFFECT ON:

<u>FACTOR</u>	<u>POROSITY</u>	<u>FUSION</u>	<u>CRACKING</u>	<u>TOUGHNESS</u>
1. Alloy	Strong	Strong	Strong	Strong
2. Filler	Minor	Minor	Minor	Minor
3. Wire size	Moderate	Moderate	Minor	Minor
4. Temper Condition	Minor	Minor	Minor	Strong
5. Post weld temper	Minor	Minor	Minor	Strong
6. Pre-heat	Minor	Minor	Minor	Minor
7. Post heat hold	Minor	Minor	Minor	Minor
8. Welder	Minor	Minor	Minor	Minor
9. Engineer	Minor	Minor	Minor	Minor
10. Shift	Minor	Minor	Minor	Minor
11. Order	Minor	Minor	Minor	Minor
12. Process	Strong	Minor	Moderate	Minor
13. Joint	Minor	Moderate	Moderate	Minor
14. Energy	Moderate	Minor	Moderate	Moderate
15. Speed	Moderate	Moderate	Moderate	Minor
16. Gas	Moderate	Moderate	Minor	Strong
17. Gas flow	Minor	Minor	Minor	Minor
18. Cup-work	Minor	Minor	Minor	Minor
19. Tip-work	Minor	Minor	Moderate	Minor
20. Filler feed	Moderate	Minor	Minor	Minor
21. Cleanliness	Minor	Minor	Minor	Minor
22. Trailer shield	Minor	Minor	Minor	Minor

TABLE XXII : MATERIAL COMPARISONS

$f_{\text{EY}}$ MIN (KSI)	WELD TOUGHNESS		CASE (1) THICKNESS ~ IN.		$(\frac{1}{4})$ CY @ PROOF ~ IN.	PROBABILITY OF LEAK BEFORE FAILURE		FORMABILITY	WELDABILITY	(2) QUALITY CONTROL	
	PROCESS	K <sub>IC</sub> KSI/IN.	260"	156"		260"	156"				
117-150	GTA GMA	200+	1.02	.61	.83+	HIGH	HIGH	EXPECTED TO BE ADEQUATE	GOOD	EXCELLENT	
12 Ni	GTA	170	.84	.50	.41	LOW	HIGH		FAIR	FAIR TO GOOD	GOOD TO FAIR
9 Ni	GTA	160	.84	.50	.36	LOW	HIGH		FAIR TO GOOD	GOOD	GOOD
18 Ni (200)	GTA	130	.71	.43	.17	NIL	LOW	GOOD	GOOD	FAIR	
18 Ni (250)	GTA	75	.60	.36	.04	NIL	NIL	GOOD	GOOD	STRINGENT	
	SUB ARC	55	.60	.36	.02						

(1) FOR : MEOP = 800  
YLD F.S. = 1.3  
WELD FACTOR = .95  
PROOF = 1.1 MEOP

(2) AS AFFECTED BY EXPECTED &  
REQUIRED QUALITY

APPENDIX A  
TO  
FIRST YEAR SUMMARY PROGRESS REPORT  
VOLUME I  
June, 1965

CONTRACT  
AF 33(615)-1623

ANALYSIS OF SECONDARY STRESSES

## TABLE OF CONTENTS

	<u>Page</u>
1. INTRODUCTION	1
1.1 Significance of Problem	1
1.2 Object and Scope	1
2. THE FLAW SIZE CORRECTION FACTOR	2
3. ANGULAR MISMATCH	3
3.1 Assumptions	3
3.2 Cylindrical Casings	3
3.2.1 Girth Welds	3
3.2.2 Longitudinal Welds	6
3.3 Spherical Heads	8
3.3.1 Girth Welds	8
3.3.2 Gore Welds	9
4. RADIAL MISMATCH	10
4.1 Assumptions	10
4.2 Cylindrical Casings	10
4.2.1 Girth Welds	10
4.2.2 Longitudinal Welds	15
4.3 Spherical Heads	16
4.3.1 Girth Welds	16
4.3.2 Gore Welds	17
5. ANALYSIS OF GEOMETRIC DISCONTINUITIES ADJACENT TO Y-RING	18

# NOTATION

$p$	Internal Pressure
$t$	Wall Thickness
$R$	Radius of Vessel
$M_{\phi}$	Circumferential Bending Moment
$M_{\phi}$	Meridional Bending Moment
$N_{\phi}$	Circumferential Force
$N_{\phi}$	Meridional Force
$Ak_{\phi}$	Meridional Flaw Size Correction Factor
$Ak_{\phi}$	Circumferential Flaw Size Correction Factor
$\beta_P, \beta_H, \beta_M$	Influence Coefficients for Rotation Due to Subscripted Force
$\delta_P, \delta_H, \delta_M$	Influence Coefficients for Radial Deflection Due to Subscripted Force

## ANALYSIS OF SECONDARY STRESSES

### 1. INTRODUCTION

#### 1.1 Significance of Problem

The welding of large motor casings can introduce both geometric discontinuities and embedded flaws into the casing wall. Secondary stresses which result from the geometric discontinuities affect the fracture resistance of the casing at the location of the embedded flaws. Hence, a knowledge of secondary stresses that can be developed by geometric discontinuities is a necessary prerequisite to the prediction of the performance capabilities of a given motor case.

#### 1.2 Object and Scope

This study has two objectives. The first is to determine the secondary stress fields which can be developed near geometric discontinuities in large rocket motor casings. The second is to establish the effect of the secondary stresses on allowable flaw size.

The study will be limited to the consideration of discontinuities which can be caused by the welding of large casings. Geometric discontinuities commonly due to welding are

- 1) angular mismatch (Figure 1a),
- 2) radial mismatch (Figure 1b).

Individual analyses are made of each of the abovementioned discontinuities at longitudinal and girth welds in both the heads and bodies of rocket motor casings.

A geometric discontinuity inherent to the design of the vessel is the head to shell juncture which is effected by means of a Y-ring. Analyses

were made of the Y-ring junctures for three different motor cases in order that the combined effects of Y-ring discontinuity, material delamination and radial mismatch could be computed. A single solution has been completed for combined effect of Y-ring discontinuity and angular mismatch.

## 2. THE FLAW SIZE CORRECTION FACTOR

Results of studies of geometric discontinuities in large rocket motor casings will be expressed in terms of a quantity called the flaw size correction factor. Critical flaw sizes are computed from the expression

$$\left(\frac{a}{Q}\right)_{cr.} = \frac{1}{1.21\pi} \cdot \frac{K_{IC}^2}{\sigma_T^2} \cdot \frac{1}{M_K} \quad (1)$$

where

$a$  is flaw size,

$Q$  is a function of the order of 1 which has a value dependent upon the flaw shape, yield strength of the material, and applied stress level.

$K_{IC}$  is plane strain fracture toughness of the material containing the flaw,

$\sigma_T$  is the component of the stress field acting perpendicularly to the plane of the crack,

$M_K$  is an approximate correction factor to account for the relative geometry of flaw and structure.

The above expression can be written as

$$\left(\frac{a}{Q}\right)_{cr.} = \frac{1}{1.21\pi} \frac{K_{IC}^2}{A_K \sigma_m^2} \frac{1}{M_K} \quad (2)$$

where

$\sigma_m$  = the component of the membrane stress solution acting perpendicularly to the plane of the crack,

$A_K$  is the flaw size correction factor.



It is now apparent that

$$A_k = \left( \frac{\sigma_T}{\sigma_m} \right)^2 \quad (3)$$

and is a scaler by which a critical flaw size associated with a given component of the membrane stress solution must be divided in order to obtain the critical flaw size associated with the corresponding component of the total stress field.

### 3. ANGULAR MISMATCH

#### 3.1 Assumptions

In the following stress analyses of angular mismatch, it will be assumed that

- 1) Plane sections remain plane and normal to the inextensional middle surface (Kirchoff Assumption)
- 2) The geometry of an angular mismatch is symmetric with respect to its cusp
- 3) The angular mismatch is sufficiently far away from other causes of secondary stress so that there is no interaction with the other causes (other mismatches, Y-rings, nozzle adapter rings, etc.).

#### 3.2 Cylindrical Casings

- 3.2.1 Girth Welds: In the analysis of angular mismatch at girth welds, it will be assumed that the angular mismatch is axisymmetric. If angular mismatch is not axisymmetric, it is suggested that the stresses at the point of maximum sink-in for the non-uniform mismatch can be approximated by the stresses in an axisymmetrically mismatched cylinder with a sink-in equal to the maximum sink-in of the non-uniform mismatch.

Secondary stresses which result from angular mismatch depend on the geometry of the mismatch. If the sink-in curve shape is described as shown in Figure 2a, three variables are needed to describe the mismatch geometry: the length  $L$ , the sink-in  $\delta$  and the curve shape  $\bar{T}$ . It was decided that a better assumption for mismatch geometry would be the shape generated by an imaginary concentrated moment assumed to act at the mismatched weld (Figure 2b). The concentrated moment is probably a good representation of the manner in which an angular mismatch is developed. The latter representation reduces the number of variables needed to describe the angular mismatch to one,  $\delta$ . Furthermore, the use of the concentrated moment representation takes into account the effect that motor case geometry would exert on angular mismatch geometry.

The problem of axisymmetric angular mismatch was solved by using the direct stiffness method described in (1). In the neighborhood of the angular mismatch, the shell was represented by a series of finite truncated conical elements connecting nodal circles (Figure 3). It was assumed that the displacements everywhere in the structure could be described in terms of the displacement of the nodal circles and that the pressure load could be replaced by a set of equivalent loads at the nodal circles. Compatibility of deformation was satisfied precisely at the nodal circles and approximately along the other elemental boundaries. The displacements were represented by the three displacement components  $u$ ,  $w$  and  $\beta$  at each nodal circle. These displacements and the corresponding equivalent loads  $T$ ,  $N$  and  $M$  are illustrated in Figure 3.

It was discovered that the angular mismatch problem exhibited a beam-column type of non-linearity. The non-linearity was taken into account by using the incremental force method described in (2). Briefly, the proof pressure load of the structure was broken into a number of increments. The deflections were computed for the first increment of load by using the stiffness matrix of the undeflected structure. The computed deflections were then added to the initial geometry and a new stiffness matrix was calculated for the partially deflected structure. The deflections for the second increment of load were then computed by using the new stiffness matrix. This procedure was repeated until the total pressure load was added to the structure.

The accuracy of this approximate solution depends on the number of increments into which the load is divided. It was found that for the particular problem of circumferential angular mismatch, division of the load into more than five increments resulted in only a very small change in the computed forces. Hence, the load was added in five increments in all of the solutions described herein.

The stresses due to the various secondary force components developed near an angular mismatch at a girth weld in a cylinder are illustrated in Figure 4. The stresses are for the particular geometry indicated on that Figure. The dominant stress is that generated by the longitudinal secondary bending moments. The longitudinal bending stress is maximum at the apex of the cusp

of the mismatch. The shear stresses are small in comparison to most of the other secondary stresses and will not be taken into account in the computation of flaw size correction factors. All other secondary forces will be taken into consideration.

The flaw size correction factors computed at the apex of the cusp are shown for three different motor casings in Figures 5, 6, and 7. The correction factors are computed using the maximum moment stresses acting in the outside fibres of the casing wall. Hence, the correction factors are conservative.

3.2.2 Longitudinal Welds: In the analyses of angular mismatch at longitudinal welds in cylinders, it was assumed that the mismatch geometry was uniform along the entire length of the cylinder. If the mismatch is not uniform, the stresses at the point of maximum sink-in can be approximated by the stresses in a uniformly mismatched cylinder which contains a sink-in equal to the maximum sink-in of the non-uniform mismatch.

The shape of the assumed angular mismatch curve is illustrated in Figure 8. This simple geometry was chosen to avoid the complexities which arise from taking the curve shape caused by a concentrated moment acting at the longitudinal weld. The solutions had to be computed by hand and a choice of a complicated mismatch geometry would have added greatly to the amount of hand calculation that was necessary. It was found in the girth weld angular mismatch problem that the solutions

derived from the curve shape of Figure 8 differed little from solutions derived for the more complicated mismatch geometry of Figure 2b. Hence, the more simple geometry was chosen for the solution of this particular problem.

In order to solve the longitudinal angular mismatch problem, it was assumed that the cylinder underwent a plane strain type of deformation. Hence a slice could be imagined to be cut from the cylinder forming a ring. Because of the plane strain assumption, the forces developed in the ring by the pressure acting on the slice are the same as the forces generated by the pressure acting on the cylinder. In the analysis of a ring, it can be imagined that the circular force line of the ring is straightened out to form a beam as in Figure 9a. For loadings symmetrical to line A-A on the same figure, the boundaries of the analagous beam would be fixed. If the beam is loaded with the longitudinal forces  $pR$  and the cylinder with the pressure  $p$ , the forces generated in the two structures at corresponding points are identical. Intuitively, it was felt that the forces developed in a pressurized ring with angular mismatch would be very nearly the same as the forces developed in the beam of Figure 9b. The only difference, in the case of uniform longitudinal mismatch, would be the "pinching effect" of the pressure acting against the mismatch. This effect is small. A linear analysis of the two structures yielded solutions which did differ only by the "pinching effect."

A non-linear numerical analysis was made of the analagous beam of Figure 9b in order to determine the forces generated by longitudinal angular mismatch. A set of deflections was assumed for a discrete

number of node points along the beam and the moments generated by the longitudinal forces acting through the deflections was computed. The deflections resulting from the moments were then determined at each node point and compared with the assumed deflections. This procedure was repeated until the assumed and computed deflections agreed at every node. The converged answer is the correct answer to the problem. The analysis was made by well known numerical techniques that can be found in most texts on numerical analyses.

The magnitude and distribution of secondary stresses developed by an angular mismatch at a longitudinal weld are shown in Figure 10. The stresses are for the particular geometry indicated on the Figure. The dominant stress is the circumferential bending stress which is maximum at the apex of the cusp. The shear stresses are small and will not be taken into account in the computation of flaw size correction factors.

The flaw size correction factors computed at the apex of the cusp are shown for three different motor casings in Figures 11, 12, and 13. The correction factors are computed using the maximum moment stresses in the outside fibres of the casing wall.

### 3.3 SPHERICAL HEADS

3.3.1 Girth Welds: The method of analysis of angular mismatch at girth welds in spherical heads was identical to the method described in connection with angular mismatch at girth welds in cylinders (Section 3.2.1). It is wished to do some final

checking of the results before they are reported. Sample results are presented for one motor case in Figure 5.

3.3.2 Gore Welds: Because of the uniform geometry of a sphere, angular mismatch at gore welds gives the same results as does angular mismatch at girth welds. It is recognized that a uniform angular mismatch will never exist in a spherical head. However, it is again suggested that the stresses at the point of maximum sink-in for a non-uniform mismatch will be equal to or less than the stresses in a uniformly mismatched gore weld which contains a sink-in equal to the maximum sink-in of the non-uniform mismatch. Hence, the same flaw size correction factor will be given for angular mismatch at both girth and gore welds in spherical heads.

#### 4. RADIAL MISMATCH

##### 4.1 Assumptions

In the analysis of radial mismatch, it will be assumed that

- 1) the Kirchoff assumption is valid,
- 2) radial mismatch results only in an offset of the middle surface of the shell and does not change the geometry of the joined shell segments, i.e., cylinders remain cylindrical and spheres remain spherical.

The first assumption reduces the radial mismatch problem to one of two dimensions so that the usual two dimensional shell theory can be applied.

The second assumption permits a general solution which is applicable to any motor casing. In motor casings, welds are used to join theoretically perfect cylindrical or spherical segments. If any radial mismatch is introduced at the weld, the joined segments cannot be geometrically perfect. However, the amounts of radial mismatch will be very small in comparison to the radii of the joined segments. The resultant deviations from the assumed geometrically perfect surfaces should normally be slight. Hence, the second assumption seems quite reasonable. If significant geometry changes are introduced by a radial mismatch, each individual problem would have to be separately analyzed.

##### 4.2 Cylindrical Casings

4.2.1 Girth Welds: Consider an axisymmetric internally pressurized shell which has an axisymmetric radial mismatch (Figure 14a).

If the shell is imagined to be cut into two pieces by a plane passing through the mismatched section, it is fundamentally possible to represent the forces at the cut section by equal and opposite shearing forces  $Q$  and equal, opposite, and col-



linear forces  $N$  acting along some unknown line of action (Figure 14b). There is no bending moment. If the longitudinal forces are moved to the middle surfaces of the shell segments, they must be accompanied by the bending moments  $M_1 = Nd$  and  $M_2 = Ng$  (Figure 14c). The two moments  $M_1$  and  $M_2$  differ by an amount  $N\delta$  because of the nonconcurrence of the middle surfaces. This imbalance in moment,  $N\delta$ , will hereafter be called the "mismatch moment."

By writing equations of continuity at the joint, it can be shown (3) that

$$M_1 = \gamma p + \rho_1 N \delta$$

$$M_2 = \gamma p + \rho_2 N \delta$$

where

$$\gamma = \frac{(\beta_{1p} - \beta_{2p})(\delta_{1H} - \delta_{2H}) - (\beta_{1H} - \beta_{2H})(\delta_{1p} - \delta_{2p})}{(\beta_{1H} - \beta_{2H})(\delta_{1M} - \delta_{2M}) - (\beta_{1M} - \beta_{2M})(\delta_{1H} - \delta_{2H})}$$

$$\rho_1 = \frac{\beta_{2M}(\delta_{1H} - \delta_{2H}) - \delta_{2M}(\beta_{1H} - \beta_{2H})}{(\beta_{1H} - \beta_{2H})(\delta_{1M} - \delta_{2M}) - (\beta_{1M} - \beta_{2M})(\delta_{1H} - \delta_{2H})} \quad (4)$$

$$\rho_2 = \frac{\beta_{1M}(\delta_{1H} - \delta_{2H}) - \delta_{1M}(\beta_{1H} - \beta_{2H})}{(\beta_{1H} - \beta_{2H})(\delta_{1M} - \delta_{2M}) - (\beta_{1M} - \beta_{2M})(\delta_{1H} - \delta_{2H})}$$

The subscripts 1 and 2 relate the subscripted quantities to the two different shell segments of Figure 14.

Since the shell geometry is assumed to be symmetrical with respect to the mismatched seam, it can be shown that

$$\gamma = 0 \quad (5)$$

$$|\rho_1| = |\rho_2| = 1/2$$

and the moments  $M_1$  and  $M_2$  take on the value

$$|M_1| = |M_2| = \frac{N\delta}{2} \quad (6)$$

A further consequence of the assumed symmetry of shell geometry is that the change in membrane force  $N$  which is caused by the radial mismatch is zero at the mismatched section. Hence, the value of  $N$  in Equation 6 can be taken as the membrane solution value of  $N\phi$ .

In general, circumferential radial mismatch will not be axisymmetric. However, the assumption of insignificant geometry change leads to the following result: if the amount of radial mismatch at any location on the non-axisymmetrically mismatched joint is  $\delta_x$ , the value of the moments  $M_1$  and  $M_2$  will be  $N\phi\delta_x / 2$  at that particular location.

The secondary forces developed by radial mismatch are distributed to the adjacent shell segments in which they attenuate to zero. A solution (4) is available for the attenuation of the forces near a axisymmetrically mismatched circumferential weld. A solution could be developed for non-axisymmetric mismatch by means of a Fourier Series analysis. However, the latter solution has not been undertaken.

The theoretical distribution of longitudinal bending moments

4.2.1 (cont'd)

developed by a axisymmetric radial mismatch is included in Figure 15. It can be seen that the peak moments occur at the mismatched weld and that the weld is located in an area of rapidly varying secondary stress. It is recognized that the peak moments computed for the idealized mismatch of Figure 1 will seldom, if ever, be realized in an actual vessel. Actual mismatches will not be as abrupt as that shown in Figure 1. However, it is conservative to use the theoretical peak moments in computing flaw size correction factor. Hence, the peak moments will be used in this appendix in the flaw size correction factor determination. Furthermore, it appears appropriate to assume that the peak secondary moments are constant over the total width of nugget and heat affected zone.

Computations have shown that stresses developed by secondary forces other than the bending moments are small. For example, if

$$\begin{aligned} R &= 130 \text{ in.} \\ t &= 0.75 \text{ in.} \\ \delta &= 0.10 \text{ in} \\ p &= 760 \text{ p.s.i.} \end{aligned}$$

the maximum bending and shearing stresses are

$$\sigma_{\text{bending}} = 26,300 \text{ psi}$$

$$\tau_{\text{shear}} = 430 \text{ psi}$$

Hence, account will be taken of only the secondary bending moments and primary membrane solution forces in computing flaw size correction factors.

4.2.1 (cont'd)

For cylindrical casings, N will be set equal to the membrane value of  $pR/2$ . The maximum value of the longitudinal bending moment is then  $pR\delta/4$  where  $\delta$  is the value of the radial mismatch at the section under investigation. The resulting circumferential bending moment is  $\mu pR\delta/4$ . The maximum longitudinal and circumferential stresses occur in the extreme fibers of the casing wall and are given by the expressions

$$\sigma_{\phi} = \frac{pR}{2t} + \frac{3\delta}{2t^2} \cdot pR \quad (7)$$

$$\sigma_{\theta} = \frac{pR}{t} + \frac{3\mu\delta}{2t^2} \cdot pR$$

The corresponding flaw size correction factors are

$$\begin{aligned} A_{K\phi} &= \left\{ 1 + \frac{3\delta}{t} \right\}^2 \\ A_{K\theta} &= \left\{ 1 + \frac{3\mu\delta}{2t} \right\}^2 \end{aligned} \quad (8)$$

Equations 8 are plotted in Figure 16.

The above flaw size correction factors are conservative values since they are based on the maximum stresses which occur in the extreme fibers of the vessel wall.

The attenuation of the values of the longitudinal flaw size correction factors in an axisymmetrically mismatched cylinder is illustrated in Figure 17.

4.2.2 Longitudinal Welds: The same assumptions and reasoning that were used in the stress analysis of mismatched circumferential welds have been used in the stress analysis of mismatched longitudinal welds. The value of  $N$  was taken as the membrane solution value of  $N_0$  which equals  $pR$ . The value of the moments  $M_1$  and  $M_2$  become  $pR\delta/2$  where  $\delta$  is the value of radial mismatch at the section under consideration. The resulting longitudinal bending moment is given with sufficient accuracy by  $\mu pR\delta/2$ . Hence, the maximum circumferential and longitudinal stresses in the case are

$$\sigma_\theta = \frac{pR}{t} + \frac{3pR\delta}{t^2} \quad (9)$$

$$\sigma_z = \frac{pR}{2t} + \frac{3\mu\delta}{t^2} \cdot pR$$

The corresponding flaw size correction factors are

$$A_{k\theta} = \left\{ 1 + 3\frac{\delta}{t} \right\}^2 \quad (10)$$

$$A_{k\phi} = \left\{ 1 + 6\mu\frac{\delta}{t} \right\}^2$$

Equations 10 are plotted in Figure 18.

A study of the attenuation of the circumferential secondary bending moments was made in (5). Solutions were derived for longitudinally mismatched cylinders with simply supported ends. However, if the mismatch is located sufficiently far away from the end support, the end support condition should not have a great deal of effect on the solution.

### 4.3 Spherical Heads

4.3.1 Girth Welds: The analysis of radially mismatched girth welds in spheres is very similar to the analysis described for radially mismatched girth welds in cylinders. If the head is imagined to be cut at the mismatch, the force system on the cut faces can be represented as in Figure 14a or 14b. If one uses the simplified theory for spherical shells (4), it is found that

$$|M_1| = |M_2| = \frac{N\delta}{2} \quad (11)$$

which is the same result as that which was derived for cylindrical shells.

The ratio of  $(R/t)$  for the heads of large rocket motor casings is very large. The simplified theory of spherical shells gives very accurate results for such heads, even near the crown of the heads. Hence, equation 11 is valid for all girth welds which do not fall within the area of influence of the Y ring or nozzle adapter ring.

The value of  $N$  is the membrane solution value of  $pR/2$ . The absolute value of the moments  $M_1$  and  $M_2$  is then  $pR\delta/4$ . The corresponding circumferential moment is  $\mu pR\delta/4$ . Ignoring the effects of shearing forces and changes in the in-plane forces of the stress state, the maximum meridional and circumferential stresses at the mismatched girth weld are

$$\sigma_\phi = \frac{pR}{2t} + \frac{3pR\delta}{2t^2} \quad (12)$$

$$\sigma_\theta = \frac{pR}{2t} + \frac{3\mu pR\delta}{2t^2}$$

#### 4.3.1 (cont'd)

The corresponding flaw size correction factors are

$$A_{\kappa\phi} = \left\{ 1 + 3 \frac{\delta}{t} \right\}^2 \quad (13)$$

$$A_{\kappa\theta} = \left\{ 1 + 3\mu \frac{\delta}{t} \right\}^2$$

Equations 13 are plotted in Figure 16.

4.3.2 Gore Welds: Using the simplified type of analysis described herein, the analysis of the secondary moments developed by mismatched gore welds is identical to the same analysis for girth welds. The resulting flaw size correction factors for mismatched gore welds is

$$\begin{aligned} A_{\kappa\theta} &= \left\{ 1 + 3 \frac{\delta}{t} \right\}^2 \\ A_{\kappa\phi} &= \left\{ 1 + 3\mu \frac{\delta}{t} \right\}^2 \end{aligned} \quad (14)$$

Equations 14 are plotted in Figure 18.

5. ANALYSIS OF GEOMETRIC DISCONTINUITIES ADJACENT TO Y-RING

When radial and angular mismatch occur adjacent to a Y-Ring, the combined effects of Y-Ring discontinuity and geometric discontinuity must be determined. Combined effects analysis were made in the usual manner. The Y-Rings were cut into a number of segments and the shears and moments on the cut faces were taken as the unknowns for which the solution was to be conducted. Equations of equilibrium and continuity were written for each joint and the resulting sets of simultaneous linear algebraic equations were solved for the unknown forces. Two-dimensional theory was used in all solutions, i.e., it was assumed that plane sections remain plane and normal to the middle surface. The elemental breakdown scheme for the forward Aerojet 260, Thiokol 260, and Thiokol 156 Y-Rings are included in Figures 19 and 20.

The major difficulty in performing the Y-ring analysis was caused by the unusual loading conditions used in the proof tests. The proof test set-up generates a large tensile stress in the heads of the casings. However, the skirts are loaded with a small compressive force in Aerojet case and it was assumed that the skirts in the Thiokol cases will be unloaded. The large differences in skirt and head forces creates a large moment at the junction of the head, skirt and thickened portion of the Y-Ring. It is recognized that the use of two-dimensional theory will result in some inaccuracies in the analysis at the above mentioned junctions. However, a three dimensional elasticity solution of the junction is prohibitively difficult. Hence, two-dimensional theory was used in the analysis described herein. A knowledge of the stress level that are developed in the junction area can best be determined from measurements of strain during proof test.



5. (cont'd)

An analysis was conducted to determine the effects, on stress, of plate delamination near a weldment. The delaminations were assumed to occur only in the parts of the casings which are to be fabricated from plate stock. The locations and magnitudes of the assumed delaminations are illustrated in Figures 19 and 20. The flaw size correction factors determined for combined delamination and radial mismatch at both head to Y-ring and shell to Y-ring welds is illustrated for both 260-inch diameter Aerojet and Thiokol casings in Figures 21 through 24 (the solution for the 156-inch diameter Thiokol casing is not complete at this time). The delaminations were assumed to occur at a depth of 0.375 t from the surface of the plate in both Thiokol casings. Analyses showed that delamination at this location resulted in maximum stress in the delaminated material. In the Aerojet casing, solutions were conducted for only mid-plane delaminations. The stress differences between mid-plane and 0.375t delaminations are small. The results show that delaminations can have a significant effect on the flaw size correction factor.

An analysis was conducted to determine the effect, on stress, of angular mismatch at the head to Y-Ring weld in the 260-inch diameter Aerojet casing. The analysis was linear and, hence, overestimates the flaw size correction factors. However, the results are conservative and are presented in Figure 25.

6. SUMMARY

Secondary stresses developed by radial and angular discontinuities at welds in large pressure vessels have been computed. The discontinuities were assumed to occur individually. The combined effects of radial and Y-ring discontinuity and angular and Y-ring discontinuity were determined. An analysis of the effects of delamination in the material adjacent to a Y-ring also was made.

The effect of the secondary stresses on the flaw sizes which can be allowed at the weld locations has been computed.

LIST OF REFERENCES

1. Grafton, P. E., and Strome, D. R., "Analysis of Axisymmetrical Shells by the Direct Stiffness Method", AIAA Journal, Vol. 1, No. 10, October 1963.
2. Turner, M. J., Dill, E. H., Martin, H. C., and Melosh, R. J., "Large Deflection of Structures Subjected to Heating and External Loads," Journal of the Aero/Space Sciences, Vol. 27, No. 1, January 1960.
3. Johns, R. H., and Orange, T. W., "Theoretical Elastic Stress Distribution Arising From Discontinuities and Edge Loads in Several Shell Type Structures", NASA TR R-103, 1961.
4. Timoshenko, S., "Theory of Plates and Shells," Book, McGraw-Hill, 1959.
5. "Large Motorcase Technology Evaluation", Progress Report, Contract AF33(615)-1623, The Boeing Company, December, 1964.

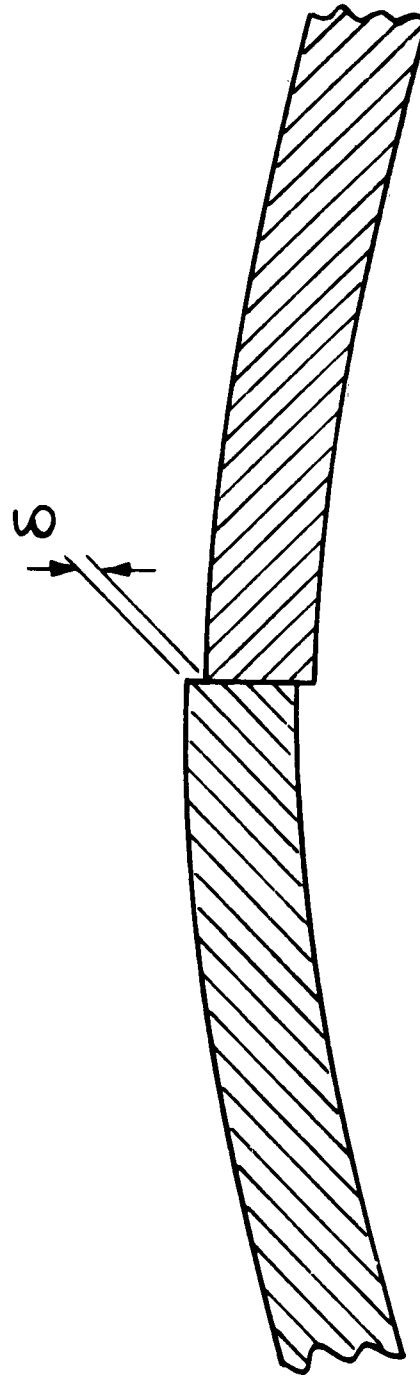
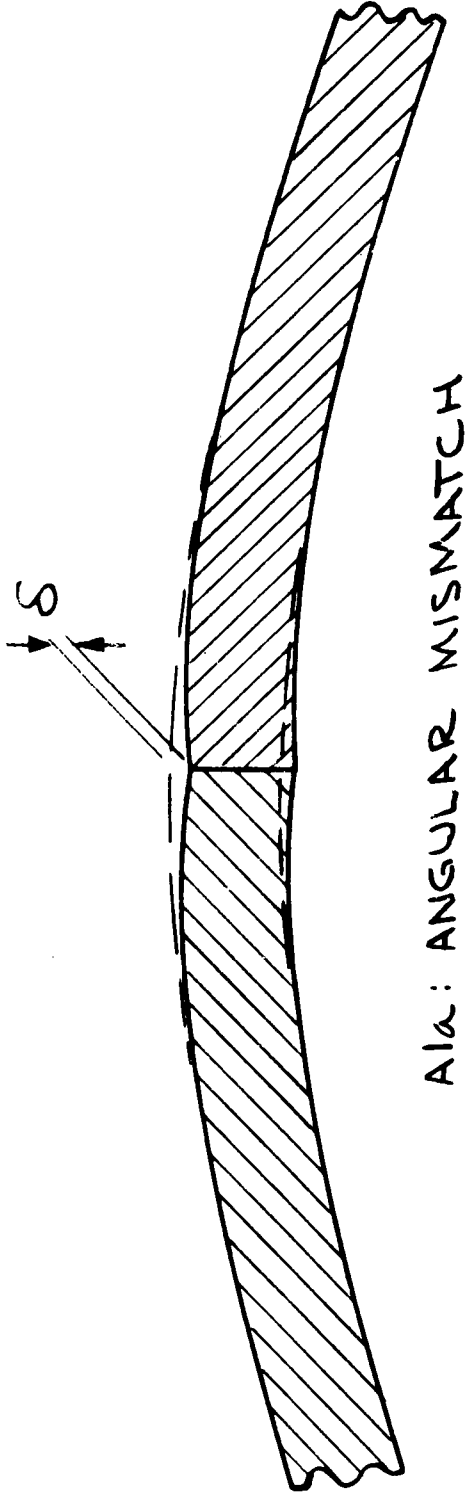


FIG. A1: MISMATCH CONFIGURATIONS

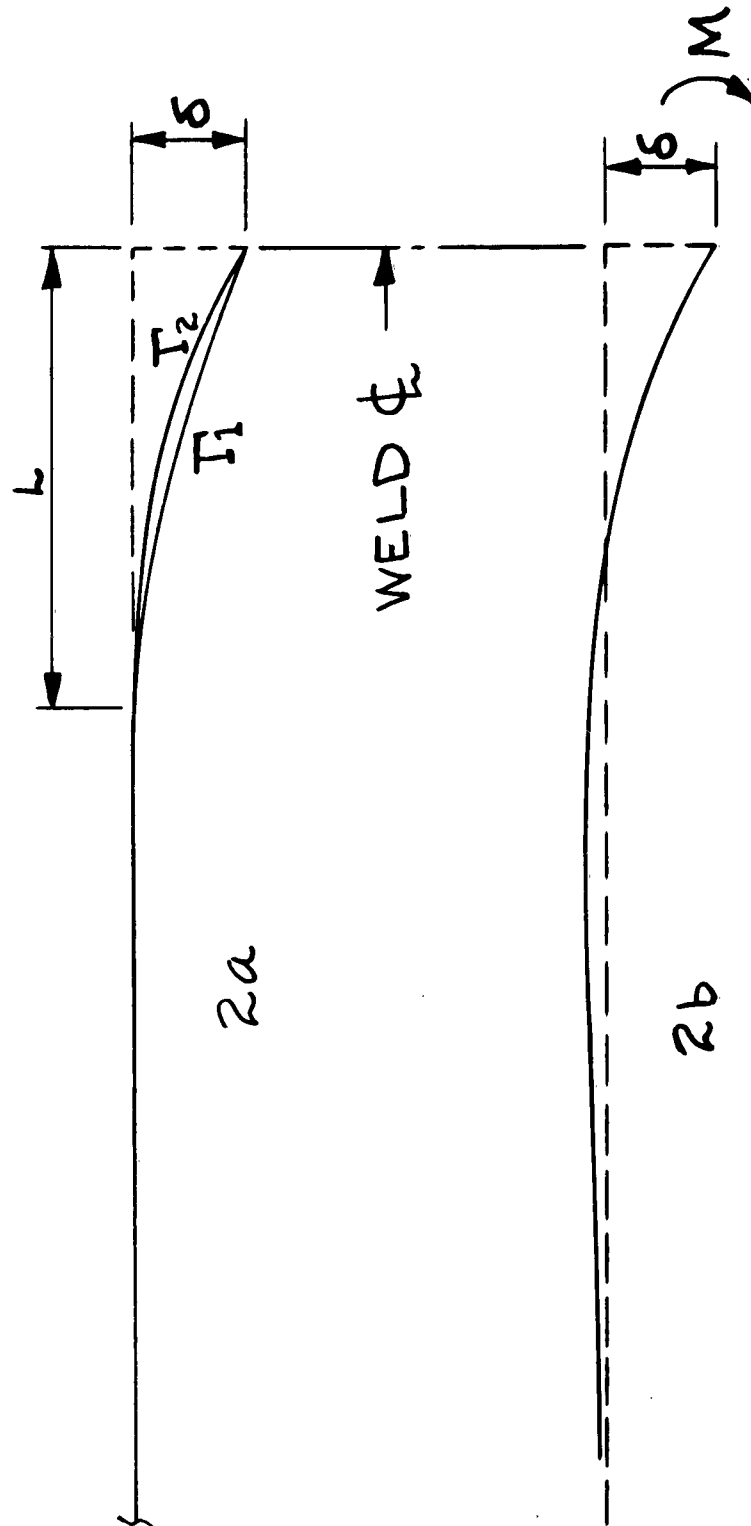


FIG. A2: ANGULAR MISMATCH

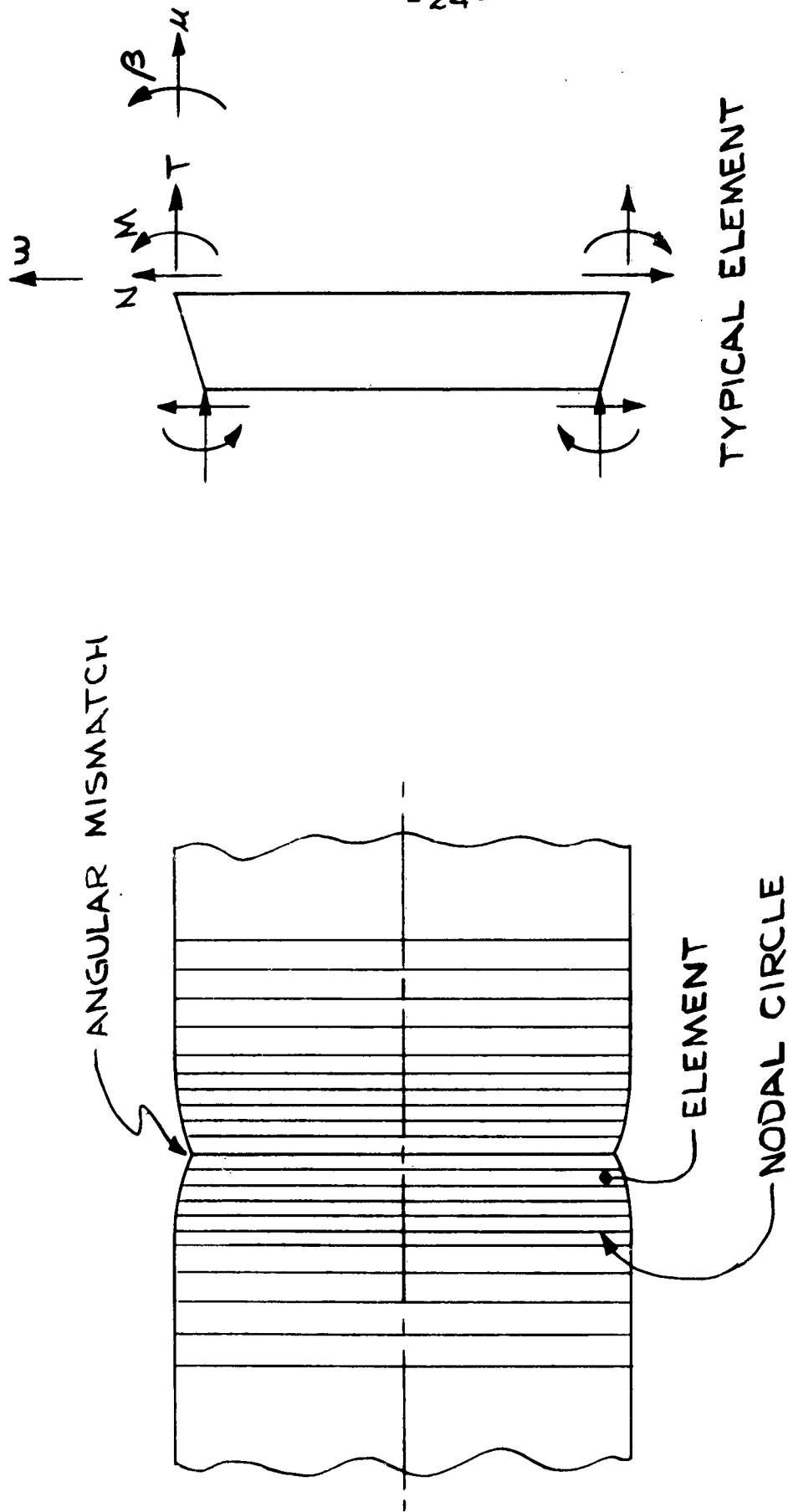


FIG. A3: ELEMENTAL BREAKDOWN OF SHELL WITH ANGULAR MISMATCH

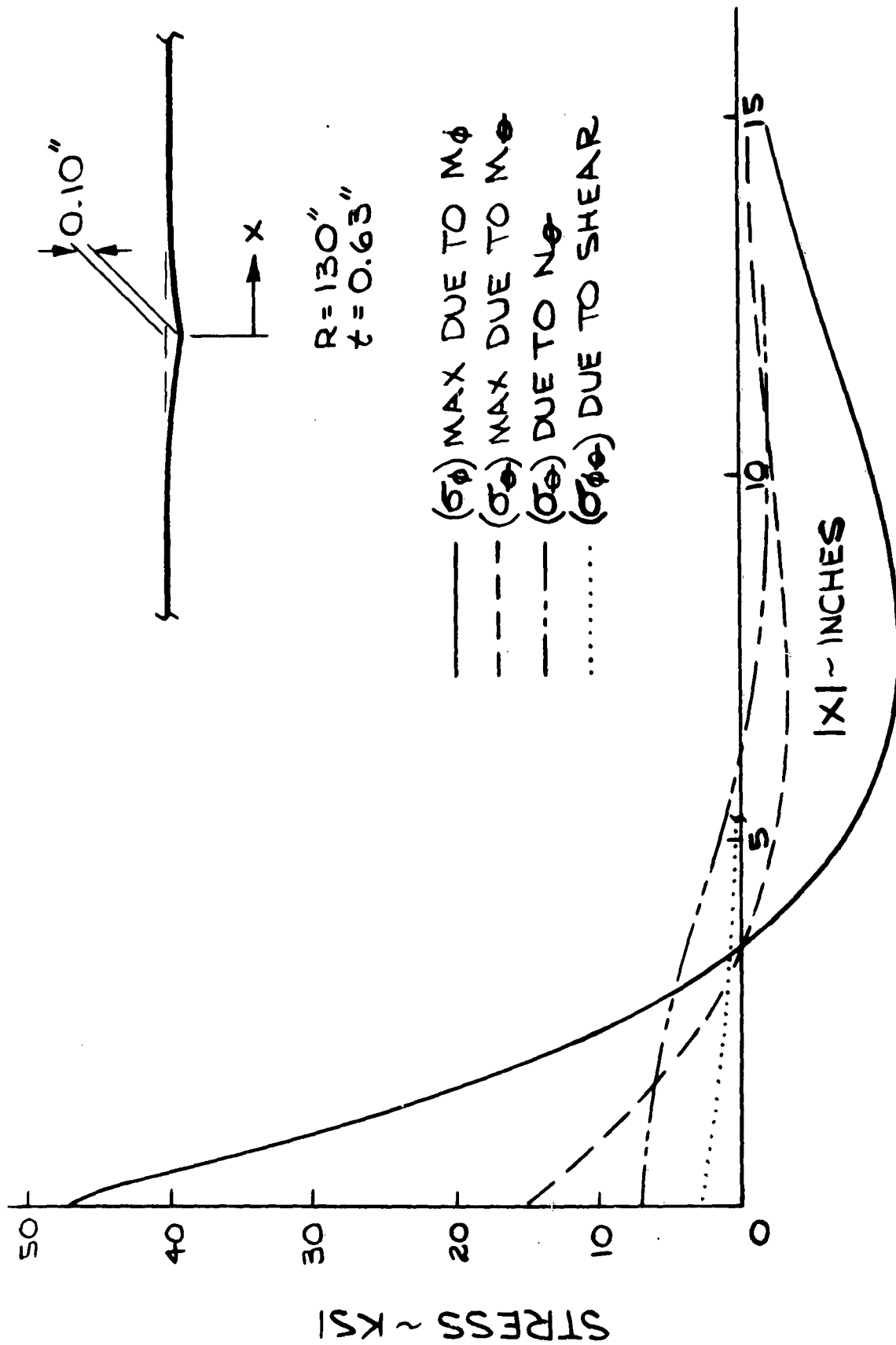


FIG. A4: SECONDARY STRESS DISTRIBUTION DUE TO ANGULAR MISMATCH AT GIRTH WELD IN AEROJET 260 INCH CYLINDER

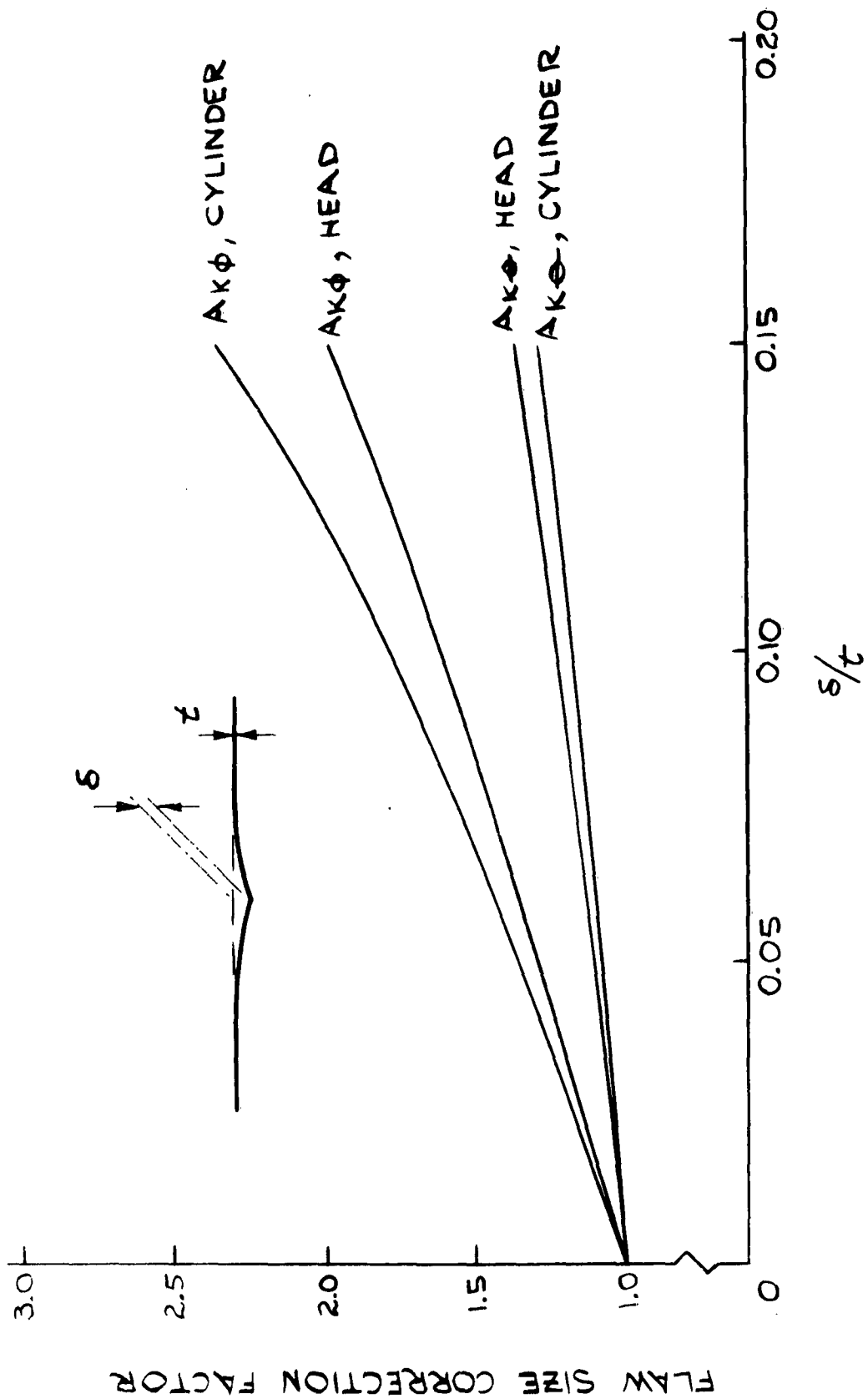


FIG. A5: FLAW SIZE CORRECTION FACTORS, ANGULAR MISMATCH, GIRTH WELDS, AEROJET 260 INCH DIA. CASE



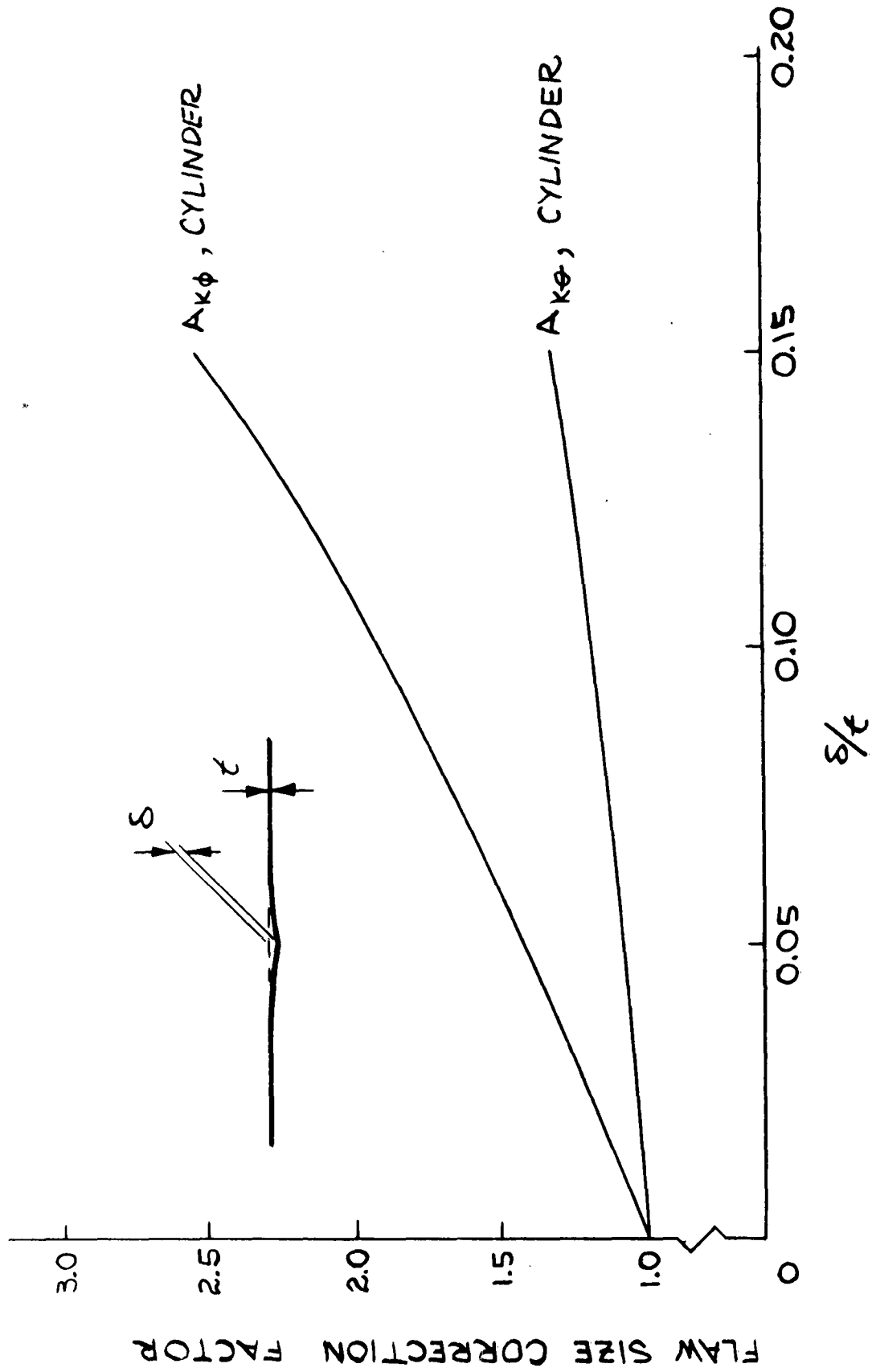


FIG. A6: FLAW SIZE CORRECTION FACTORS, ANGULAR MISMATCH GIRTH WELDS, THIOKOL 260 INCH DIA CASE

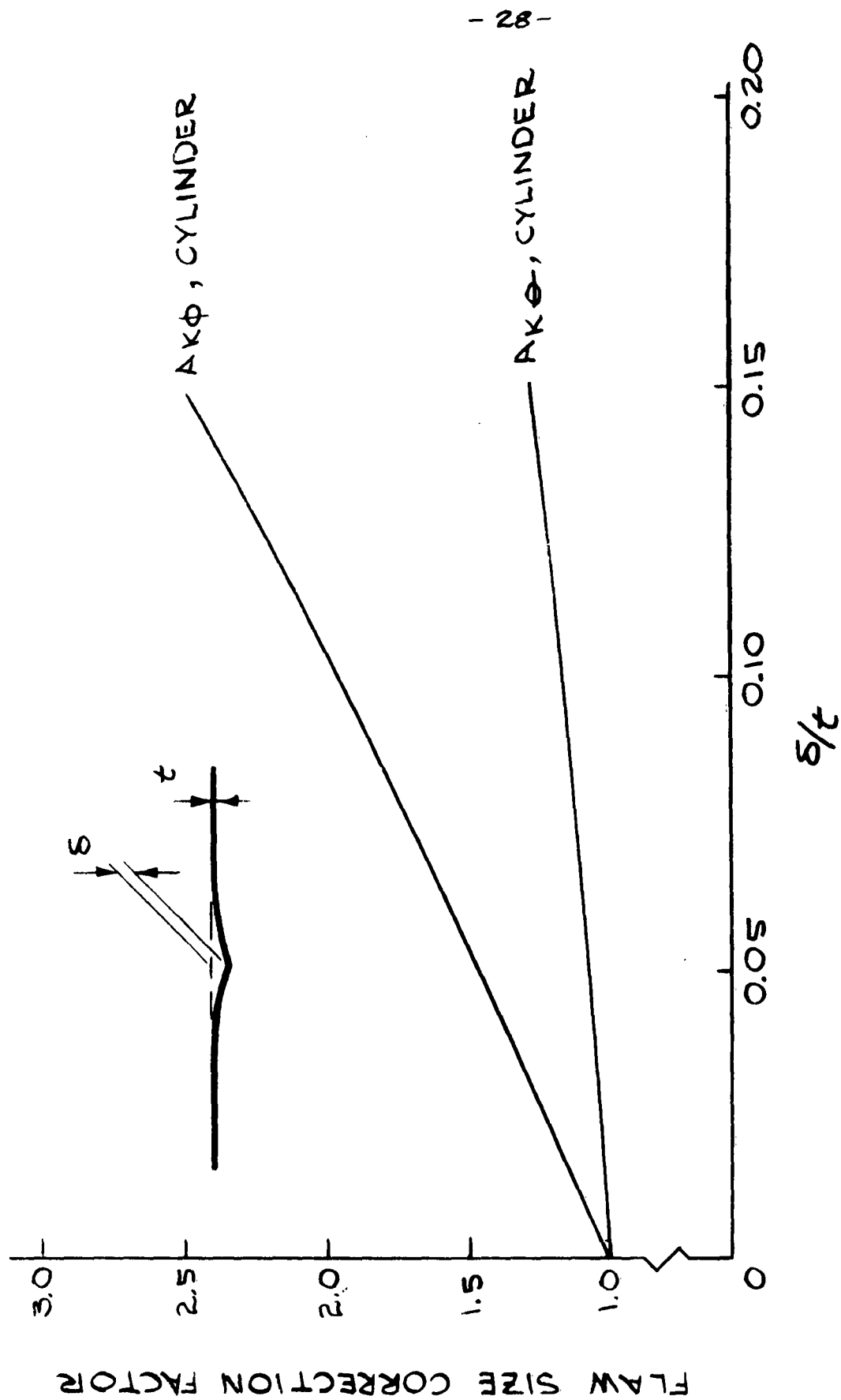


FIG. A7: FLAW SIZE CORRECTION FACTORS, ANGULAR MISMATCH, GIRTH WELDS, THICKOL 156 INCH DIA. CASE

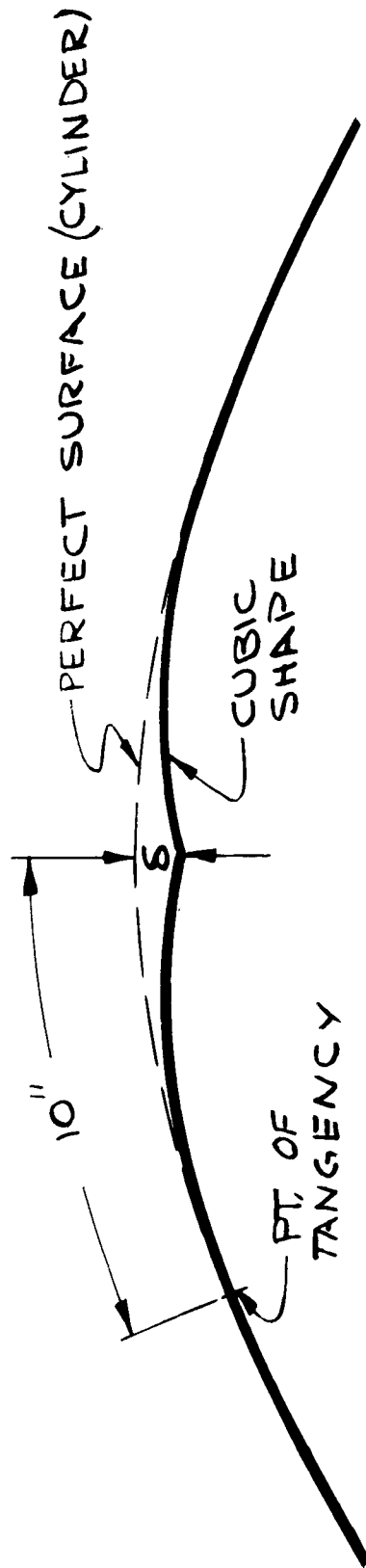


FIG. A8: ANGULAR MISMATCH CONFIGURATION ASSUMED FOR LONGITUDINAL WELDS IN CYLINDERS

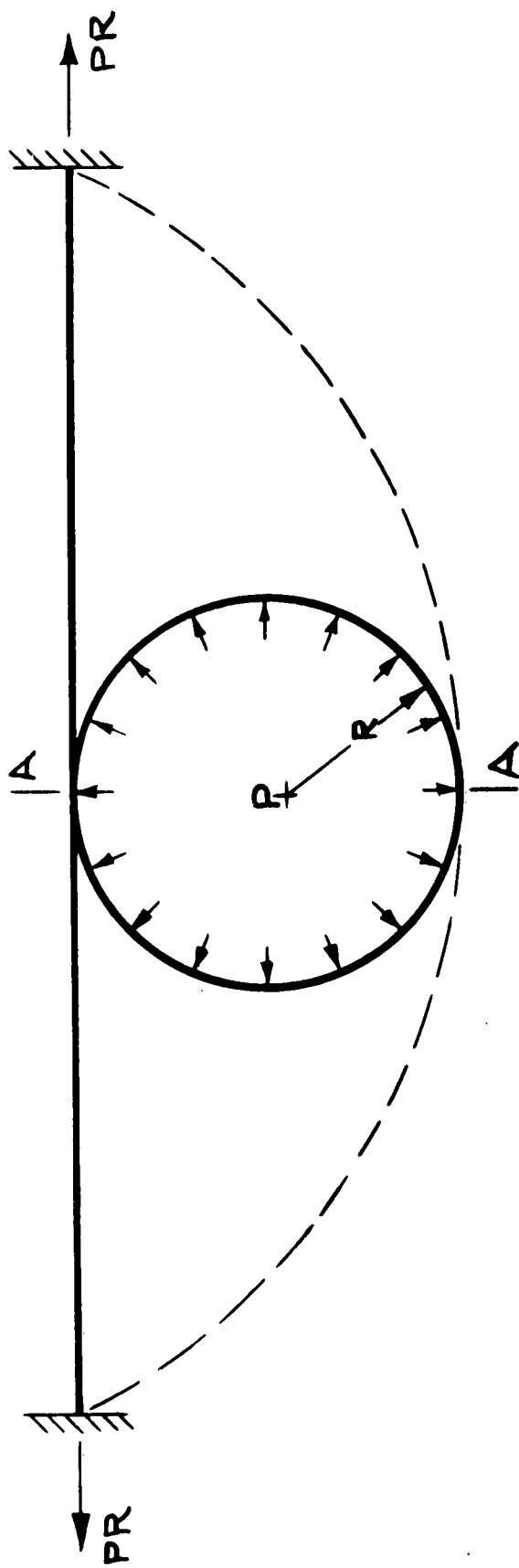


FIG. A9a



FIG. A9b

FIG. A9: LONGITUDINAL ANGULAR MISMATCH ANALYSIS

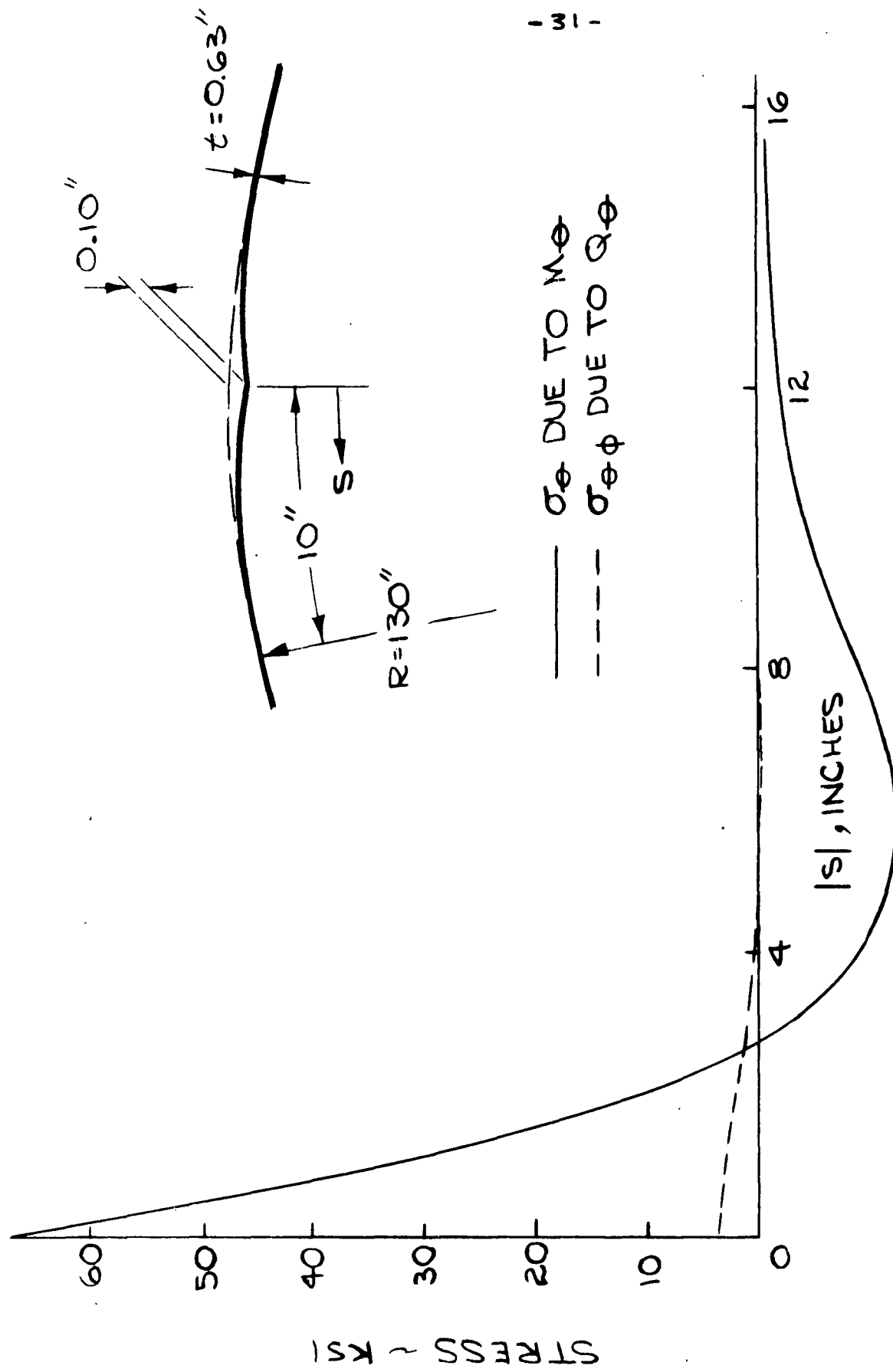
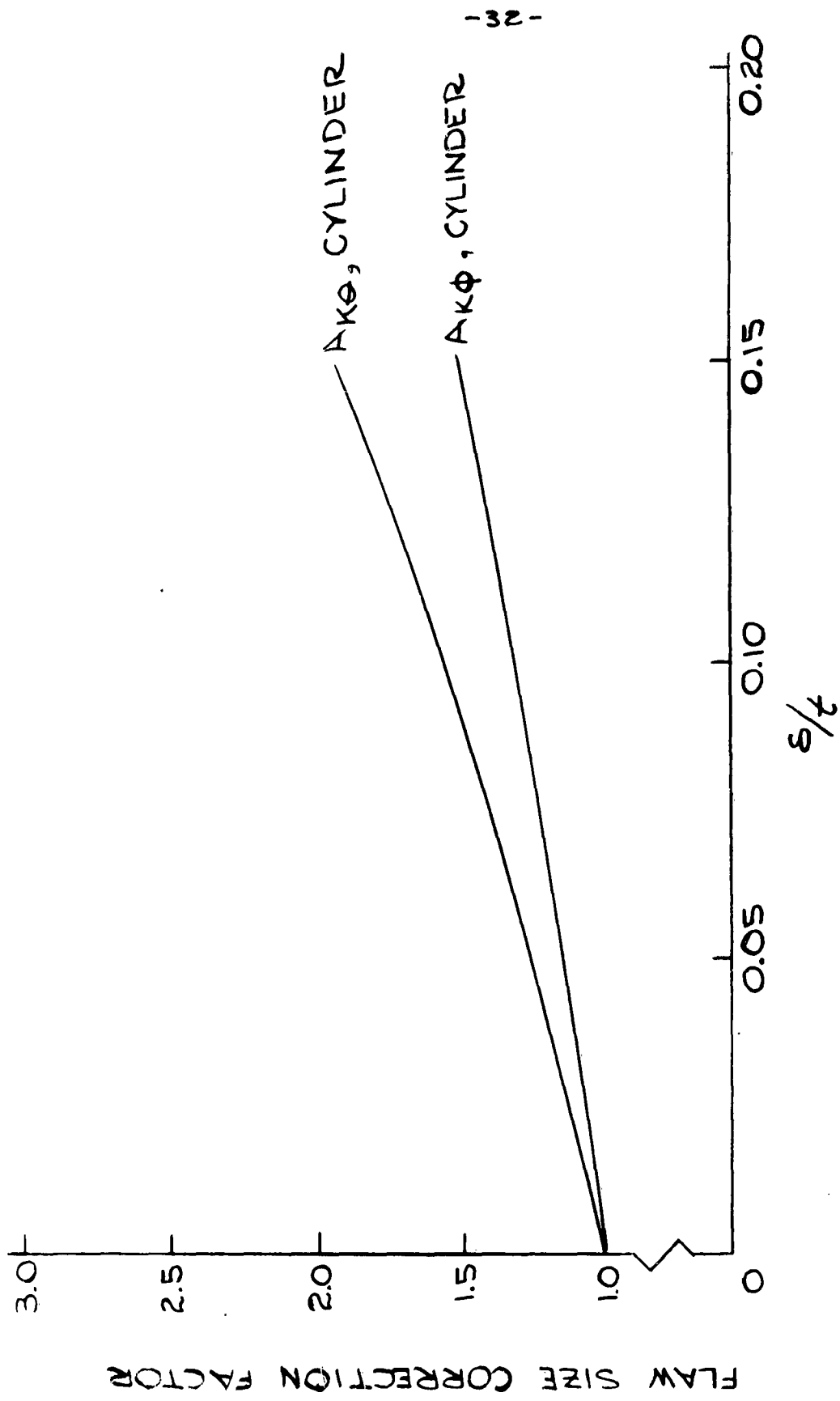


FIG. A10: SECONDARY STRESS DISTRIBUTION DUE TO ANGULAR MISMATCH AT LONGITUDINAL WELD IN AEROJET CYLINDER



- 32 -

FIG. A11: FLAW SIZE CORRECTION FACTORS, ANGULAR MISMATCH, LONGITUDINAL (GORE) WELDS, AEROJET 260 INCH DIA CASE

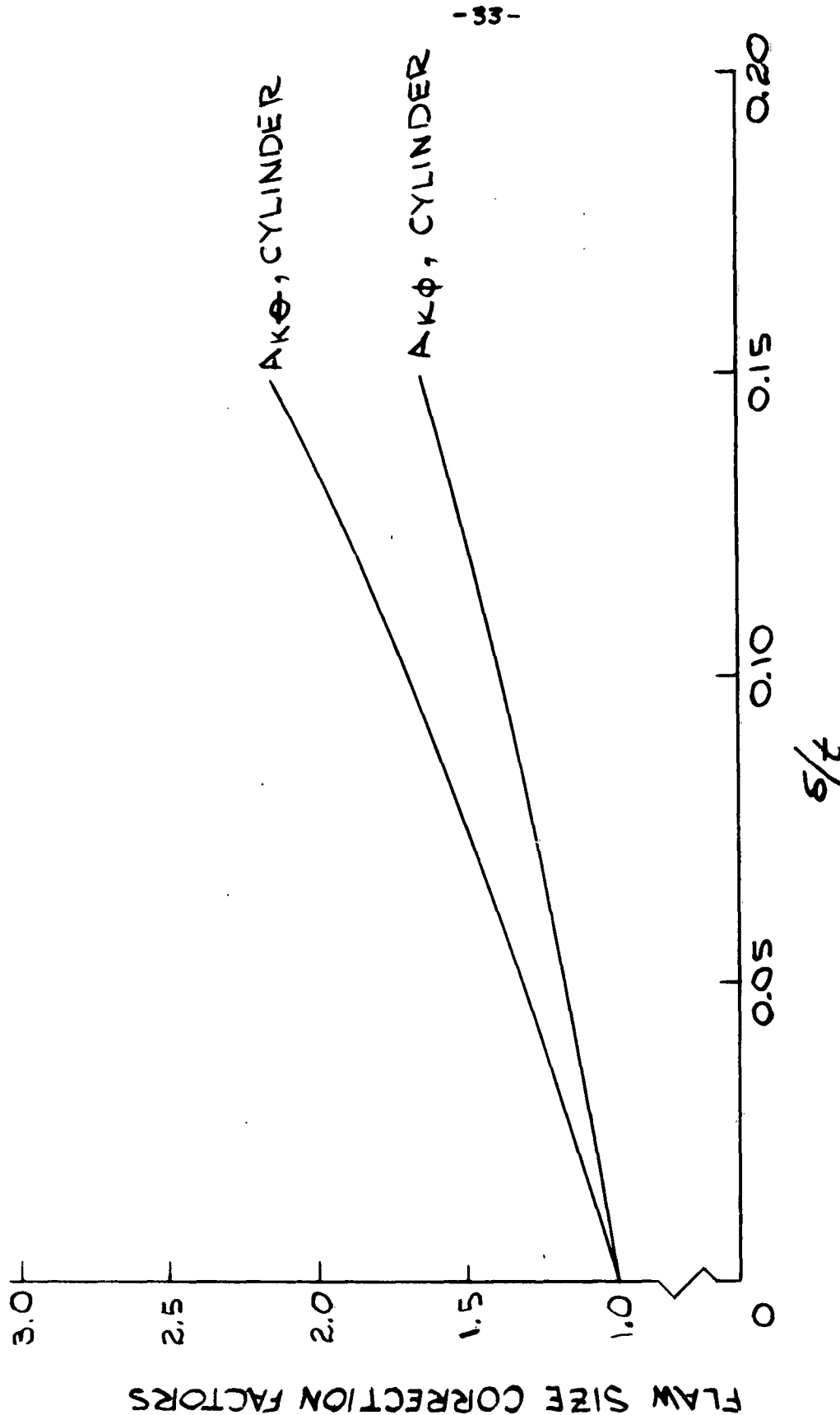
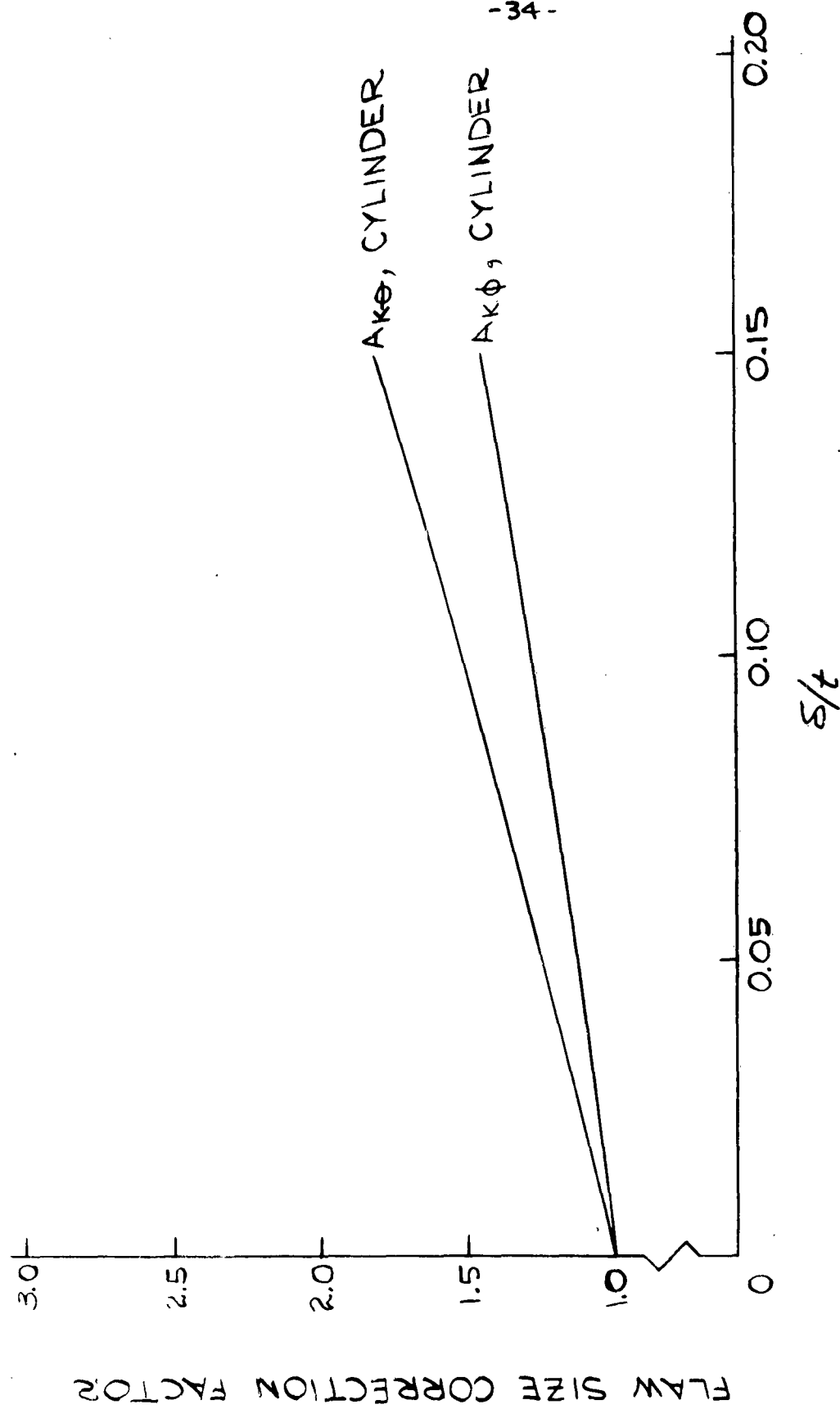


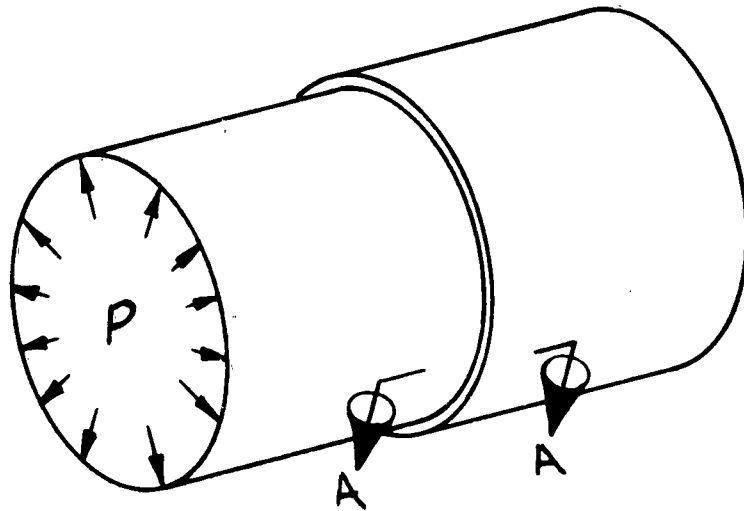
FIG. A12: FLAW SIZE CORRECTION FACTORS, ANGULAR  
MISMATCH, LONGITUDINAL (GORE) WELDS,  
THICKOL 260 INCH DIA. CASE



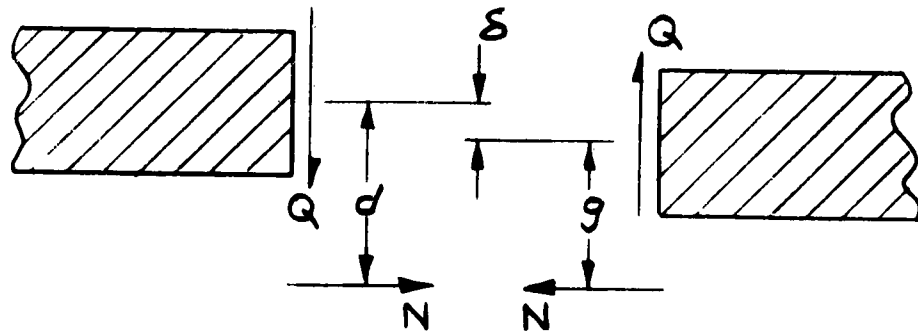
-34-

FIG. A13: FLAW SIZE CORRECTION FACTORS, ANGULAR  
MISMATCH, LONGITUDINAL (GORE) WELDS, THIOKOL  
156 INCH DIA CASE

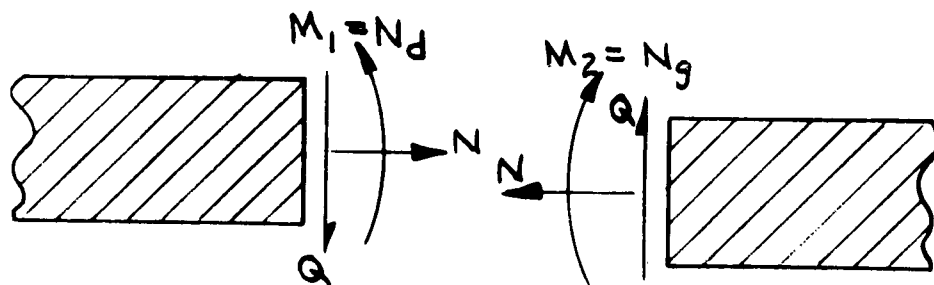




14a



14b



14c

SECTION A-A

FIG. A14: AXISYMMETRIC RADIAL MISMATCH

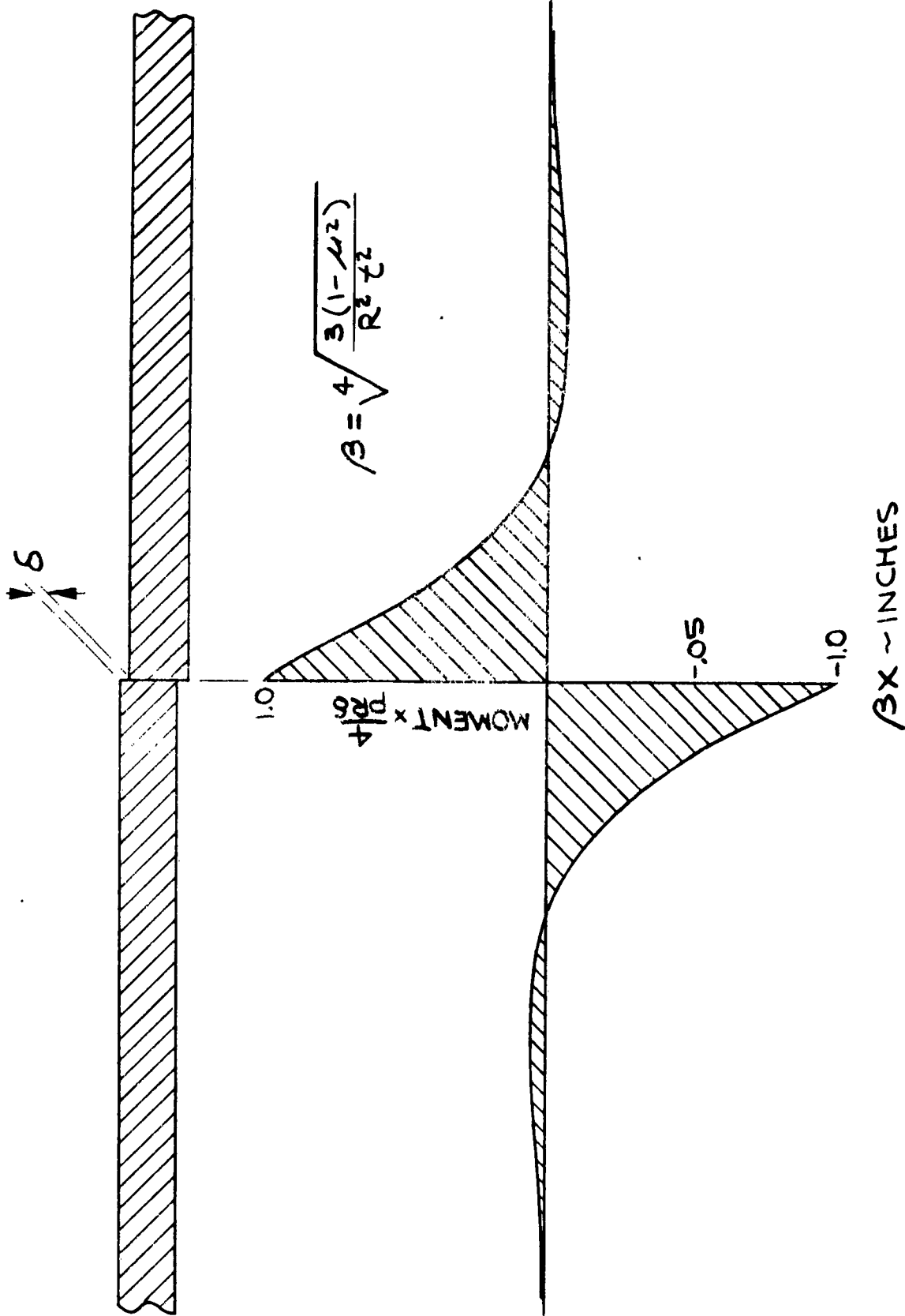


FIG. A15: DISTRIBUTION OF LONGITUDINAL SECONDARY BENDING MOMENT AT AXISYMMETRIC CIRCUMFERENTIAL MISMATCH IN CYLINDERS

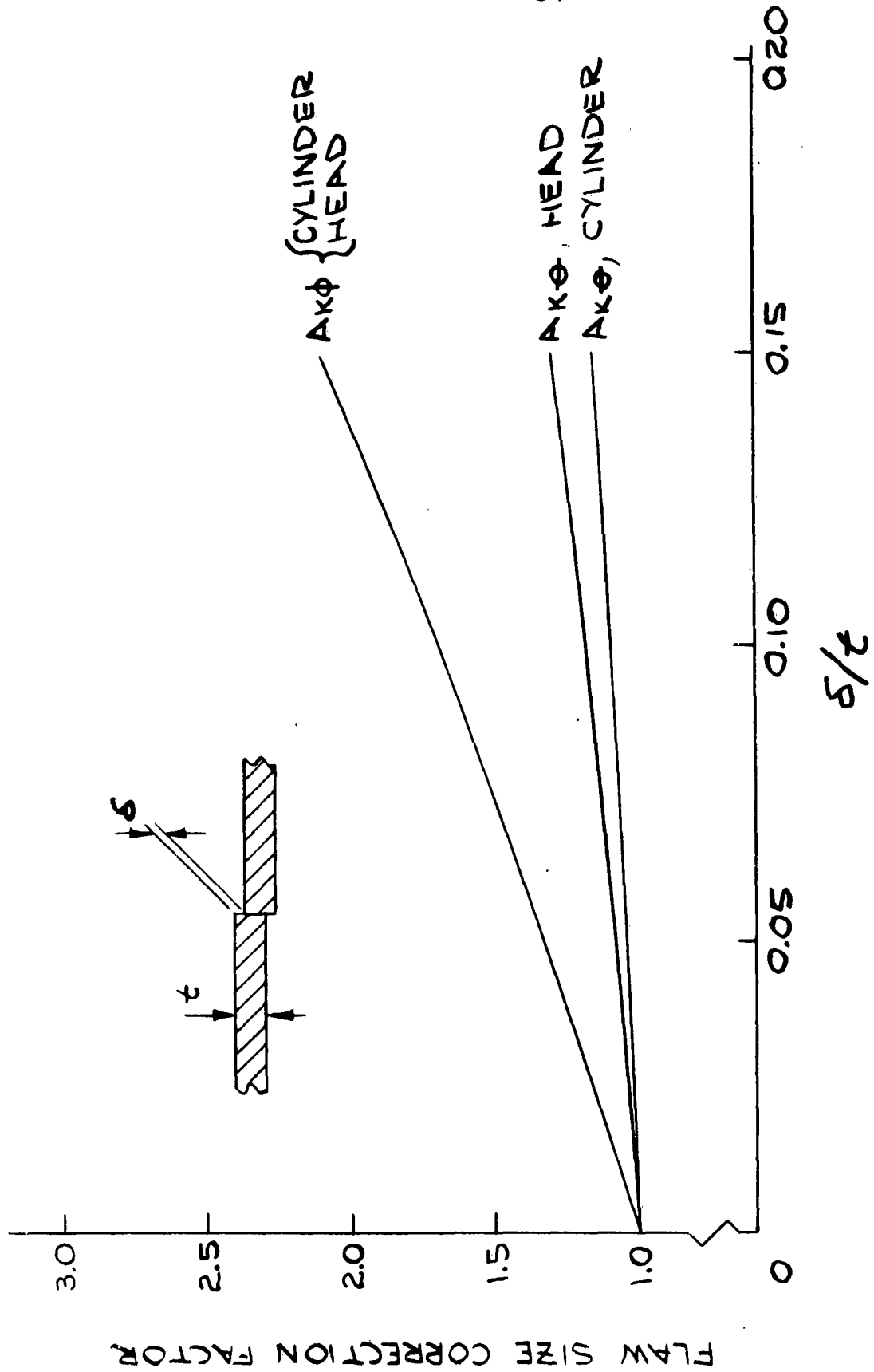


FIG. A16: FLAW SIZE CORRECTION FACTORS, RADIAL MISMATCH AT GIRTH WELDS

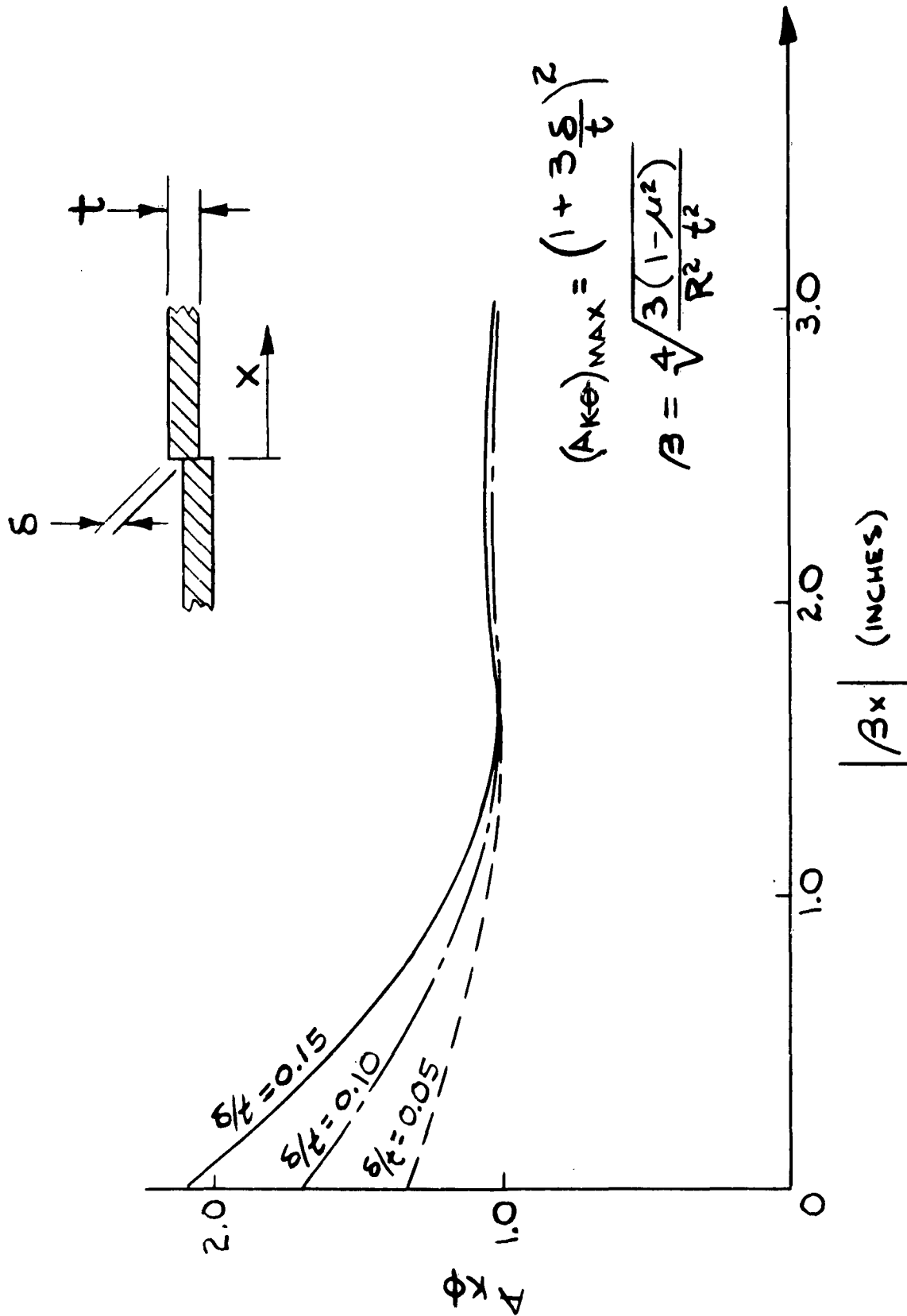


FIG. A17: FLAW SIZE CORRECTION FACTORS FOR CIRCUMFERENTIAL RADIAL MISMATCH IN CYLINDERS

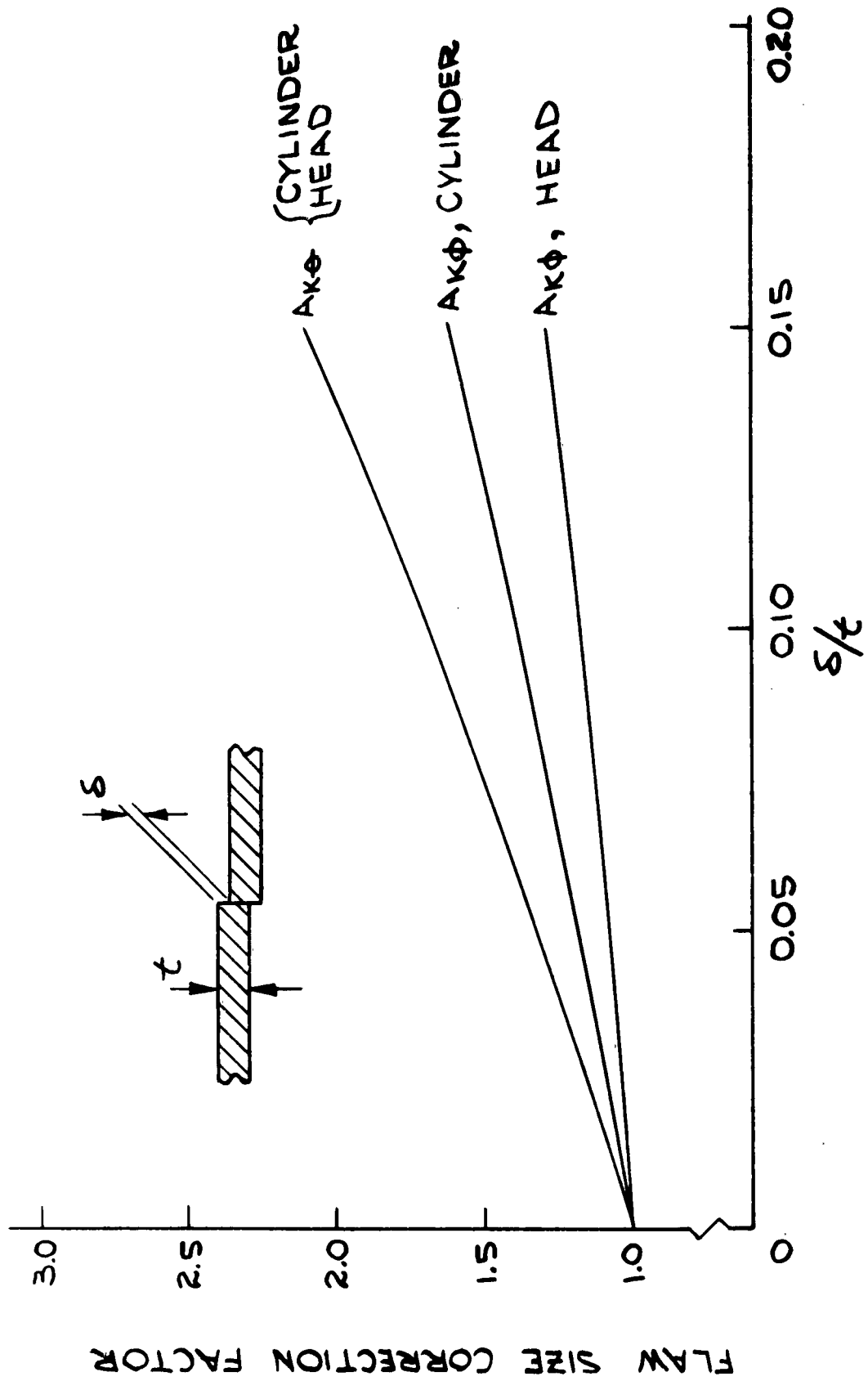
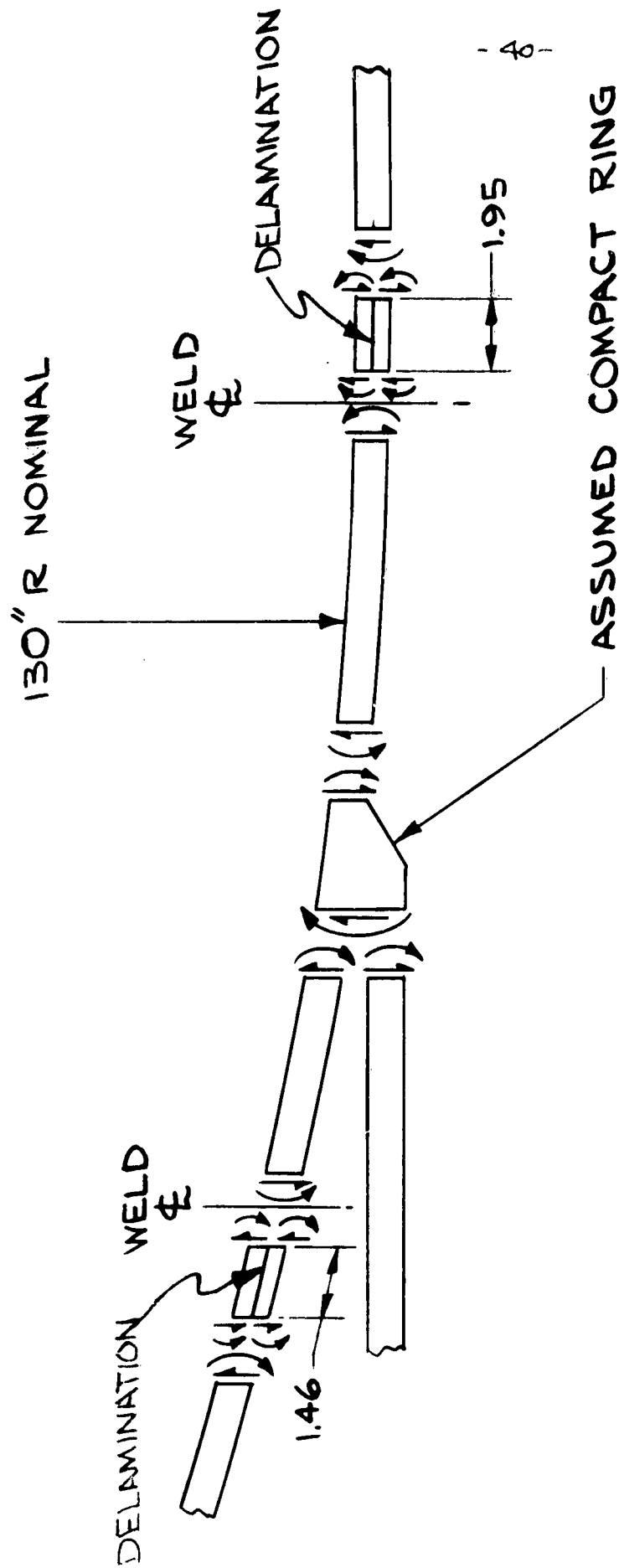
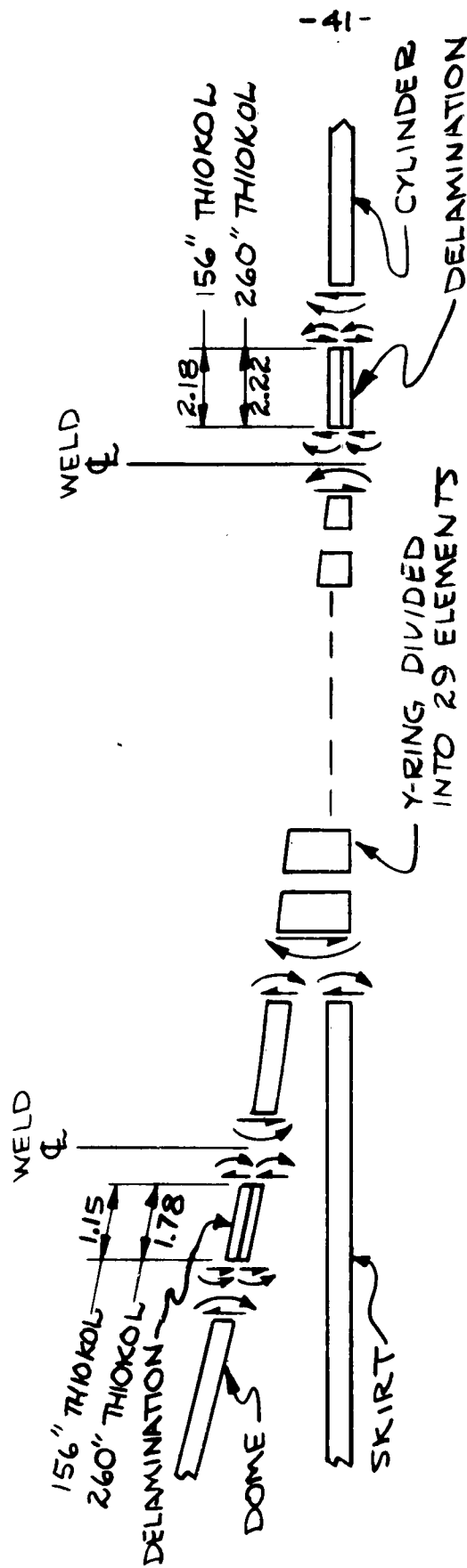


FIG. A18: FLAW SIZE CORRECTION FACTORS, RADIAL MISMATCH AT LONGITUDINAL (GORE) WELDS



A-40

FIG. A19: FORWARD BULKHEAD - Y RING - CYLINDRICAL SHELL  
 CONNECTIONS, DELAMINATED BULKHEAD & CYLINDER,  
 260 SL AEROJET CASE



A-41

FIG. A20: FORWARD BULKHEAD - Y RING - CYLINDRICAL SHELL JUNCTION, DELAMINATED BULKHEAD AND CYLINDER, 260" DIA AND 156" DIA THICKOL CASES

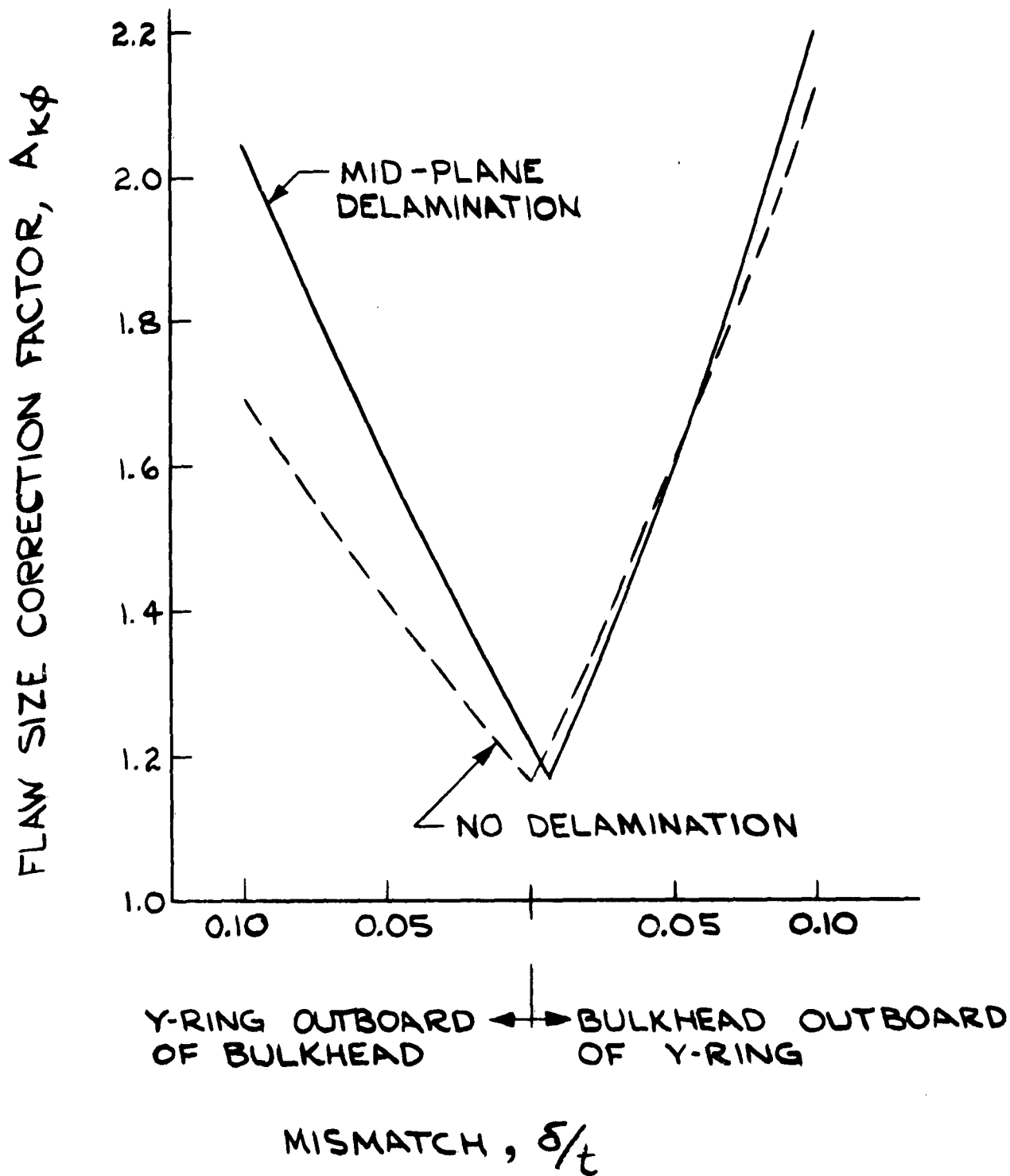


FIG. A21: FLAW SIZE CORRECTION FACTOR FOR BULKHEAD TO Y-RING WELD WITH GROSS DELAMINATION AND MISMATCH, 260 SL AERO JET CASE



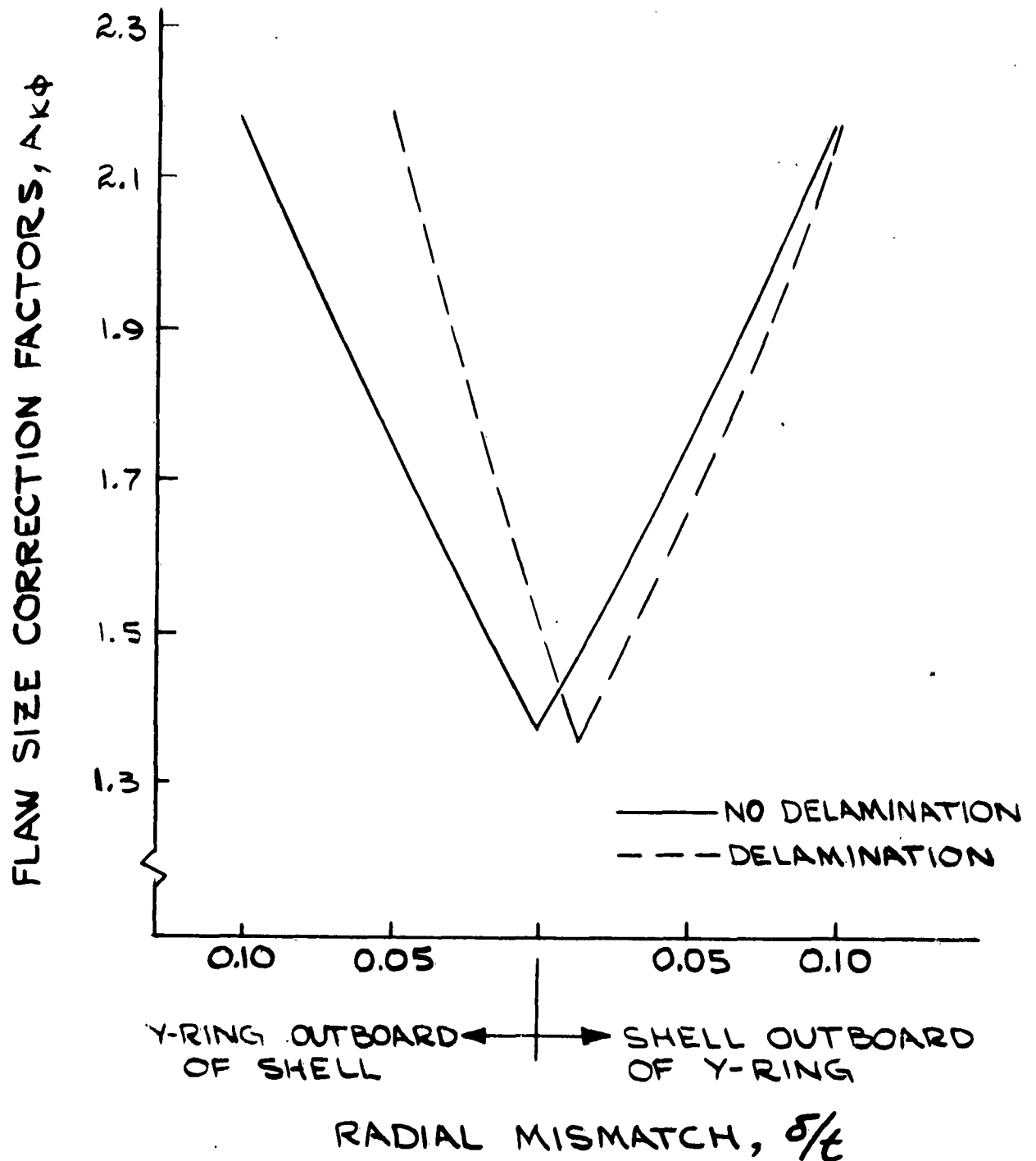


FIG. A22: FLAW SIZE CORRECTION FACTORS, SHELL TO Y-RING WELD, DELAMINATION AND RADIAL MISMATCH, 260 SL AEROJET CASE

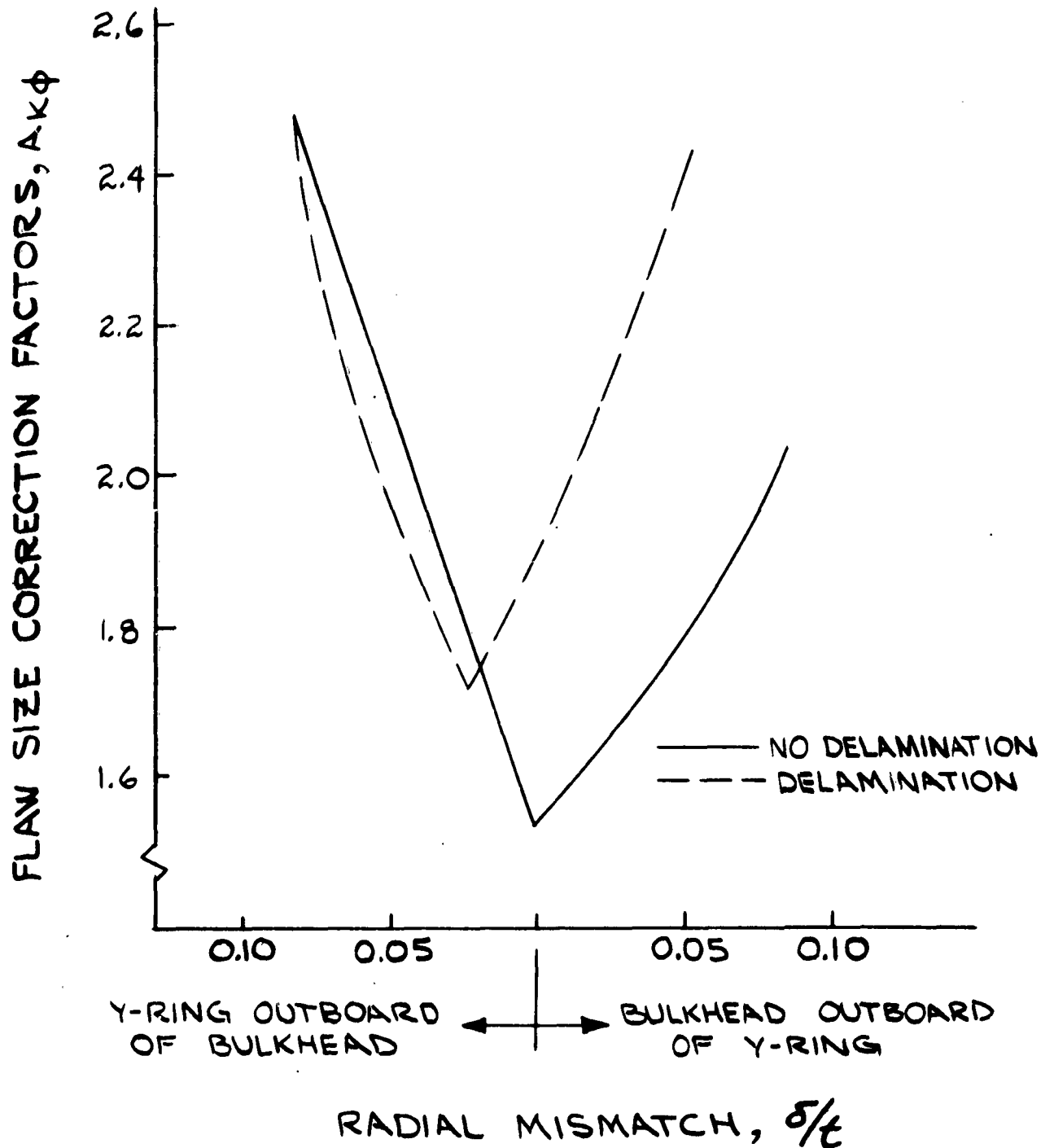


FIG. A23: FLAW SIZE CORRECTION FACTORS  
FOR BULKHEAD TO Y-RING WELD,  
DELAMINATION AND RADIAL MISMATCH,  
260 SL THIOKOL CASE

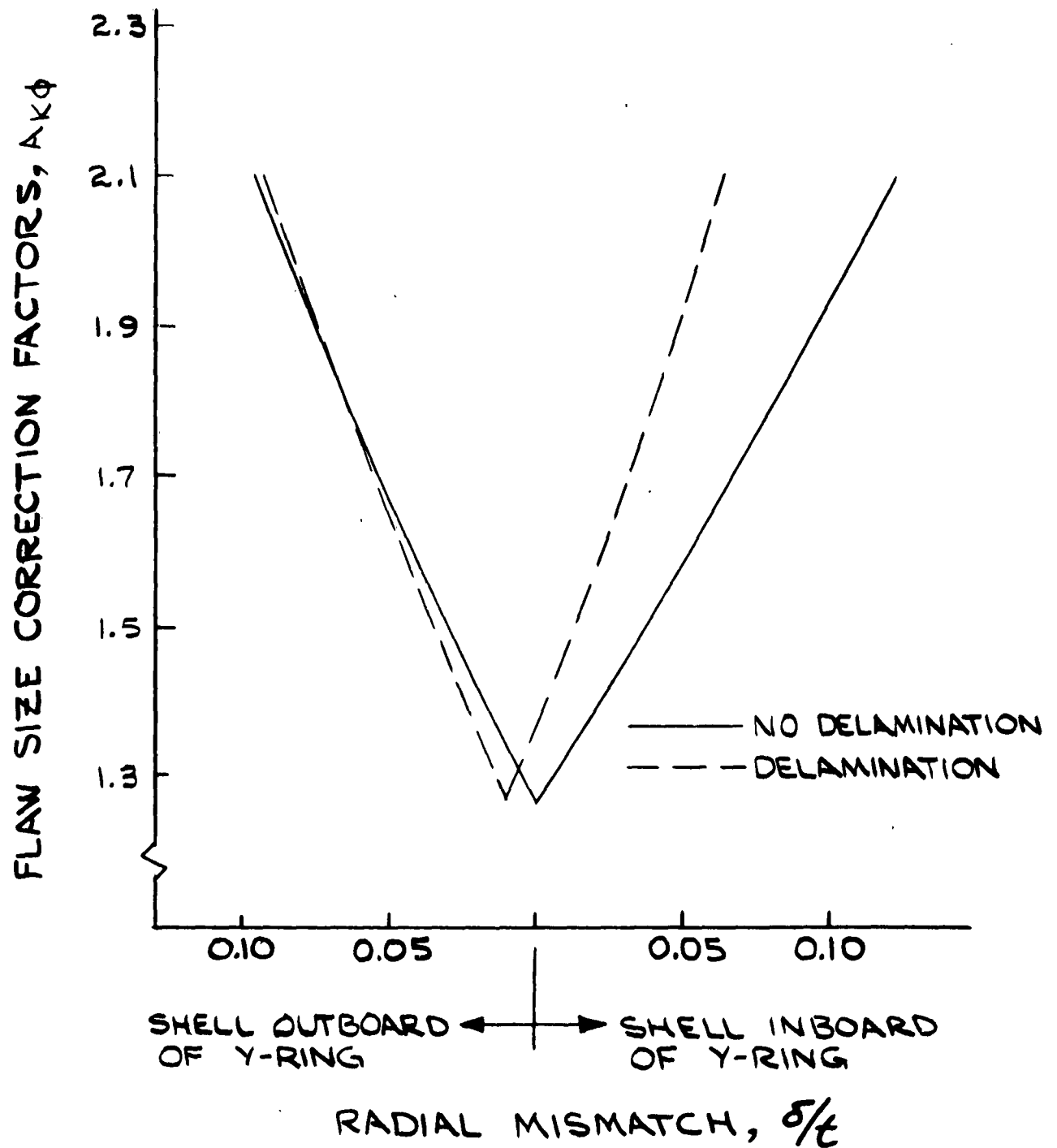


FIG. A24: FLAW SIZE CORRECTION FACTORS, SHELL TO Y-RING WELD, DELAMINATION AND RADIAL MISMATCH, 260 SL THIOKOL CASE

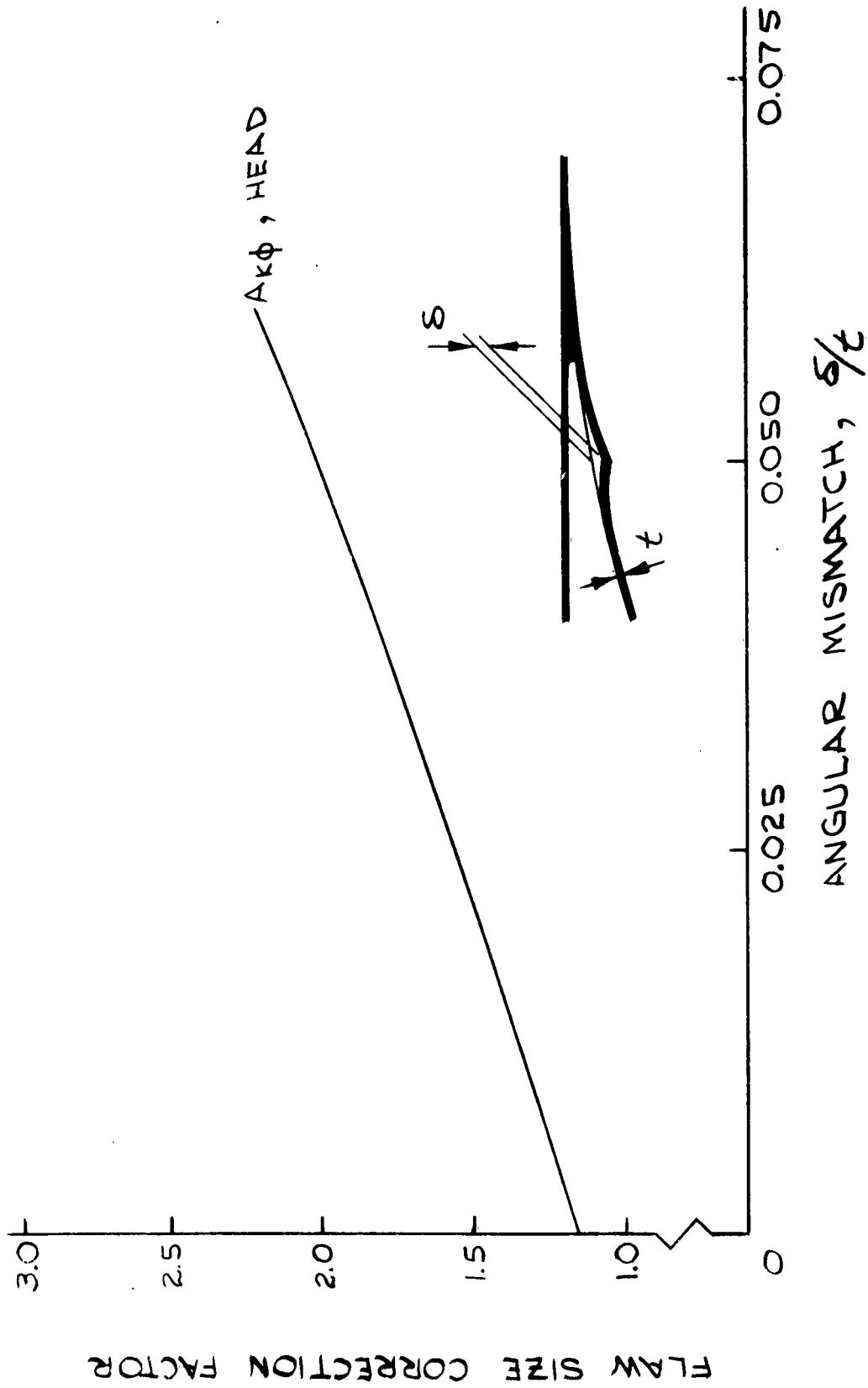


FIG. A25: FLAW SIZE CORRECTION FACTORS, ANGULAR MISMATCH, HEAD TO Y-RING WELD, 260 SL AEROJET CASE

DISTRIBUTION LIST FOR AF 33(615)-1623

National Aeronautics & Space Admin.  
Lewis Research Center  
21000 Brookpark Road  
Cleveland, Ohio 44135  
Attn: Library

National Aeronautics & Space Admin.  
Launch Operations Center  
Cocoa Beach, Florida 32931  
Attn: Library

National Aeronautics & Space Admin.  
Manned Spacecraft Center  
P. O. Box 1537  
Houston, Texas 77001  
Attn: Library

National Aeronautics & Space Admin.  
George C. Marshall Space Flight Center  
Huntsville, Alabama 35800  
Attn: Library

National Aeronautics & Space Admin.  
Langley Research Center  
Langley Air Force Base  
Virginia 23365  
Attn: Library

National Aeronautics & Space Admin.  
Washington, D. C. 20546  
Attn: Office of Technical Information  
and Educational Programs, Code ETL

Scientific and Tech. Info. Facility  
P. O. Box 5700  
Bethesda, Maryland 20014  
Attn: NASA Representative

National Aeronautics & Space Admin.  
Washington, D. C. 20546  
Attn: R. W. Ziem (RPS)

National Aeronautics and Space Admin.  
Goddard Space Flight Center  
Greenbelt, Maryland 20771  
Attn: Library

Defense Documentation Center  
Cameron Station  
Alexandria, Virginia 22314  
(19)

Air Force Systems Command  
Attn: SCTAP  
Andrews AFB  
Washington, D. C. 20331

Arnold Eng. Development Center  
Attn: AEOIM  
Air Force Systems Command  
Tullahoma, Tennessee 37389

AFRPL (RPR)  
Edwards, California 93523

AFRPL (RPMB)  
Edwards, California 93523 (2 copies)

AFRPL (RPLL)  
WPAFB, Ohio 45433

Office of Research Analysis  
Attn: RRRT  
Holloman AFB, New Mexico 88330

Wright-Patterson AFB, Ohio 45433  
Attn: AFML (MAAE) (3 Copies)

Wright-Patterson AFB, Ohio 45433  
Attn: AFML (MAAM)

Commander  
AFSC  
Foreign Technology Division  
Wright-Patterson AFB, Ohio 45433  
Attn: RTD(TD-E3b)

Commanding Officer  
U. S. Army Research Office (Durham)  
Box CM, Duke Station  
Durham, North Carolina 27706

Commanding Officer  
Frankford Arsenal  
Philadelphia, Pennsylvania 19137  
Attn: Metallurgical Research Lab.

Commanding Officer  
Picatinny Arsenal  
Dover, New Jersey 07801  
Attn: Library

Commanding Officer  
Picatinny Arsenal  
Liquid Rocket Propulsion Laboratory  
Dover, New Jersey 07801  
Attn: Technical Library

U. S. Army Missile Command  
Redstone Scientific Info. Center  
Redstone Arsenal, Alabama 35808  
Attn: Chief, Document Section

Bureau of Naval Weapons  
Department of the Navy  
Washington, D. C. 20360  
Attn: DLI-3

Bureau of Naval Weapons  
Department of the Navy  
Washington, D. C. 20360  
Attn: RMMP-2

Bureau of Naval Weapons  
Department of the Navy  
Washington, D. C. 20360  
Attn: RRRE-6

Commander  
U. S. Naval Missile Center  
Point Mugu, California 93041  
Attn: Technical Library

Commander  
U. S. Naval Ordnance Laboratory  
White Oak  
Silver Spring, Maryland 20910  
Attn: Library

Commander (Code 753)  
U. S. Naval Ordnance Test Station  
China Lake, California 93557  
Attn: Technical Library

Commanding Officer  
U. S. Naval Propellant Plant  
Indian Head, Maryland 20640  
Attn: Technical Library

Commanding Officer  
Office of Naval Research  
1030 E. Green Street  
Pasadena, California 91101

Director (Code 6180)  
U. S. Naval Research Lab.  
Washington, D. C. 20390  
Attn: H. W. Carhart

Commanding Officer  
U. S. Naval Underwater Ordnance  
Station  
Newport, Rhode Island 02844  
Attn: W. W. Bartlett

Commander  
U. S. Naval Weapons Laboratory  
Dahlgren, Virginia 22448  
Attn: Technical Library

Aerojet-General Corporation  
P. O. Box 296  
Azusa, California 91703  
Attn: Librarian

Aerojet-General Corporation  
11711 South Woodruff Avenue  
Downey, California 90241  
Attn: Florence Walsh, Librarian

Aerojet-General Corporation  
P. O. Box 1947  
Sacramento, California 95809  
Attn: Technical Information Office

Aeronutronic Div. Philco Corporation  
Ford Road  
Newport Beach, California 92600  
Attn: Dr. L. H. Linder, Manager  
Technical Information Department

Aerospace Corporation  
P. O. Box 95085  
Los Angeles, California 90045  
Attn: Library-Documents

Allied Chemical Corporation  
General Chemical Division  
Research Lab., P. O. Box 405  
Morristown, New Jersey 07960  
Attn: L. J. Wiltrakis, Security  
Officer

Ancel Propulsion Company  
Box 3049  
Asheville, North Carolina 28802

IIT Research Institute  
Technology Center  
Chicago, Illinois 60616  
Attn: C. K. Hersh, Chemistry  
Division

ARO, Inc.  
Arnold Engineering Dev. Center  
Arnold AF Station, Tennessee 37389  
Attn: Dr. B. H. Goethert  
Director of Engrg.

Atlantic Research Corporation  
Shirley Highway and Edsall Road  
Alexandria, Virginia 22314  
Attn: Library

Atlantic Research Corporation  
Western Division  
209 Easy Street  
El Monte, California 91731  
Attn: H. Niederman

Battelle Memorial Institute  
505 King Avenue  
Columbus, Ohio 43201  
Attn: Report Library, Room 6A

Chemical Propulsion Information  
Agency  
Applied Physics Laboratory  
8621 Georgia Avenue  
Silver Spring, Maryland 20910

Defense Metals Information Center  
Battelle Memorial Institute  
505 King Avenue  
Columbus, Ohio 43201

Douglas Aircraft Co., Inc.  
Santa Monica Division  
Santa Monica, California 90405  
Attn: Mr. J. L. Waisman

The Dow Chemical Company  
Security Section  
Box 31  
Midland, Michigan 48641  
Attn: Dr. R. S. Karpiuk, 1710 Bldg.

E. I. duPont de Nemours and Company  
Eastern Laboratory  
Gibbstown, New Jersey 08027  
Attn: Mrs. Alice R. Steward

Esso Research and Engineering Company  
Special Projects Unit  
P. O. Box 8  
Linden, New Jersey 07036  
Attn: Mr. D. L. Baeder

General Electric Company  
Cincinnati, Ohio 45215  
Attn: Technical Information Center

Allison Division  
General Motors Corporation  
Indianapolis, Indiana 46206  
Attn: Plant 8, Tech. Library  
Mr. L. R. Smith

Hercules Powder Company  
Allegheny Ballistics Laboratory  
P. O. Box 210  
Cumberland, Maryland 21501  
Attn: Library

Jet Propulsion Laboratory  
4800 Oak Grove Drive  
Pasadena, California 91103  
Attn: Library (TDS)  
Mr. N. E. Devereux

Lockheed Propulsion Company  
P. O. Box 111  
Redlands, California 92374  
Attn: Miss Belle Berlad, Librarian

Martin Company  
Baltimore, Maryland 21203  
Attn: Science - Technology  
Library - Mail 398

Martin Company  
Advanced Technology Library  
P. O. Box 1176  
Denver, Colorado 80201

Minnesota Mining & Manufacturing Co.  
900 Bush Avenue  
St. Paul, Minnesota 55106  
Attn: J. D. Ross  
VIA: H. C. Zeman  
Security Administrator

Monsanto Research Corporation  
Boston Labs., Everett Station  
Boston, Massachusetts 02149  
Attn: Library

New York University  
Dept. of Chemical Engineering  
New York, New York 10053  
Attn: P. F. Winternitz

North American Aviation, Inc.  
Space and Information Systems Div.  
12214 Lakewood Boulevard  
Downey, California 90242  
Attn: W. H. Morita

Rocketdyne  
6633 Canoga Avenue  
Canoga Park, California 91304  
Attn: Library, Dept. 596-306

Space Technology Laboratory, Inc.  
1 Space Park  
Redondo Beach, California 90200  
Attn: STL Tech. Lib. Doc.  
Acquisitions

Texaco Experiment Incorporated  
P. O. Box 1-T  
Richmond, Virginia 23203  
Attn: Librarian

Thiokol Chemical Corporation  
Alpha Division, Huntsville Plant  
Huntsville, Alabama 35800  
Attn: Technical Director

Thiokol Chemical Corporation  
Alpha Division  
Space Booster Plant  
Brunswick, Georgia 31500

Thiokol Chemical Corporation  
Elkton Division  
Elkton, Maryland 21921  
Attn: Librarian

Thiokol Chemical Corporation  
Reaction Motors Division  
Denville, New Jersey 07834  
Attn: Librarian

Thiokol Chemical Corporation  
Wasatch Division  
P. O. Box 524  
Brigham City, Utah 84302  
Attn: Library Section

Thompson Ramo Wooldridge  
23555 Euclid Avenue  
Cleveland, Ohio 44117  
Attn: Librarian

United Aircraft Corporation  
Corporation Library  
400 Main Street  
East Hartford, Connecticut 06118  
Attn: Dr. David Rix

United Aircraft Corporation  
Pratt & Whitney Fla. Res. & Dev.  
Ctr.  
P. O. Box 2691  
W. Palm Beach, Florida 33402  
Attn: Library

United Technology Center  
P. O. Box 358  
Sunnyvale, California 94088  
Attn: Librarian

General Electric Company  
Apollo Support Department  
P. O. Box 2500  
Daytona Beach, Florida 32015

Mr. W. F. Brown, Jr.  
NASA/Lewis Research Center  
21000 Brookpark Road  
Cleveland, Ohio 44135

Central Intelligence Agency  
2430 E. Street, N. W.  
Washington, D. C. 20505  
Attn: OCD, Standard Dist.

Bureau of Ships  
Code 634B  
Washington D. C. 20390  
Attn: T. J. Griffin

United States Steel Corporation  
Applied Research Lab.  
P. O. Box 38  
Monroeville, Pennsylvania  
Attn: Dr. J. H. Gross



Rensselaer Polytechnic Institute  
Materials Engineering Department  
Troy, New York  
Attn: Mr. W. F. Savage

AFFDL (FDTR/Mr. Royce Forman)  
Wright-Patterson AFB, Ohio 45433

AFML (MAA/Lt Col. W. Postelnek)  
Wright-Patterson AFB, Ohio 45433

AFML (MAX/Dr. A. M. Lovelace)  
Wright-Patterson AFB, Ohio 45433

AFML (MAAA/Lt. Col. G. W. Roust)  
Wright-Patterson AFB, Ohio 45433

AFML (MAAE/Lt. R. Roeschlein)  
Wright-Patterson AFB, Ohio 45433

AFML (MAAE/W. P. Conrardy)  
Wright-Patterson AFB, Ohio 45433

AFML (MAAE/E. W. McKelvey)  
Wright-Patterson AFB, Ohio 45433

AFML (MAAM/S. O. Davis)  
Wright-Patterson AFB, Ohio 45433

AFML (MAAM/M. Knight)  
Wright-Patterson AFB, Ohio 45433

AFML (MAAM/D. Shinn)  
Wright-Patterson AFB, Ohio 45433

AFML (MAAM/Lt. N. G. Tupper)  
Wright-Patterson AFB, Ohio 45433

AFML (MAMD/ J. A. Holloway)  
Wright-Patterson AFB, Ohio 45433

AFML (MAMD/ R. Rowand)  
Wright-Patterson AFB, Ohio 45433

AFML (MAMP/I. Perlmutter)  
Wright-Patterson AFB, Ohio 45433

AFML (MAMP/R. E. Bowman)  
Wright-Patterson AFB, Ohio 45433

AFML (MAMP/R. T. Ault)  
Wright-Patterson AFB, Ohio 45433

AFML (MATB/G. Glenn)  
Wright-Patterson AFB, Ohio 45433

AFML (MAT/Col. M. E. Fields)  
Wright-Patterson AFB, Ohio 45433

AFML (MATF/Mr. F. R. Miller)  
Wright-Patterson AFB, Ohio 45433

AFRPL (RPMB/Mr. D. Hart)  
Edwards AFB, California 93523

AFRPL (RPMB/Maj. O. Krone)  
Edwards AFB, California 93523

SSD (SSBS/Maj. E. Dabrowski)  
AF Unit Post Office  
Los Angeles California 90045

SSD (SSTR/Mr. P. Propp)  
AF Unit Post Office  
Los Angeles California 90045

HQ. U. S. Army Materiel Command  
Attn: AMCRD-RC-M (Mr. L. S. Croan)  
Building T-7  
Washington, D. C. 20315

Army Tank-Automotive Center  
Materials Laboratory  
Attn: Mr. Charles J. Kropf/SMOTA-RCM)  
28251 Van Dyke  
Warren, Michigan 48090

Commanding Officer  
Frankford Arsenal - U. S. Army  
Attn: D. F. Armiento/SMUFA-L 7400  
Bridge & Tacony Streets  
Philadelphia, Pennsylvania 19137

U. S. Army Missile Command  
Directorate of Research & Development  
Propulsion Laboratory  
Attn: Mr. W. S. Crownover/AMSMI-RKP  
Redstone Arsenal, Alabama 35809

Commanding Officer  
2705 Ammunition Wing  
Ogden, Utah

NASA  
Marshall Space Flight Center  
Attn: Dr. W. R. Lucas  
M-P&VE-M  
Huntsville, Alabama

NASA Headquarters  
Attn: Mr. R. A. Wasel  
Code RPM  
Washington, D. C.

NASA  
Attn: Mr. Harry Williams  
150 Pico Blvd.  
Santa Monica, California

NASA - Lewis Research Center  
Attn: Mr. J. Kramer  
MS 500-209  
21000 Brookpark Road  
Cleveland, Ohio

NASA - Marshall Space Flight Center  
Attn: Mr. M. G. Olsen  
R-P&VE-MMJ  
Huntsville, Alabama

NASA-Marshall Space Flight Center  
Attn: Mr. John Miller  
R-P & VE-PP  
Huntsville, Alabama

Bureau of Naval Weapons  
Department of the Navy  
Attn: RRMA-24 (Mr. Roy Gustafson)  
Washington, D. C. 20360

Chief,  
Bureau of Naval Weapons  
Department of the Navy  
Attn: Mr. S. J. Matesky  
Washington, D. C. 20360

Chief,  
Bureau of Naval Weapons  
Department of the Navy  
Attn: Mr. N. E. Promisel  
Washington, D. C. 20360

Chief,  
Bureau of Ships  
Department of the Navy  
Attn: Code 634B (Mr. T. J. Griffin)  
Washington, D. C. 20390

Chief,  
Bureau of Ships  
Department of the Navy  
Attn: Code 314A (Mr. G. Sorkin)  
Washington, D. C. 20390

U. S. Naval Research Laboratory  
Navy Department  
Attn: Mr. C. D. Beachem (Code 6322)  
Washington, D. C. 20390

U. S. Naval Research Laboratory  
Department of the Navy  
Attn: Dr. B. F. Brown (Code 6320)  
Washington, D. C. 20390

U. S. Naval Research Laboratory  
Attn: Mr. Steven Hart  
Washington, D. C. 20390

U. S. Naval Research Laboratory  
Attn: Dr. G. R. Irwin (Code 6212)  
Mechanics Division  
Washington, D. C. 20390

U. S. Naval Research Laboratory  
Attn: Dr. H. Romine (Code 6212)  
Mechanics Division  
Washington, D. C. 20390

U. S. Naval Research Laboratory  
Attn: Mr. J. M. Krafft  
Mechanics Division  
Washington, D. C. 20390

Aerojet-General Corporation  
Solid Rocket Plant  
Attn: Mr. R. Cottrell  
P. O. Box 1947  
Sacramento, California

Aerojet-General Corporation  
Solid Rocket Plant  
Attn: Mr. P. P. Crimmins  
P. O. Box 1947  
Sacramento, California

Aerojet-General Corporation  
Solid Rocket Plant  
Attn: Mr. W. S. Tenner  
P. O. Box 1947  
Sacramento, California

Aerospace Corporation  
Attn: Mr. John C. Batteiger  
1111 Mill Street  
P. O. Box 1308  
San Bernardino, California

Aerospace Corporation  
El Segundo Corporation  
Attn: Dr. George Kendall  
2350 East El Segundo  
El Segundo, California 90045

Aerospace Corporation  
Attn: Mr. Harold Smullen  
Engineering Division  
2400 E. El Segundo Blvd  
El Segundo, California

Air Reduction Company  
Attn: Mr. K. E. Dorschu  
Process & Equipment Development  
Mountain Avenue  
Murray Hill, New Jersey

Allegheny Ballistics Laboratory  
Attn: Mr. R. Randolph  
Hercules Powder Company  
Cumberland, Maryland

Allison Division/GMC  
Attn: Mr. D. Hanink  
Indianapolis 6, Indiana

ARDE, Incorporated  
Attn: Mr. Ralph H. Alper  
100 West Century Road  
Paramus, New Jersey

Automation Industries, Inc.  
Research Laboratory  
Attn: Dale Maley  
Industrial Park  
Boulder, Colorado

Automation Industries, Inc.  
Attn: Jerry Posakony  
Industrial Park  
Boulder, Colorado

AVCO Manufacturing Corporation  
Research & Advanced Development Division  
Attn: C. H. Hastings  
201 Lowell Street  
Wilmington, Massachusetts

Bell Aerosystems Company  
Attn: Mr. J. R. Piselli  
Director of Engineering  
Buffalo 5, New York

Branson Instrument Incorporated  
Attn: Peter Bloch  
57 Brown House Road  
Standford, Connecticut 06902

The Budd Company  
Attn: Walter J. Hauck  
2450 Huntingpark Avenue  
Philadelphia, Pennsylvania 19132

California Institute of Technology  
Attn: Dr. M. L. Williams  
1201 E. California Blvd.  
Pasadena, California 91109

Chicago Bridge & Iron Company  
Attn: Mr. C. D. Miller  
25 Prospect Avenue, West  
Cleveland 15, Ohio

Curtiss-Wright Corporation  
Attn: Mr. E. P. Gilewicz  
Wright Aeronautical Division  
Passaic Avenue  
Woodridge, New Jersey

Curtiss-Wright Corporation  
Attn: Mr. S. Kirschener  
Wright Aeronautical Division  
Passaic Avenue  
Woodridge, New Jersey

Curtiss-Wright Corporation  
Attn: Mr. J. Sohn, Manager  
Metallurgy  
Wright Aeronautical Division  
Passaic Avenue  
Woodridge, New Jersey

DMIC  
Battelle Memorial Institute  
Attn: Mr. G. T. Hahn  
505 King Avenue  
Columbus 1, Ohio

DMIC  
Battelle Memorial Institute  
Attn: Mr. R. J. Runck  
Columbus, Ohio 43201

Douglas Aircraft Company, Inc.  
Missiles and Space Systems Division  
Attn: C. J. Adams, Group Engineer  
Mechanical & NDT Section  
Santa Monica, California

Douglas Aircraft Company  
Attn: Mr. R. H. Christensen  
3000 Ocean Park Blvd  
Santa Monica, California

Excelco Developments, Incorporated  
Attn: Mr. Ward Abbott  
Mill Street  
Silvercreek, New York 14136

Foster Wheeler Corporation  
Attn: Mr. E. L. Daman  
Director of Research  
110 South Orange Avenue  
Livingston, New Jersey 07039

General Dynamics/Convair  
Attn: Mr. H. F. Greet  
P. O. Box 1108  
San Diego, California 92112

General Dynamics Corporation  
Electric Boat Division  
Attn: Mr. L. A. Luini  
R. & D Department  
Groton, Connecticut

General Dynamics/Electric Boat  
Attn: Dr. H. E. Sheets  
Director of R & D  
Groton, Connecticut

General Electric Company  
Attn: D. C. Barnes  
Rocket Case Section, Bldg. 700  
Cincinnati 15, Ohio

General Electric Company  
Research Laboratory  
Attn: Dr. John R. Low, Jr.  
P. O. Box 1088  
Schenectady, New York

Grand Central Rocket Company  
Attn: E. F. Harris  
P. O. Box 11  
Redlands, California

Hughes Aircraft Company  
Attn: Robert W. Jones  
Culver City, California

International Nickel Co., Inc.  
Attn: Mr. R. E. Decker  
Research Laboratories  
30 Oak Street  
Bayonne, New Jersey

Ladish Company  
Attn: Mr. Robert Daykin  
Metallurgical Department  
Cudahy, Wisconsin

Linde Company  
Union Carbide Corporation  
Attn: Mr. R. L. Hackman  
Electric Welding Development  
P. O. Box 2819  
Newark, New Jersey 07114

Lockheed-Missile & Space Company  
Attn: Mr. R. E. Lewis  
Dept. 52-30, B204  
3251 Hanover Street  
Palo Alto, California

Lockheed-Missile & Space Company  
Attn: Dr. Leo Schapiro  
52-30/201/2  
3251 Hanover Street  
Palo Alto, California

Lockheed Propulsion Company  
Attn: Mr. J. S. Coverdale  
P. O. Box 111  
Redland, California

Magnaflux Corporation  
Attn: D. O'Connor  
7300 West Lawrence Avenue  
Chicago 31, Illinois

ManLabs, Incorporated  
Attn: Dr. B. S. Lement  
21 Erie Street  
Cambridge 39, Massachusetts

Mellon Institute  
Attn: Dr. G. K. Bhat  
4400 Fifth Avenue  
Pittsburgh, Pennsylvania 15213

National Science Foundation  
Undergraduate Education in the Sciences  
Attn: Dr. Paul C. Paris  
1730 K Street, N. W.  
Washington, D. C. 20550

Newport News Shipbuilding & Dry Dock Co.  
Attn: Mr. G. S. Barlow, Jr.  
New port News, Virginia

Newport News Shipbuilding & Dry Dock Co.  
Attn: Mr. Frank Duffey  
Newport News, Virginia

Newport News Shipbuilding & Dry Dock Co.  
Attn: Mr. W. L. Lamerdin  
Newport News, Virginia

North American Aviation, Inc.  
Rocketdyna Division  
Attn: Mr. E. L. Klein,  
Manager-Advanced Products  
Solid Rocket Division  
McGregor, Texas

North American Aviation, Inc.  
Los Angeles Division  
Attn: Mr. William D. Padian  
Welding Laboratory  
International Airport  
Los Angeles, California 90009

North American Aviation  
Los Angeles Division  
Attn: Dr. C. S. Yen  
International Airport  
Los Angeles, California 90009

NTW Missile Engineering, Inc.  
4820 Alcoa Avenue  
Los Angeles, California 90058

The Ohio State University  
Department of Metallurgical Engineering  
Attn: Prof. J. W. Spretnak  
116 West 19th Avenue  
Columbus, Ohio 43210

Republic Steel Corporation  
Research Center  
Attn: Mr. S. J. Matas  
P. O. Box 7806  
6801 Brecksville Road  
Cleveland, Ohio 44131

Republic Steel Corporation  
Attn: Mr. T. J. Shimmin  
Central Alloy District  
Massillon, Ohio

Republic Steel Corporation  
Attn: Mr. R. J. Place  
Alloy Steel Division  
410 Oberlin Avenue, S. W.  
Massillon, Ohio

Rocketdyna  
Attn: Mr. R. L. Black  
Solid Rocket Division  
Johnson Drive  
McGregor, Texas

Rohr Corporation  
Attn: Mr. T. R. Bradley  
P. O. Box 878  
Chula Vista, California

Sandia Corporation  
Attn: Mr. C. H. Maak  
Materials Laboratory 1121  
Sandia Base  
Albuquerque, New Mexico

Southwest Research Institute  
Attn: Mr. J. R. Barton  
8500 Culebra Road  
San Antonio, Texas 78206

Southwest Research Institute  
Attn: Mr. L. U. Rastrelli  
8500 Culebra Road  
San Antonio, Texas 78206

Space Technology Laboratories  
Attn: Dr. P. N. Randall  
Materials Sciences  
Redondo Beach, California

Sperry Products Company  
Attn: Mr. H. E. Van Valkenburg  
Danbury, Connecticut

Sun Shipbuilding & Dry Dock Company  
Rocket Fabrication Division  
Attn: Mr. Charles Garland  
Chester, Pennsylvania

Sun Shipbuilding & Dry Dock Company  
Attn: Mr. Byron Nierenberg  
Chester, Pennsylvania

Syracuse University  
Attn: Dr. Volker Weiss  
Bldg D6 Collendale Campus  
Syracuse, New York 13210

Thiokol Chemical Corporation  
Attn: Mr. P. Craig,  
Technical Director  
Space Booster Division  
Brunswick, Georgia 31520

Thiokol Chemical Corporation  
Alpha Division  
Attn: Mr. T. H. Burns,  
Metallurgist  
Huntsville, Alabama

Thiokol Chemical Corporation  
Attn: Mr. J. F. Douglas  
Space Booster Division  
Brunswick, Georgia

Thiokol Chemical Corporation  
Attn: Mr. A. G. Melville  
Materials Department  
Wasatch Division  
Brigham City, Utah 84302

TRW, Incorporated  
Equipment Laboratories  
Attn: Dr. J. M. Gerken  
23555 Euclid Avenue  
Cleveland, Ohio 44117

TRW  
Electromechanical Division  
Attn: Mr. E. A. Steigerwald  
23555 Euclid Avenue  
Cleveland, Ohio 44117

United Technology Center  
Attn: Mr. S. M. Jacobs  
P. O. Box 358  
Sunnyvale, California 94088

University of Illinois  
Attn: Dr. Herbert T. Corten  
Dpt. of Theoretical & Applied Mechanics  
Urbana, Illinois

U. S. Steel Corporation  
Applied Research Laboratory  
Attn: Mr. J. H. Gross, Chief  
Ordnance Products Division  
Monroeville, Pennsylvania 15146

U. S. Steel Corporation  
Applied Research Laboratory  
Attn: Mr. G. E. Pellissier (MS-16)  
Monroeville, Pennsylvania 15146

U. S. Steel Corporation  
Attn: Elgin Van Meter  
525 William Penn Place  
Pittsburgh, Pa.

Westinghouse Electric Corporation  
Advanced Development/Rocket Motor Case  
Department  
Attn: Mr. G. W. Ellenburg, Manager  
Lester Branch P. O. Box 9175  
Philadelphia, Pennsylvania 19113

Westinghouse Electric Corporation  
Research & Development Center  
Attn: H. Greenberg, Manager  
Beulah Road, Churchill Boro  
Pittsburgh, Pa. 15235

Westinghouse Electric Corporation  
Research Laboratory  
Attn: Mr. E. T. Wessel  
Beulah Road, Churchill Boro  
Pittsburgh, Pa. 15235

Syman-Gordan Company  
Research & Development Department  
Attn: Mr. Robert B. Sparks  
Worcester, Massachusetts